ITERATIVE ACCELERATION METHODS FOR MONTE CARLO AND DETERMINISTIC CRITICALITY CALCULATIONS

by

Todd James Urbatsch

A dissertation submitted in partial fulfillment
of the requirements for the degree of
Doctor of Philosophy
(Nuclear Engineering and Scientific Computing)
in The University of Michigan
1995

Doctoral Committee:

Professor E. W. Larsen, Chairperson
Professor T. I. Gombosi
Professor J. C. Lee
Professor W. R. Martin

To my parents, Jim and Dee Urbatsch, and my sisters, Kathy and Stacy

ACKNOWLEDGEMENTS

I owe many thanks to a large group of people who, in some way, educated me, encouraged me, kicked me in the right direction, cried when I laughed, laughed at me when I cried, or otherwise helped me out.

First and foremost, thanks to Ed Larsen. Experiencing his lectures, watching him work, working with him, and getting caught up in his contagious enthusiasm were truly educational highlights. He's the only other person I know of, besides J. Robert Oppenheimer, who was so caught up in his thoughts, that he ran his car off the road. Thank you, Dr. Larsen, for not running into a tree.

Thanks to Mom and Dad for everything, especially for trying to explain to others what I was doing; hopefully this explains everything. And thanks to the rest of the family: my vengeful, witty sisters Stacy and Kathy (& Corey, too), Grandma and Jack, and Grump.

Warm thanks to Art Forster for taking me under his wing, in ways of Monte Carlo and otherwise, and letting me be a part of his family: Deanna, Michael, and David, and Mindy and Bruiser.

I extend thanks to the supervisors who have provided much needed guidance: Art Forster and Tom Booth (LANL); Roger Blomquist (ANL-East); George Imel, Darrell Cutforth, and Charlie Lahm (ANL-West), and to the managers who worked to make it possible, Bob Little and Pat Soran (LANL), and Michael Lineberry (ANL-West). I will try to make good use of your investments. Thanks to other professionals in

the field for their advice and help: Jim Rathkopf (LLNL), and Forrest Brown, Dick Mendelson, and Tom Sutton (KAPL). And thanks to the late Wally Walters (LANL); this wasn't how I wanted you to miss out on harassing me at my defense.

Thank you Dr. Martin, Dr. Lee, and Dr. Gombosi for accepting the dubious honor of serving on my committee.

Thanks to several friends who shaped me and made me what I am and am not: from Osage, Iowa: Russell Johnson and Mike "Stokes" O'Connor; from Iowa State University: Mike "M.R." Smith, J.P. "Jet Pilot" Martin, Rick Ruddy, Greg "G.I." and Jeannette Derner, Mike Ross, Ryan and Melissa Brookhart, Mike and Debbie Jessen, the Lehr Sisters, Deb Haugen, Ellen Schwictenberg, and Steff Stiegelmeyer; from Idaho: Cliff "Jag" Russell, Cal "Captain" Morgan and Samantha, Bonnie Bean, Santiago Parra, Tom Fanning, and Robert Canaan; from Illinois: Jenny Joseph; from the University of Michigan: Amit Majumdar and Mieko Ueno, Todd and Teri Palmer, Todd Wareing, Chris Gesh, Eric Hawkes, Djordje Tomasevic, Scott and Anna Turner, Moaied Miften, Tarek Al-Nahlawi, Marie-Anne Descalle, Joe Schumer, Craig Holmes, Eric Smith, Denise Pareventi, Helen Lum, Sue Greenwood, Karen Balson, Ann Bell, and Alice Cook; and from Los Alamos: Reid Rivenburgh, Kevin Barbour, Dr. Robert "The Big Sperm" Seamon, Tammy Palmer, Debbie Apodaca, John Wagner, Jason Lashley, Lori Brockway, Shelley Thompson, Denise Soran, and Travis and Cheryl Brown. To Beth Mele, thanks for the Louisiana influences (including your grandma Margie) and for helping me through some particularly trying times. Thanks to Carol Tallman for the great times and putting up with me.

Thank you and much appreciation to Los Alamos National Laboratory, the University of Michigan Nuclear Engineering Department, and the Michigan Regents. Without their funding, none of this would have been possible.

TABLE OF CONTENTS

LIST OF FIGURES

LIST OF APPENDICES

Appendix

CHAPTER I

Introduction

If you have ever given up on a nuclear criticality calculation and terminated it because it took so long to converge, you might find this thesis of interest. We develop three methods for improving the fission source convergence in nuclear criticality calculations for physical systems with high dominance ratios for which convergence is slow. The Fission Matrix Acceleration Method and the Fission Diffusion Synthetic Acceleration (FDSA) Method are acceleration methods that speed fission source convergence for both Monte Carlo and deterministic methods. The third method is a hybrid Monte Carlo method that also converges for difficult problems where the unaccelerated Monte Carlo method fails.

1.1 Criticality Calculations

The *criticality* of a system containing fissionable material is described by its multiplication factor. The *multiplication factor* is the ratio of the number of neutrons in one generation to the number of neutrons in the previous generation. A generation is essentially the lifetime of a neutron. For finite systems, the multiplication factor is denoted as $k_{effective}$, or k_{eff}. When a system is critical, it sustains a steady-state chain reaction of nuclear fissioning, and k_{eff}=1. The average neutron population

in a critical system stays constant in time. A subcritical system has $k_{eff}<1$ and the neutron population dies off in time. The neutron population in a supercritical system, where $k_{eff}>1$, grows without bound in time [Dud76].

Knowledge of k_{eff} is necessary when designing nuclear reactors and handling nuclear waste. With reactor design at a lull and waste production not, the latter has become a dominant application for criticality calculations, or, more appropriately, *criticality safety calculations.* Criticality has been a concern since the first criticality experiments. Experiments are the best benchmarks for criticality safety, but they are costly and specific only to the particular geometry of the experiment. Hand calculations have been used for arrays of fissionable material [Tho73]. However, numerical computer methods are used almost exclusively for criticality calculations at this time. Deterministic and Monte Carlo methods are both used. However, because of complicated geometries and increasing computer power, Monte Carlo methods are emerging as the tool of choice for criticality safety engineers. In the United States, three production Monte Carlo computer codes are widely used: MCNP^{TM} [1] [Bri93][For94] from Los Alamos National Laboratory, KENO [Bow95] from Oak Ridge National Laboratory, and MONK from AEA Technology in the United Kingdom [Smi95]. VIM [Blo95] is used extensively at Argonne National Laboratory. We have implemented one of our new methods, the Fission Matrix Acceleration Method, in MCNP.

1.2 Difficulties with Criticality Calculations

For some systems, criticality calculations take an enormous amount of time to converge. Both deterministic and Monte Carlo criticality calculations are based

[1] MCNP is a trademark of the Regents of the University of California, Los Alamos National Laboratory

on the source (or power) iteration method. A deterministic calculation is finished upon source convergence, but a Monte Carlo calculation begins accumulating useful random variable data only after the (fission) source is converged. The error in the source iteration method decreases with each iteration, where the speed of the decrease is dictated by the dominance ratio. The *dominance ratio* is the ratio of the second eigenvalue to the first, or dominant, eigenvalue (k_{eff}). If the dominance ratio is near unity, the source iteration error will decrease slowly, and thus convergence to the dominant eigenmode (the converged fission source) is slow. Two types of systems that have high dominance ratios (near unity) are large thermal reactors and arrays of nuclear waste components. A system's high dominance ratio is synonymous with weak neutron communication between distant regions of the system.

Slow source convergence is less of a problem when the initial fission source guess is very close to the converged fission source. However, sometimes knowledge of the solution beforehand is evasive. Sometimes the typically available initial source shapes (flat, or uniform, over the fissionable regions, or maybe a cosine shape) in a production code are very different from the converged source shape. So, in practice, slow source convergence can be quite troublesome. In fact, for some difficult problems, Monte Carlo may never converge.

1.3 History of the Fission Matrix

The fission matrix is mainly associated with Monte Carlo criticality calculations, but it also has applications in deterministic criticality calculations. The (i,j)th element of the fission matrix is the probability that a fission source neutron born in region j of the system causes the subsequent birth of a fission source neutron in region i. The fission matrix may be somewhat tediously estimated from a set of

deterministic calculations.

The fission matrix may also be estimated in a Monte Carlo calculation by keeping track of what happens to the Monte Carlo–simulated neutrons. Each element (i, j) of the fission matrix is the number of neutrons produced in region i due to neutrons starting in region j divided by the number of neutrons starting in region j. Because the fission matrix elements are ratios (and probabilities), they may be closer to truth than the Monte Carlo fission source. For example, suppose the source in region j is lower than its converged value. Both the numerators and denominators in the fission matrix elements associated with region j will be lower than their converged values. The errors tend to cancel out in the fission matrix elements, and are more representative of the converged solution. Thus, the eigenvector of the fission matrix tends to converge faster than the Monte Carlo fission source. Note that, because it is spatially discretized, the fission matrix eigenvector does not converge exactly to the spatially continuous Monte Carlo fission source. The eigenvector has a second–order spatial truncation error [Kap58][Car75].

The idea of using the fission matrix as a separate and faster calculation was developed by Morton [Mor56] and Kaplan [Kap58]. Morrison, Mihalczo, and Irving of Oak Ridge National Laboratory implemented a fission matrix calculation into the Monte Carlo code O5R [Mor66]. They used the number of iterations required to converge the fission matrix eigenvector as a guide to know how many Monte Carlo iterations it would take the regular Monte Carlo to converge. Both Mihalczo [Mih67] and Mendelson [Men68] used the fission matrix calculations in calculations for real systems. The Oak Ridge code, KENO, has the capability of performing fission matrix calculations. Unfortunately, hardly anyone uses this option [Pet92]. We speculate that the major reason this KENO option is largely unused is the user community's

lack of familiarity with the fission matrix.

Both Kaplan [Kap58] and Kalos, et al. [Gre68] suggested using the fission matrix eigenvector to adjust the regular Monte Carlo fission source distribution through variance reduction techniques (Splitting and Russian roulette). Carter and McCormick [Car69] presented a method in which the regular Monte Carlo fission source distribution is adjusted by the ratio of successive fission matrix eigenvectors. They demonstrated the potential acceleration by performing calculations that used diffusion methods to simulate Monte Carlo. Kadontani, et al. [Kad91] attempted accelerating the Monte Carlo fission source by setting it equal to the fission matrix eigenvector at each iteration. These attempts met with limited success.

The big culprit behind these failures of Monte Carlo source acceleration methods is the statistical noise inherent in the Monte Carlo algorithm. The acceleration attempts may be carried over from successful deterministic methods, or they may just be inherently deterministic, but whatever the reason, they cannot handle statistical noise. However, Swaja [Swa72] successfully accelerated Monte Carlo fission source convergence with Source Extrapolation, a deterministic acceleration method. He filtered the statistical noise by a Kalman filter. Embedded in the Kalman filtering process was the fission matrix to account for the dynamic state of the converging source.

We consider a numerical acceleration method as a method that converges to a solution equivalent to the unaccelerated solution, only faster. Since the fission matrix is estimated in discrete space, it has a truncation error. Therefore, unless the fission matrix has the same spatial discretization as the regular calculation, a direct adjustment of the regular fission source to the fission matrix eigenvector is not an acceleration method. (Depending on how the method of Kalos, et al. [Gre68] is

implemented, it may or may not be an acceleration method.) Monte Carlo calculations are usually performed in continuous space and the fission matrix is estimated in finite discretized space.

The Fission Matrix Acceleration method derived in this thesis converges to the regular, unaccelerated Monte Carlo fission source. It uses the fission matrix as a low-order operator to determine an additive correction to the fission source. However, it does require filtering the statistical noise.

1.4 The New Methods and Testing Their Feasibility

We develop three new methods that have not been tried before. The Fission Matrix Acceleration method and the Fission Diffusion Synthetic Acceleration method are accelerated versions of the regular, unaccelerated Source Iteration method. Each iteration contains an additional step in which a low-order approximation to an exact additive correction is applied to the fission source. Although each accelerated iteration entails more work, the method accelerates the source convergence such that significantly fewer iterations are required for convergence. The low-order approximations to the exact corrections are what differentiate the two methods: the fission matrix and the diffusion approximation. The third method, the Hybrid Monte Carlo method, is not an acceleration method, but rather a modified Monte Carlo source iteration method. The source at each iteration is sampled not from the Monte Carlo tracking, but from the solution of an elliptic equation, some of whose coefficients are determined by the Monte Carlo simulation.

We determine the feasibility of the new methods by testing them on idealized problems. The problems are far from reality, but nevertheless, they contain enough "truth" to determine the merit and behavior of the methods.

Verification of the testbed's validity is found by implementing the Fission Matrix Acceleration method in the production code MCNP. Its behavior for a real, three-dimensional, continuous-energy problem is the same as its behavior in the idealized problems.

In a valid testbed then, we demonstrate that these methods are successful and warrant further adaptation to real problems. Projected speedups will reduce computational time investments, thus permitting better evaluation of criticality scenarios.

1.5 Thesis Synopsis

We present an overview of the thesis.

Chapter II: Criticality Calculations

In Chapter II we begin with the general neutron transport equation and derive the analytic fixed-source and the analytic criticality equations for one energy group, isotropic scattering, and one-dimensional slab geometry. We also derive the adjoint transport equation. We derive and present the numerical method of solution for deterministic and Monte Carlo methods and the difficulties they have with high dominance ratio problems. Lastly, we describe the fission matrix and how it is estimated.

Chapter III: Fourier Analysis and Damped Acceleration

The acceleration methods we derive produce an additive correction for the fission source. We will find that sometimes the correction needs to be scaled back, or damped, because applying the entire correction results in instability or highly oscillatory behavior. Usually the oscillatory behavior is found in Monte Carlo calculations and is due to the statistical noise. Sometimes deterministic acceleration

has to be scaled back if the system and solution are extremely heterogeneous or contain severe transport effects. We do not have a direct theoretical justification for this damping. However, we gain some indirect theoretical insight by looking at Diffusion Synthetic Acceleration (DSA), an acceleration method for fixed-source calculations. We find, through a Fourier analysis, that when the acceleration equation is discretized inconsistently with the transport equation, damping is required for certain mesh sizes in order to inhibit instability. We note that, in methods for accelerating the Monte Carlo fission source convergence, the acceleration equations are inherently inconsistently discretized with Monte Carlo. Fission source convergence acceleration methods are not amenable to this type of Fourier analysis, so we use the inconsistently-discretized fixed-source analysis as a foundation for damping fission source convergence acceleration.

Chapter IV: Experimental Fourier Analysis Tool

This shortest chapter in this thesis explains the tool we use to measure the convergence of a fission source. The experimental Fourier analysis tool is used throughout the thesis to gauge the convergence of various modes of the fission source.

Chapter V: Diffusion-Simulated Monte Carlo Calculations

In Chapter V we present Carter and McCormick's acceleration method [Car69] and propose an improvement to it. All neutron transport in this chapter is simulated by diffusion calculations.

Chapter VI: Fission Matrix Acceleration Method

We develop the Fission Matrix Acceleration method in Chapter VI. We derive it and explain the statistical filtering necessary for accelerating Monte Carlo. We

present the three one-dimensional slab geometry test problems that we use throughout the thesis: a homogeneous slab, a uniform lattice, and a one-dimensional model of the "k_{eff} of the world" problem. We present both deterministic and Monte Carlo acceleration results.

We also extend the Fission Matrix Acceleration method to the production Monte Carlo code MCNP and demonstrate the acceleration for the real, three-dimensional, continuous energy- and space-dependent "k_{eff} of the world" problem.

Chapter VII: Fission Diffusion Synthetic Acceleration

Chapter VII contains the derivation of the Fission Diffusion Synthetic Acceleration (FDSA) method and the results for both deterministic and Monte Carlo criticality calculations for the one-dimensional problems.

Chapter VIII: A Hybrid Monte Carlo Method for Improved Source Convergence

Sometimes Monte Carlo does not converge to the correct fission source. An example of a system where this is the case is the uniform lattice problem. Since a true acceleration method converges to the unaccelerated solution, the method cannot overcome inherent Monte Carlo deficiencies. We present a hybrid Monte Carlo method in Chapter VIII that converges when regular, or accelerated, Monte Carlo cannot. This method also results in reduced statistical noise.

Chapter IX: Summary, Conclusions, and a Look Ahead

In Chapter IX we summarize, draw conclusions, and list some activities for future work.

CHAPTER II

Criticality Calculations

This thesis investigates the acceleration of Monte Carlo (and, to a lesser extent, deterministic) nuclear criticality calculations. Criticality calculations, due to the presence of fissioning, are an extension of fixed-source calculations. We first present the fixed-source neutron transport equation and sketch the derivation of its monoenergetic, isotropic scattering, one-dimensional slab geometry form. We then introduce fissioning to obtain the criticality form of the neutron transport equation that provides the groundwork for much of this thesis. We also present the diffusion equation, an approximation to the transport equation. We use the diffusion equation and its associated approximations to develop and study acceleration methods.

2.1 Analytic Equations

2.1.1 Analytic Fixed Source Neutron Transport Equation

A fixed-source calculation solves the neutron transport equation, which is a linearized version of the Boltzmann equation [Cas67][Dud76]. The neutron transport equation, for both fixed-source and criticality calculations, is a neutron balance equation. In general geometry, the time-independent fixed-source transport equation is [Lew84],

$$\Omega \cdot \nabla\psi(\mathbf{r}, E, \Omega) + \Sigma_t(\mathbf{r}, E)\psi(\mathbf{r}, E, \Omega) =$$
$$\int\int \Sigma_s(\mathbf{r}, \Omega' \cdot \Omega, E' \to E)\psi(\mathbf{r}, E', \Omega')\, d\Omega'\, dE' + \frac{1}{4\pi}Q(\mathbf{r}, E) \quad , \qquad (2.1)$$

where

$$\Omega = \text{direction of particle} \quad , \qquad (2.2)$$

$$\mathbf{r} = \text{position of particle} \quad , \qquad (2.3)$$

$$E = \text{energy of particle} \quad , \qquad (2.4)$$

$$\Sigma_t(\mathbf{r}, E) = \text{total cross section} \qquad (2.5)$$
$$= \text{probable number of interactions a particle at } \mathbf{r} \text{ with energy } E \text{ undergoes per unit path length} \quad , \qquad (2.6)$$

$$\Sigma_s(\mathbf{r}, \Omega' \cdot \Omega, E' \to E)\, d\Omega\, dE = \text{probability per unit path length that a particle at } \mathbf{r} \text{ with energy } E' \text{ traveling in direction } \Omega' \text{ scatters into } dE \text{ about } E \text{ and } d\Omega \text{ about } \Omega \quad , \qquad (2.7)$$

$$\frac{1}{4\pi}Q(\mathbf{r}, E) = \text{external (independent of } \psi\text{) source of particles} \quad , \qquad (2.8)$$

$$\psi(\mathbf{r}, E, \Omega) = \text{angular flux} \qquad (2.9)$$
$$= vn(\mathbf{r}, E, \Omega) \quad . \qquad (2.10)$$

Here

$$v = \text{particle speed} \quad , \qquad (2.11)$$

$$n(\mathbf{r}, E, \Omega) = \text{particle density distribution} \quad , \qquad (2.12)$$

and

$$n(\mathbf{r}, E, \Omega)\, dr\, dE\, d\Omega = \text{expected number of particles in } dr \text{ about } \mathbf{r} \text{ with energy } dE \text{ about } E \text{ and traveling in direction } d\Omega \text{ about } \Omega \quad . \qquad (2.13)$$

In this thesis, we make three simplifications to the neutron transport equation. First, we consider only monoenergetic (or, one-group) problems, thereby eliminating the dependence on E. Second, we consider only isotropic scattering. All angles are equiprobable in isotropic scattering, so the dependence of Σ_s on angle is eliminated. Third, our analysis is restricted to one-dimensional slab geometry. These are harsh restrictions and deviate greatly from reality, but they provide an appropriate platform for methods development. If a method is successful under these simplifications, extensions of it may be successful for higher-dimensioned, more complicated problems. In fact, we have successfully implemented the Fission Matrix Acceleration method in MCNP and applied it to a three-dimensional, continuous energy problem. (See Section 6.6.) The characteristics of the simplified, one-dimensional acceleration method extend to the more complicated three-dimensional method.

Let us express the direction vector, Ω, in spherical coordinates. We consider a right-hand coordinate system with orthogonal unit directions $(\mathbf{i},\mathbf{j},\mathbf{k})$ in the (x,y,z) directions. Then the direction vector, Ω, emanating from the origin is

$$\begin{aligned} \Omega &= \Omega_x\,\mathbf{i} + \Omega_y\,\mathbf{j} + \Omega_z\,\mathbf{k} && (2.14)\\ &= \sin\theta\cos\phi\,\mathbf{i} + \sin\theta\sin\phi\,\mathbf{j} + \cos\theta\,\mathbf{k} && (2.15)\\ &= \sqrt{1-\mu^2}\cos\phi\,\mathbf{i} + \sqrt{1-\mu^2}\sin\phi\,\mathbf{j} + \mu\,\mathbf{k}\ , && (2.16) \end{aligned}$$

where

$$\theta = \text{angle between } \Omega \text{ and } \mathbf{k}\ , \quad (2.17)$$

$$\begin{aligned} \phi &= \text{azimuthal angle} && (2.18)\\ &= \text{angle between } \mathbf{i} \text{ and the projection of } \Omega \text{ onto the } xy \text{ plane}\ , && (2.19) \end{aligned}$$

$$\mu = \cos\theta\ . \quad (2.20)$$

Then, for any function $f(\Omega)=f(\mu,\phi)$, we have that

$$\int_{4\pi} f(\Omega)\,d\Omega = \int_{\phi=0}^{2\pi}\int_{\mu=-1}^{1} f(\mu,\phi)\,d\mu\,d\phi \quad . \tag{2.21}$$

An explicit expression for the monoenergetic scattering cross section is that of linearly anisotropic scattering,

$$\Sigma_s(\mathbf{r},\Omega'\cdot\Omega) = \frac{1}{4\pi}\left(\Sigma_{s0} + 3\Omega\cdot\Omega'\Sigma_{s1}\right) \quad , \tag{2.22}$$

where, for isotropic scattering, $\Sigma_{s1}=0$.

In one-dimensional slab geometry, there is no dependence upon y or z or the azimuthal angle ϕ. Thus, by renormalizing ψ,

$$\psi(x,\mu) \leftarrow \int_{\phi=0}^{2\pi}\psi(x,\mu)\,d\phi = 2\pi\psi(x,\mu) \quad , \tag{2.23}$$

we obtain the monoenergetic, one-dimensional slab geometry transport equation for isotropic scattering:

$$\mu\frac{\partial}{\partial x}\psi(x,\mu) + \Sigma_t(x)\psi(x,\mu) = \frac{1}{2}\int_{-1}^{1}\Sigma_{s0}(x)\psi(x,\mu')\,d\mu' + \frac{Q(x)}{2} \quad , \tag{2.24}$$

where

$$\Sigma_{s0}(x) = \int_{-1}^{1}\Sigma_{s0}(x,\mu')\,d\mu' \quad . \tag{2.25}$$

For a slab of width L, $0\le x\le L$, the boundary conditions specify ψ for incoming directions,

$$\psi(0,\mu) = \psi^{+}(\mu) \ , \ \mu>0 \quad , \tag{2.26}$$

$$\psi(L,\mu) = \psi^{-}(\mu) \ , \ \mu<0 \quad . \tag{2.27}$$

2.1.2 Analytic Criticality Neutron Transport Equation

We obtain the one-group analytic criticality neutron transport equation for isotropic scattering and one-dimensional slab geometry by introducing a fission term

to Equation 2.24:

$$\mu\frac{\partial}{\partial x}\psi(x,\mu)+\Sigma_t(x)\psi(x,\mu)= \frac{1}{2}\Sigma_s(x)\int_{-1}^{1}\psi(x,\mu')\,d\mu'+\frac{1}{2}\frac{\nu\Sigma_f(x)}{k}\int_{-1}^{1}\psi(x,\mu')\,d\mu' \quad , \tag{2.28}$$

where

$$\Sigma_f(x) = \text{fission cross section} \tag{2.29}$$

$$= \text{probability per unit path length that a particle at } x \text{ undergoes a fission} \quad , \tag{2.30}$$

$$\nu = \text{average number of neutrons produced in a fission event} \quad , \tag{2.31}$$

$$k = k_{eff} = k_{effective} \tag{2.32}$$

$$= \text{the multiplication factor} \quad , \tag{2.33}$$

For simplicity, we denote Σ_{s0} as Σ_s. For our criticality calculations, we only consider sources from fission, no external (either interior or incident) sources. Therefore, we have vacuum boundary conditions:

$$\psi(0,\mu)=0 \ , \ \mu>0 \quad , \tag{2.34}$$

$$\psi(L,\mu)=0 \ , \ \mu<0 \quad . \tag{2.35}$$

Since the source depends on ψ, Equation 2.28 defines an eigenvalue problem, where k=k_{eff} is the dominant eigenvalue. k can be viewed as the number by which ν needs to be divided to make the system model critical, that is, where a nuclear chain reaction is just sustainable. It follows that, for $k > 1$, the system model is supercritical and the neutron population would grow in time. For $k < 1$, the system model is subcritical and the neutron population would die out.

2.1.3 Analytic Diffusion Equation

Solving the transport equation is typically difficult. Employing the diffusion approximation in the transport equation yields the diffusion equation, which is simpler

to solve. The diffusion approximation rests on the assumption that the angular flux is linear in angle:

$$\psi(x,\mu) \approx \frac{1}{2}\left(\phi_0(x) + 3\mu\phi_1(x)\right) \quad . \tag{2.36}$$

Here we have defined

$$\phi_n(x) \equiv \int_{-1}^{1} \mu^n \psi(x,\mu) d\mu \quad , \quad n = 0, 1 \quad , \tag{2.37}$$

where $\phi_0(x)$ is the scalar flux, $\phi(x)$. Immediately, we substitute the scalar flux into Equation 2.28 and obtain

$$\mu\frac{\partial}{\partial x}\psi(x,\mu) + \Sigma_t(x)\psi(x,\mu) = \frac{1}{2}\Sigma_s(x)\phi(x) + \frac{1}{2}\frac{\nu\Sigma_f(x)}{k}\phi(x) \quad . \tag{2.38}$$

Now, we take the zeroth angular moment of Equation 2.38 by operating on it by

$$\int_{-1}^{1} (\cdot)\, d\mu \tag{2.39}$$

and obtain

$$\frac{\partial}{\partial x}\phi_1(x) + \Sigma_t(x)\phi_0(x) = \Sigma_s(x)\phi_0(x) + \frac{\nu\Sigma_f(x)}{k}\phi_0(x) \quad . \tag{2.40}$$

Operating on Equation 2.38 by

$$\int_{-1}^{1} \mu(\cdot)\, d\mu \quad , \tag{2.41}$$

we obtain its first angular moment,

$$\frac{\partial}{\partial x}\int_{-1}^{1} \mu^2\psi(x,\mu)\, d\mu + \Sigma_t(x)\phi_1(x) = 0 \quad . \tag{2.42}$$

Substituting the linear approximation of ψ, Equation 2.36, into Equation 2.42, we obtain

$$\frac{1}{3}\frac{\partial}{\partial x}\phi_0(x) + \Sigma_t(x)\phi_1(x) = 0 \quad , \tag{2.43}$$

from which we obtain Fick's Law,

$$\phi_1(x) = -\frac{1}{3\Sigma_t(x)}\frac{\partial}{\partial x}\phi_0(x) \quad . \tag{2.44}$$

Substituting Equation 2.44 into Equation 2.40 and using the identity that the total cross section is the sum of the scattering and absorption cross sections,

$$\Sigma_t(x) = \Sigma_s(x) + \Sigma_a(x) \quad , \tag{2.45}$$

we obtain the diffusion equation:

$$-\frac{\partial}{\partial x}\frac{1}{3\Sigma_t(x)}\frac{\partial}{\partial x}\phi_0(x) + \Sigma_a(x)\phi_0(x) = \frac{\nu\Sigma_f(x)}{k}\phi_0(x) \quad . \tag{2.46}$$

The boundary conditions are obtained by utilizing the linear approximation, Equation 2.36, and the first moment equation, Equation 2.42, and integrating over incoming directions. At the left side,

$$\begin{aligned} 0 &= \int_0^1 \mu\psi(0,\mu)\,d\mu & (2.47)\\ &= \frac{1}{2}\phi_0(0)\int_0^1 \mu\,d\mu + \frac{3}{2}\phi_1(0)\int_0^1 \mu^2\,d\mu & (2.48)\\ &= \frac{1}{4}\phi_0(0) + \frac{1}{2}\phi_1(0) & (2.49)\\ 0 &= \phi_0(0) - \frac{2}{3\Sigma_t(0)}\frac{\partial}{\partial x}\phi_0(0) \quad . & (2.50) \end{aligned}$$

Similarly, on the right side,

$$\begin{aligned} 0 &= \int_{-1}^0 \mu\psi(L,\mu)\,d\mu & (2.51)\\ &= \frac{1}{2}\phi_0(L)\int_{-1}^0 \mu\,d\mu + \frac{3}{2}\phi_1(L)\int_{-1}^0 \mu^2\,d\mu & (2.52)\\ &= -\frac{1}{4}\phi_0(L) + \frac{1}{2}\phi_1(L) & (2.53)\\ 0 &= \phi_0(L) + \frac{2}{3\Sigma_t(L)}\frac{\partial}{\partial x}\phi_0(L) \quad . & (2.54) \end{aligned}$$

These boundary conditions are commonly called the Marshak boundary conditions [Bel70].

Equation 2.46 is the diffusion equation. The diffusion equation and its associated boundary conditions are obtained from the neutron transport equation by assuming that the angular flux is linear in angle. The transport equation is a hyperbolic equation, but the diffusion equation is an elliptic equation. Hyperbolic equations are associated with wave propagation, giving rise to distinctly different domains of dependence and zones of influence for a point in phase phase. Elliptic equations are associated with diffusion processes where, for a phase space point, the domain of dependence is equal to the zone of influence [Hir88]. For example, a localized perturbation in a finite system would be propagated to the rest of the system in finite time by the transport equation, while the diffusion equation would diffuse the effects across the entire system instantaneously.

2.1.4 Analytic Adjoint Transport Equation

The solution of the adjoint transport equation is a valuable tool. Suppose a system of volume V consists of a volume source of neutrons in a nonmultiplying (nonfissioning) medium and a detector located some distance away from the source, as shown in Figure 2.1. In the world of Monte Carlo, where individual particles are simulated, the adjoint calculation is referred to as "running the particles backward from the detector." The adjoint solution is the system-wide importance at each point in phase space for a particle to reach the detector [Bel70]. The three main uses for the adjoint solution are perturbation calculations, Monte Carlo biasing [Lew84], and variational calculations [Bel70]. We briefly present the adjoint equation because we find it is necessary in our acceleration methods.

Given an operator $\mathbf{R}$ and the functions $\psi(x,\mu)$ and $\psi^*(x,\mu)$ that satisfy the necessary boundary and continuity conditions, the adjoint operator $\mathbf{R}^*$ is defined by

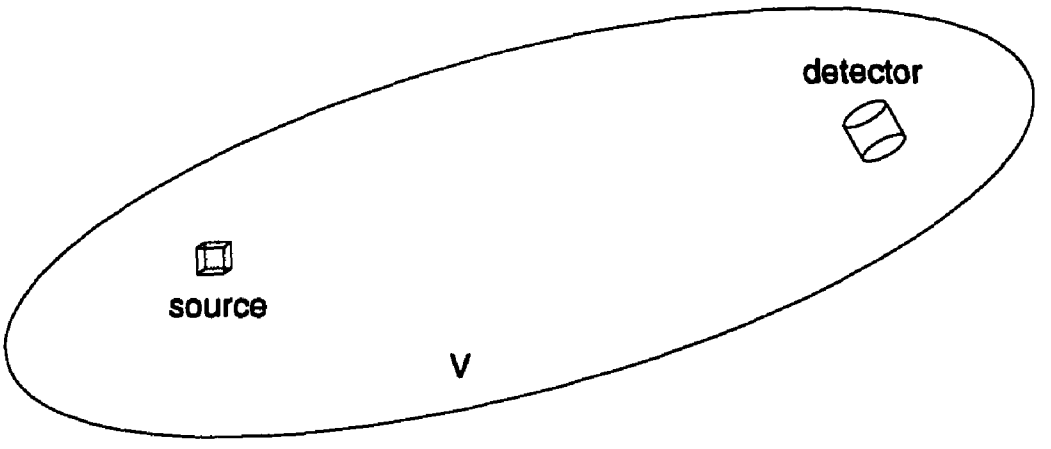

Figure 2.1: Three-dimensional fixed-source system.

the following equation [Lew84][Bel70],

$$(\psi^*, \mathbf{R}\psi) = (\psi, \mathbf{R}^*\psi^*) \quad , \tag{2.55}$$

where $(\cdot, \cdot)$ is the inner product,

$$(\cdot, \cdot) = \int\int (\cdot)(\cdot)\, d\mu\, dx \quad . \tag{2.56}$$

Suppose $\mathbf{R}$ is the criticality transport operator from Equation 2.28:

$$\mathbf{R} = \mathbf{M} - \frac{1}{k}\mathbf{N} \quad , \tag{2.57}$$

where

$$\mathbf{M}\psi(x,\mu) = \mu\frac{\partial}{\partial x}\psi(x,\mu) + \Sigma_t(x)\psi(x,\mu) - \frac{1}{2}\Sigma_s(x)\int_{-1}^{1}\psi(x,\mu')\, d\mu' \quad , \tag{2.58}$$

and

$$\mathbf{N}\psi(x,\mu) = \frac{1}{2}\nu\Sigma_f(x)\int_{-1}^{1}\psi(x,\mu')\, d\mu' \quad . \tag{2.59}$$

Then the criticality transport equation is

$$\mathbf{R}\psi(x,\mu) = 0 \quad , \tag{2.60}$$

which is called the *forward problem* in the adjoint context. Considering the fixed-source part of **R** first, the adjoint of **M** is defined by

$$(\psi^*, \mathbf{M}\psi) = (\psi, \mathbf{M}^*\psi^*) \quad . \tag{2.61}$$

Multiplying **M** by the adjoint angular flux, ψ^*, and taking the inner product, the form of $\mathbf{M}^*$ is found as [Lew84]

$$\mathbf{M}^*\psi^*(x,\mu) = -\mu\frac{\partial}{\partial x}\psi^*(x,\mu) + \Sigma_t(x)\psi^*(x,\mu) - \frac{1}{2}\Sigma_s(x)\int_{-1}^{1}\psi^*(x,\mu')\,d\mu' \quad . \tag{2.62}$$

The difference between the forward operator **M** and its adjoint, $\mathbf{M}^*$, is a negative sign on the streaming term. Similarly, the adjoint of the fission operator **N** is defined by

$$(\psi^*, \mathbf{N}\psi) = (\psi, \mathbf{N}^*\psi^*) \quad , \tag{2.63}$$

where

$$\mathbf{N}^*\psi^*(x,\mu) = \frac{1}{2}\nu\Sigma_f(x)\int_{-1}^{1}\psi^*(x,\mu')\,d\mu' \quad . \tag{2.64}$$

Since $\mathbf{N}=\mathbf{N}^*$, **N** is *self-adjoint.* (When energy dependence is taken into account, the fission operator is not self-adjoint.) The adjoint criticality transport operator is

$$\mathbf{R}^* = \mathbf{M}^* - \frac{1}{k^*}\mathbf{N}^* \quad , \tag{2.65}$$

Utilizing Equations 2.61 and 2.63, we see that, for Equation 2.55 to hold, we must have

$$\left(\frac{1}{k} - \frac{1}{k^*}\right)(\psi^*, \mathbf{N}\psi) = 0 \quad . \tag{2.66}$$

Since the inner product is not zero for positive ψ and ψ^*, the forward and adjoint eigenvalues must be equal,

$$k = k^* \quad . \tag{2.67}$$

We will discover that we need the solution of the adjoint diffusion equation for the Fission Diffusion Synthetic Acceleration method. Without energy dependence, the diffusion operator in Equation 2.46 is self-adjoint. For a system with a non-reentrant vacuum boundary, the adjoint boundary condition is zero for outgoing fluxes. This boundary condition coincides with the physical interpretation of the adjoint flux as the neutron importance. Neutrons escaping the system have zero chance of causing a fission, therefore they have zero importance.

2.2 Numerical Methods for Solving the Neutron Transport Equation

Analytically solving the transport and diffusion equations is possible only for simple, idealized systems. Therefore, people resort to numerical, or computational, methods to solve the equations on a computer. Computational methods are either *deterministic* or *stochastic*.

Deterministic methods typically require discretizing the equations in every independent variable and using finite differencing methods to approximate derivatives of functions. An alternative to finite differencing is the finite element method, but we will not consider that in this thesis. In neutron transport, a popular way to discretize the angular variable is the discrete-ordinates, or S_N, method, where the Gauss-Legendre quadrature set is used to approximate integrals over angle. The main source of error in a deterministic method is the spatial discretization. For finite spatial cells, the discretized equation differs from the analytic equation by a truncation error that should disappear as the spatial cells go to zero.

The Monte Carlo method is a stochastic method. Instead of solving a discretized equation, the Monte Carlo method simulates actual particles. Using pseudo-random

numbers, all events that a particle undergoes are sampled from known probability density functions. The location, energy, and angle of a source particle are sampled from a source distribution. The distance the particle travels to a collision, whether it is absorbed or scatters, and its properties after a scatter are all sampled according to probability density functions. Since Monte Carlo can handle the energy, spatial, and angular variables continuously, it does not suffer from truncation errors. However, since results are obtained by averaging the individual results from many particles, all Monte Carlo solutions have statistical error.

The advantage of the Monte Carlo method is that it is able to model continuous energy, space, and angle in irregular, complicated geometries. The advantage of deterministic methods over Monte Carlo is that they have no statistical errors.

Figure 2.2 qualitatively shows how Monte Carlo and S_N compare. The S_N method considers an infinite number of particles in a finitely resolved system. Monte Carlo considers a finite number of particles in an infinitely resolved system. The "degree of variable resolution" axis could also be, in some sense, "number of collisions." Monte Carlo particles either explicitly or probabilistically experience all of their collisions from birth to death. However, in a discrete-ordinates calculation, the nth iteration on the scattering source produces the nth-collided flux.

2.2.1 Deterministic Methods

By discretizing the independent variables, the integro-differential transport equation is converted to a system of equations amenable to solving on a computer.

Angular Discretization

For discrete-ordinates, or S_N, the angular variable, μ, is divided into bins such that particles only travel in discrete angles. The S_N Gauss-Legendre quadrature set

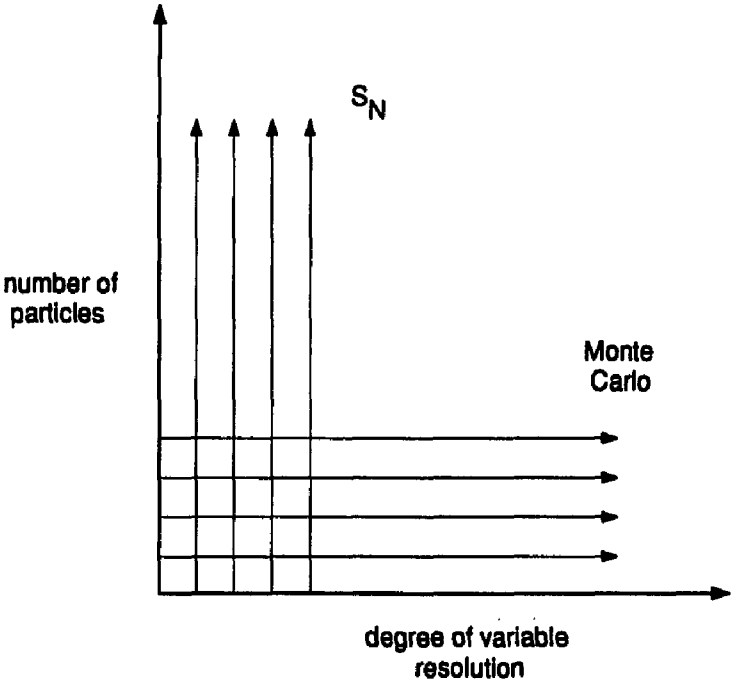

Figure 2.2: A qualitative comparison of discrete-ordinates S_N and Monte Carlo.

defines the discrete angle, μ_m, and weight, w_m, in each bin. (An alternative to S_N quadrature sets is the spherical harmonics, or Legendre polynomial approximations (P_N). The S_N and P_{N-1} equations are equivalent in one-dimensional slab geometry [Lew84].) Integrals over angle are approximated in S_N by summations over the quadrature set:

$$\int_{-1}^{1} \mu \, d\mu \approx \sum_{m=1}^{N} \mu_m \, w_m \quad . \tag{2.68}$$

In one-dimensional geometries, even-order quadrature sets are almost exclusively employed. The even order quadrature sets are symmetric about, but do not include μ=0. They exactly integrate polynomials up to order $2N$-1 [Bel70]. We use the convention that the weights sum to 2:

$$\sum_{m=1}^{N} w_m = 2 \quad . \tag{2.69}$$

Thus, the angular flux is converted from a continuous function to a discrete vector whose N elements at a particular point in space (and energy, if considered) are the angular flux in each discrete angle. So, for $\mu \approx \mu_m$,

$$\psi(x,\mu) \approx \psi_m(x) \equiv \psi(x,\mu_m) \quad . \tag{2.70}$$

The scalar flux, for instance, is approximated as

$$\phi(x) = \int_{-1}^{1} \psi(x,\mu)\, d\mu \tag{2.71}$$

$$\approx \sum_{m=1}^{N} \psi_m(x)\, w_m \quad . \tag{2.72}$$

Spatial Discretization

Spatially, the one-dimensional slab of width L is discretized by dividing it into J cells, as shown in Figure 2.3. The interior cell edges are specified by $x_{j+1/2}$,

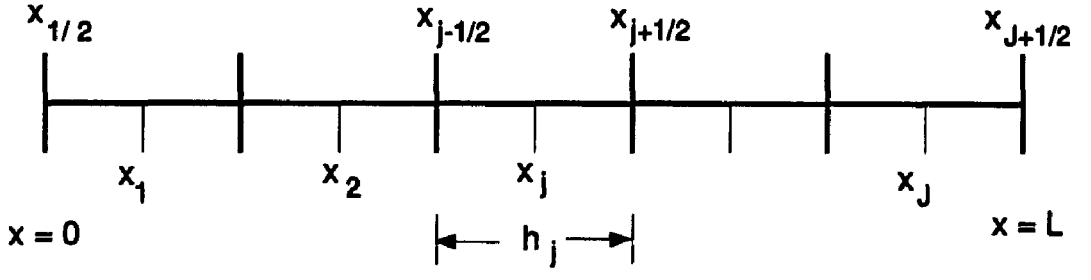

Figure 2.3: Discretized one-dimensional slab geometry.

$1 \leq j \leq J\text{-}1$. The left boundary is denoted by $x_{1/2}$ and the right boundary by $x_{J+1/2}$. The cells have width h_j,

$$h_j = x_{j+1/2} - x_{j-1/2} \quad , \tag{2.73}$$

with the cell center, x_j, located at

$$x_j = \frac{1}{2}\left(x_{j+1/2} + x_{j-1/2}\right) \quad . \tag{2.74}$$

Cross sections and any external fixed-sources in the interior of the system are to be constant across a cell. The spatially discretized angular flux is assumed to reside on the cell edges. The spatially analytic S_N transport equation for a particular direction m is

$$\mu_m \frac{\partial}{\partial x}\psi_m(x) + \Sigma_t(x)\psi_m(x) = \frac{1}{2}\Sigma_s(x)\sum_{n=1}^{N}\psi_n(x)\,w_n + \frac{1}{2}\frac{\nu\Sigma_f(x)}{k}\sum_{n=1}^{N}\psi_n(x)\,w_n \quad . \tag{2.75}$$

Integrating Equation 2.75 over the jth cell or, specifically, operating on it by

$$\frac{1}{h_j}\int_{x_{j-1/2}}^{x_{j+1/2}}(\cdot)\,dx \quad , \tag{2.76}$$

we obtain

$$\frac{\mu_m}{h_j}\left(\psi_{m,j+1/2} - \psi_{m,j-1/2}\right) + \Sigma_{t,j}\psi_{m,j} = \frac{1}{2}\Sigma_{s,j}\sum_{n=1}^{N}\psi_{n,j}\,w_n + \frac{1}{2}\frac{\nu\Sigma_{f,j}}{k}\sum_{n=1}^{N}\psi_{n,j}\,w_n \quad , \tag{2.77}$$

where $1 \leq m \leq N$, $1 \leq j \leq J$, and the cell-averaged angular flux for direction m is

$$\psi_{m,j} = \frac{1}{h_j}\int_{x_{j-1/2}}^{x_{j+1/2}}\psi_m(x)\,dx \quad . \tag{2.78}$$

Differencing Scheme

Equation 2.77, together with specified incoming boundary conditions, constitutes $JN+N$ equations in $2JN+N$ unknowns ($(J+1)N$ cell-edge fluxes and JN cell-average fluxes). The required extra JN equations are auxiliary equations that approximate Equation 2.78 and relate the cell-average flux to the cell-edge flux. A common differencing scheme for the auxiliary equations, and one that we use in this thesis, is the *Diamond Differencing Scheme*,

$$\psi_{m,j} = \frac{1}{2}\left(\psi_{m,j-1/2} + \psi_{m,j+1/2}\right) \quad . \tag{2.79}$$

The Diamond Differencing scheme is second order accurate, but it produces negative fluxes in some cases, and attempts to alleviate the negativity may cause inaccuracies. There are several other differencing schemes. For example, one new differencing scheme that is positive and very accurate is a nonlinear characteristic scheme [Wal95].

Order of Accuracy

In Equation 2.77, the derivative of the angular flux is represented as a finite difference. The finite difference method is based on the definition of the derivative of ψ at x:

$$\frac{d\psi}{dx} = \lim_{\Delta x \to 0} \frac{\psi(x+\Delta x) - \psi(x)}{\Delta x} \quad . \tag{2.80}$$

Representing a derivative as a finite difference is an approximation. The order of the accuracy of the approximation is determined by the power n, when the truncation error goes to zero as $(\Delta x)^n$ [Hir88].

We use Taylor series expansions to show that both the Diamond Differencing Scheme and the centrally differenced approximation to the first derivative of the flux in Equation 2.77 are second order accurate. First, the Diamond Difference scheme, for a particular angle m, is shown to be second order accurate as follows:

$$\begin{aligned}
\psi_j &= \frac{1}{2}\left(\psi_{j-1/2} + \psi_{j+1/2}\right) && (2.81)\\
&= \frac{1}{2}\left(\psi(x_j) - \frac{d\psi(x_j)}{dx}\frac{h}{2} + \frac{d^2\psi(x_j)}{dx^2}\frac{h^2}{8} + \mathcal{O}(h^3)\right. \\
&\quad \left. +\psi(x_j) + \frac{d\psi(x_j)}{dx}\frac{h}{2} + \frac{d^2\psi(x_j)}{dx^2}\frac{h^2}{8} + \mathcal{O}(h^3)\right) && (2.82)\\
&= \psi(x_j) + \mathcal{O}(h^2) \quad , && (2.83)
\end{aligned}$$

where $\mathcal{O}(h^n)$ represents terms of, at most, order h^n. Second, the centrally differenced first derivative of the angular flux is, expanded in Taylor series, also shown to be

second order accurate:

$$\frac{d\psi_j}{dx} = \frac{\psi_{j+1/2} - \psi_{j-1/2}}{h} \tag{2.84}$$

$$= \frac{1}{h}\left(\psi(x_j) + \frac{d\psi(x_j)}{dx}\frac{h}{2} + \frac{d^2\psi(x_j)}{dx^2}\frac{h^2}{8} + \mathcal{O}(h^3)\right.$$

$$\left. -\psi(x_j) + \frac{d\psi(x_j)}{dx}\frac{h}{2} - \frac{d^2\psi(x_j)}{dx^2}\frac{h^2}{8} + \mathcal{O}(h^3)\right) \tag{2.85}$$

$$= \frac{d\psi(x_j)}{dx} + \mathcal{O}(h^2) \quad . \tag{2.86}$$

Fixed-Source Method of Solution

The method of solution for fixed-source, one-dimensional slab geometries is sweeping left to right, considering the left-going angular fluxes separately from the right-going angular fluxes. Equation 2.77 becomes a fixed-source problem if the entire fission source is instead a fixed-source, Q_j, that is constant within each cell:

$$\frac{\mu_m}{h_j}\left(\psi_{m,j+1/2} - \psi_{m,j-1/2}\right) + \Sigma_{t,j}\psi_{m,j}$$

$$= \frac{1}{2}\Sigma_{s,j}\sum_{n=1}^{N}\psi_{n,j}\,w_n + Q_j \quad . \tag{2.87}$$

The procedure is to guess the scalar flux for the scattering source, then lump the scattering source and fixed-source together on the right hand side. Beginning at the left boundary, for instance, a transport sweep is made to the right, one cell at a time, for particles flowing to the right. Equations 2.87 and 2.79 are solved for the exiting flux. Given the incoming flux, the exiting flux from the first cell provides the incoming flux for the next cell. The procedure is repeated for each cell, marching to the right boundary. Then a transport sweep is made from right to left, where the equations are solved for the exiting *left-going* flux. Upon returning to the left boundary, an updated scalar flux is available for each cell. Substituting the updated scalar flux into the scattering source, the transport sweep is performed again. The

whole sweep (back and forth) is repeated until the fluxes converge to within some specified criterion.

Criticality Method of Solution

Solving the discretized criticality transport equation requires more work. Guesses are made for the scattering source as well as for the fission source and the eigenvalue. Just as in the fixed-source solution, the flux is converged for the scattering source. This allows for updating the fission source. Then all the fluxes are normalized to the fission source. Again, the fluxes are converged upon the scattering source, at which time the fission source is updated. Thus, there is a hierarchy of iterations. The iterations that converge the scattering source are called *inner iterations* and those that converge the fission source are called *outer iterations.*

Solving the Discretized Diffusion Equation

For fixed-source problems, solving the discretized diffusion equation is similar to solving the discretized transport equation. However, the resulting equations are not explicitly dependent upon angle like the S_N equations. They form a tridiagonal system that can be explicitly solved by matrix methods, such as Gaussian Elimination, instead of iterating with transport sweeps. For criticality problems, the tridiagonal system must be solved repeatedly until the fission source converges. That is, there are only "outer" iterations in a criticality diffusion calculation. The explicit solving of the tridiagonal matrix replaces the criticality transport "inner" iterations.

2.2.2 Monte Carlo Method

The Monte Carlo Method is based upon an entirely different model than deterministic methods. Instead of solving equations that describe an infinite number of

particles, Monte Carlo simulates enough individual particles to statistically describe the actual number of particles. Typically, thousands or millions of simulated particles represent an actual number of particles on the order of 10^8 to 10^{16}.

The relation between fixed-source and criticality calculations in Monte Carlo is similar to the relation in deterministic calculations. Each "outer iteration" consists of an entire fixed-source calculation.

Sampling from a Probability Density Function

Analog Monte Carlo is conceptually the simplest form of Monte Carlo. Analog Monte Carlo is direct, explicit representation of particles. We consider analog Monte Carlo for a fixed-source calculation. The foundation of Monte Carlo simulation is sampling from probability density functions (pdf). Each event that a particle undergoes is randomly sampled from the appropriate pdf. Therefore, the life of a particle is a sequence of random events.

Suppose a *probability density function* (pdf) is $p(y)$ defined on $a \leq y \leq b$. The pdf must be positive or zero over the interval, so that

$$p(y)\,dy = \text{the probability that } y \text{ lies between } y \text{ and } dy, \tag{2.88}$$

and the pdf is normalized over the range $a \leq y \leq b$,

$$\int_a^b p(y)\,dy = 1 \quad . \tag{2.89}$$

We see then that

$$\int_{y_1}^{y_2} p(y)\,dy = \text{the probability that } y \text{ lies between } y_1 \text{ and } y_2. \tag{2.90}$$

We define the *cumulative distribution function* (cdf), $P(x)$, as

$$P(x) = \int_a^x p(y)\,dy \tag{2.91}$$

$$= \text{the probability that } y \text{ lies between } a \text{ and } x, \tag{2.92}$$

so that

$$P(a) = 0 \quad , \tag{2.93}$$

$$P(b) = 1 \quad . \tag{2.94}$$

Given that we have available a pseudorandom number, ξ, between 0 and 1, we can sample x from the cdf as follows:

$$\xi = P(x) = \int_a^x p(y)\,dy \quad . \tag{2.95}$$

If x is not easily tractable from Equation 2.95, one may need to resort to rejection techniques [Ham64][Car75][Kal86]. Rejection techniques may require many sampled ξ's before an x is found.

The Life of a Monte Carlo Particle

Let us traverse the lifeline of a Monte Carlo fixed-source particle. First, we must sample the source. In one-dimensional slab geometry, suppose the source is isotropic and uniform between x=3.5 and x=7.0 cm. The pdf for its location is

$$p(x) = \frac{1}{6.0 - 3.5} \quad , \quad 3.5 \le x \le 6.0 \quad , \tag{2.96}$$

and the cdf is

$$P(x) = \int_{3.5}^x \frac{1}{6.0 - 3.5}\,dy \tag{2.97}$$

$$= \frac{x - 3.5}{6.0 - 3.5} \quad . \tag{2.98}$$

Drawing a random number, ξ, setting it equal to $P(x)$, and solving for x, we have

$$x = (6.0 - 3.5)\xi + 3.5 \quad . \tag{2.99}$$

We sample its isotropic direction cosine, μ, from a cdf obtained similarly as before

$$\mu = -1 + 2\xi \quad . \tag{2.100}$$

Now that we know the particle's initial location and direction, we must determine how far it will travel to its first (next) collision. In order to determine the pdf for this event, we consider the transport equation without scattering for a particle traveling along the determined direction. We may, with no loss of generality, consider a coordinate system along the direction of travel, and set μ=1. Therefore, we have

$$\frac{d\psi(x)}{dx} + \Sigma_t \psi(x) = 0 \quad , \quad \psi(0) = 1 \quad . \tag{2.101}$$

The solution is

$$\psi(x) = e^{-\Sigma_t x} \quad , \tag{2.102}$$

such that the collision rate, and the pdf, is

$$\Sigma_t \psi(x) = \Sigma_t e^{-\Sigma_t x} \quad . \tag{2.103}$$

The cdf for traveling a distance d is

$$P(d) = \int_0^d \Sigma_t e^{-\Sigma_t x} \, dx \quad . \tag{2.104}$$

Drawing a random number, ξ, setting it equal to $P(d)$, we solve for d, obtaining,

$$d = -\frac{1}{\Sigma_t} \ln(1 - \xi) \quad , \tag{2.105}$$

or, since 1-ξ is distributed equivalently to ξ,

$$d = -\frac{1}{\Sigma_t} \ln(\xi) \quad . \tag{2.106}$$

After transporting the simulated Monte Carlo particle to its collision site, we use the cross sections to determine what happens to the particle. Assume, for simplicity, that we have only absorption and isotropic scattering, so that the total cross section is

$$\Sigma_t = \Sigma_s + \Sigma_a \quad . \tag{2.107}$$

With probability

$$p_s = \frac{\Sigma_s}{\Sigma_t} \quad , \tag{2.108}$$

the particle scatters, and with probability 1-p_s, it is absorbed. The particle continues its random walk until its death, through absorption or leakage out the system.

Implicit capture is a non-analog variance reduction technique that does not allow the particle to be absorbed. Instead, the particles are assigned a weight (initially one) and, at every collision, the weight is reduced, such that only p_s of the weight continues. If the system is highly scattering, the weight may become too low to justify the computer time spent on it. Low weight particles are terminated by an unbiased technique called Russian Roulette [Car75][Spa69].

Obtaining Monte Carlo Results

Information is weaned from the Monte Carlo method by running thousands or millions of particles and accumulating random variable data of interest. For instance, one may be interested in the flux in a region of the system, or the current across a surface, or leakage out a boundary, etc. One may accumulate random variable data, say g_n, for events n=1,...N, where N is large, and build an average:

$$\bar{g} = \frac{1}{N}\sum_{n=1}^{N} g_n \quad , \tag{2.109}$$

where the average is an estimate of the true value g. Suppose the probability density function of g is $f(g)$ and g_i is sampled from $f(g)$. Then $\bar{g}$ is an unbiased estimator of g if its expected value is g [Lew84]:

$$E[\bar{g}] = E[\frac{1}{N}\sum_{n=1}^{N} g_n] \tag{2.110}$$

$$= \frac{1}{N}\sum_{n=1}^{N} E[g_n] \tag{2.111}$$

$$= E[g] \quad , \tag{2.112}$$

where

$$E[g] = \int_{-\infty}^{\infty} g f(g)\, dg \quad , \tag{2.113}$$

and

$$E[g_i] = E[g] \quad , \tag{2.114}$$

since g_n is sampled from $f(g)$.

According to the Central Limit Theorem [Kal86][Spa69][Car75][Lew84], $\bar{g}$ approaches a Gaussian, or normal, distribution, such that we can build a confidence interval from $\bar{g}$. A confidence interval is a range of values that contains, with probability p, the true value:

$$[\bar{g} - t_{p,N-1} s_{\bar{g}} \ , \ \bar{g} + t_{p,N-1} s_{\bar{g}}] \quad , \tag{2.115}$$

where

$$s_{\bar{g}} = \text{estimate of the true standard deviation, } \sigma_{\bar{g}}, \text{ of the mean, and} \tag{2.116}$$

$$t_p = \text{Student's } t\text{-percentile for confidence level } p \text{ and } N\text{-}1 \text{ degrees of freedom.} \tag{2.117}$$

The sample standard deviation of the mean is obtained from the sample standard deviation of the population with the following relation:

$$s_{\bar{g}} = \frac{s_g}{\sqrt{N}} \quad , \tag{2.118}$$

where the sample standard deviation is [Lew84]

$$s_g = \sqrt{\frac{N}{N-1}} \left(\frac{1}{N} \sum_{n=1}^{N} g_n - \bar{g} \right)^{1/2} \quad . \tag{2.119}$$

The Central Limit Theorem states that $\bar{g}$ approaches a normal distribution as $N \to \infty$. However, for finite N, the distribution is not exactly normal. To build confidence

intervals, the departure from a normal distribution is accounted for by the Student's t-percentile [Stu08][Ait57]. The Student's t-percentile multiplies the estimated standard deviation and gives a confidence interval, in Equation 2.115, at the p confidence level and for $N-1$ degrees of freedom.

The collision estimator for the scalar flux in a volume V is

$$\phi_c = \frac{1}{V\Sigma_t}\frac{1}{N}\sum_{n=1}^{N} w_n \quad , \tag{2.120}$$

where w_n is the total collided weight for the nth history. The collision flux estimator is based on the expression for the average number of collisions per unit time in volume V [Lew84]:

$$\bar{c} = V\Sigma_t\phi \quad . \tag{2.121}$$

Monte Carlo Criticality Calculations

Just like in deterministic calculations, Monte Carlo criticality calculations have "outer" iterations, each one consisting of a fixed-source calculation. In Monte Carlo, the outer iterations are called *cycles*. The typical criticality procedure is to make an initial fission source guess and run enough cycles to converge the source. These cycles are called the *inactive cycles*, or settling cycles. The difference between deterministic and Monte Carlo criticality calculations is that once the deterministic source is converged the calculation is finished, whereas, Monte Carlo data accumulation can begin only *after* the Monte Carlo source is converged. The cycles after the source is converged are called *active cycles*. Deciding that the source is converged and active cycles may begin is not an easy, well-defined task. It requires experience, knowledge of the system and quality of the initial source guess, and luck.

During a cycle, the particle tracks determine the initial location of the fission source particles for the next cycle. If, at a collision, a fission event occurs, and a

fission particle is deemed to be born, then its position is banked (stored) until the next cycle. At a collision, the fission weight, based upon the collision flux estimator, is

$$\text{fission weight} = w_n \frac{\nu\Sigma_f}{\Sigma_t} \quad . \tag{2.122}$$

Although there are other ways, the typical method involves dividing the fission weight by the old (currently available) k_{eff}. Thus, at each collision,

$$\gamma = \frac{w_n}{k_{eff}} \frac{\nu\Sigma_f}{\Sigma_t} \tag{2.123}$$

fission source particles are produced for the next cycle. For example, if γ=0.7, a source particle is produced with probability 0.7; or if γ=1.2, one particle is produced with probability 0.8, and two particles are produced with probability 0.2. The result of scaling the fission weight by k_{eff} is that each cycle has roughly the same number of histories. With cycles having the same number of histories, computational difficulties of an increasing (problems with storage) or decaying (no particles!) source are eliminated. However, the estimate of the scaled fission weight is biased, because both the numerator and denominator are random variables, and the ratio of random number averages is not equal to the average of the ratios [Elp85]. The bias is usually insignificant because it is inversely proportional to the number of histories per cycle [Gas75][Bow83][Bri86][Gel90][Gel91][Gel94].

We use three k_{eff} estimators [Lew84]: collision, absorption, and track length. Contributions to the collision estimator are made at every collision, so that the collision k_{eff} estimate at each cycle is

$$k^{\text{collision}} = \sum_{n=1}^{N} \sum_{m_n=1}^{M_n} w_{m_n} \frac{\nu\Sigma_f}{\Sigma_t} \quad , \tag{2.124}$$

where there are N histories in the cycle and M_n collisions in the nth history. Contributions to the absorption estimator are made at every absorption, so that, for N

histories, the cycle absorption k_{eff} estimate is

$$k^{\text{absorption}} = \sum_{n=1}^{N} w_n \frac{\nu\Sigma_f}{\Sigma_a} \quad . \tag{2.125}$$

The cycle track length k_{eff} estimator is accumulated over distances traveled, not at particular points. It is

$$k^{\text{track length}} = \sum_{n=1}^{N} \sum_{m_n=1}^{M_n} \ell_{m_n} w_{m_n} \frac{\nu\Sigma_f}{\Sigma_t} \quad , \tag{2.126}$$

where M_n is the number of track length segments, ℓ_{m_n}, in the nth history. The cycle k_{eff} estimators are averaged over the active cycles to give an average k_{eff} estimate for each estimator type,

$$\bar{k}^{\,\text{type}} = \frac{1}{N} \sum_{n=1}^{N} k^{\text{type}} \quad , \tag{2.127}$$

where "type" is collision, absorption, or track length.

Assuming a limited amount of computer resources, there are optimal values of the number of histories per cycle and number of active cycles. The number of histories per cycle should be large enough to diminish the bias in the k_{eff} estimate, but not so large that only a small number of cycles can be run. Small numbers of cycles may result in large estimated variances in k_{eff}, and, hence, meaningless confidence intervals. Conversely, too many cycles may reduce the estimated variance enough such that the bias is no longer negligible [Gel94].

Determining the number of cycles to skip (the number of inactive cycles) is not a trivial task. It depends on the quality of the initial fission source guess, the dominance ratio of the system, and the computational parameters (and model). Usually, it is difficult to know for sure if the source is converged. Section 2.3 discusses computational difficulties and this thesis addresses accelerating source convergence and decreasing the number of necessary inactive cycles.

2.3 Calculational Difficulties

Monte Carlo criticality calculations sometimes have difficulties that manifest themselves in inaccurate results or unacceptably large computer times to achieve accurate results. These difficulties may originate from the actual physical system being modeled, or from computational situations, or both. In this section, we discuss *sampling* and the *dominance ratio* of the system. Generally, if a problem is inadequately sampled, or if the dominance ratio is close to unity, there will be computational difficulties. The discussion regarding the dominance ratio applies equally to deterministic criticality calculations.

2.3.1 Sampling Difficulties

When parts of phase space are not sampled adequately, the solution is likely to be inaccurate. Such an inaccuracy is considered a *bias* due to an improper model. The best example of this sampling difficulty is G. Elliott Whitesides' "k_{eff} of the world" problem [Whi71]. Whitesides used a Monte Carlo code to obtain k_{eff} for a $9 \times 9 \times 9$ array of plutonium spheres. All the spheres were identical with radii of about 4 cm and separated by 60 cm. The entire array was surrounded by a water reflector. This array is a loosely-coupled, subcritical system with $k_{eff} \approx 0.93$. Whitesides found k_{eff} as about 0.93 with 300 histories per cycle. He undoubtedly did not obtain the correct fission source shape, because the spheres are very independent and there were not even enough histories per cycle to have one particle in each sphere! However, since this problem is similar to a homogeneous, infinite medium, the value of k_{eff} is not highly dependent upon where the particles are located. When there is little communication between the spheres, the k_{eff} of the system is about the k_{eff} of an individual sphere. Indeed, Whitesides obtained the correct k_{eff}.

However, when Whitesides replaced the center sphere of the model with a larger, critical sphere, he obtained what he called the "k_{eff} of the world" problem. The name comes from the fact that the world is about critical since it has critical reactors, but if you were not near a critical reactor, it would be difficult to calculate the critical k_{eff}. After 200 active cycles [Dic76], his Monte Carlo estimate of k_{eff} was about the same as before. With so few particles, the hot center sphere was not detected. In this problem, the fission source shape is very important. It is highly peaked at the hot center sphere–very different from a typical initial flat source guess. Once the particles can "see" the hot center sphere, the Monte Carlo k_{eff} estimate begins drifting upward toward unity. In addition to the poor sampling in this problem, the system has a high dominance ratio, resulting in slow convergence.

2.3.2 Dominance Ratio

The *dominance ratio* is the ratio of the second highest eigenvalue to the dominant eigenvalue, k_{eff}. In a source (or power) iteration method, the dominance ratio dictates the rate of the slowest error decay, that of the lowest order error mode. When the dominance ratio is near one, the low order error decays very slowly, thus requiring many iterations for convergence.

Rate of Convergence for High Dominance Ratios

To demonstrate the relevance of the dominance ratio in source iteration, we investigate its effect on the rate of convergence. We consider the transport equation,

$$\mathbf{T}\psi \;=\; \mathbf{S}\psi + \frac{1}{k}\chi\mathbf{F}\psi \quad , \tag{2.128}$$

where

$$\mathbf{T}\psi = \mathbf{\Omega}\cdot\nabla\psi(\mathbf{r},E,\mathbf{\Omega}) + \sigma_t(\mathbf{r},E)\psi(\mathbf{r},E,\mathbf{\Omega}) \quad , \tag{2.129}$$

$$\mathbf{S}\psi = \int\int \sigma_s(\mathbf{r},\mathbf{\Omega}'\cdot\mathbf{\Omega},E'\rightarrow E)\psi(\mathbf{r},E',\mathbf{\Omega}')\,d\mathbf{\Omega}'\,dE' \quad , \tag{2.130}$$

$$\mathbf{F}\psi = \int\int \nu\sigma_f(\mathbf{r},E')\psi(\mathbf{r},E',\mathbf{\Omega}')\,d\mathbf{\Omega}'\,dE' \quad . \tag{2.131}$$

We manipulate Equation 2.128 as follows,

$$(\mathbf{T}-\mathbf{S})\psi = \frac{1}{k}\chi\mathbf{F}\psi \tag{2.132}$$

$$\psi = \frac{1}{k}(\mathbf{T}-\mathbf{S})^{-1}\chi\mathbf{F}\psi \quad , \tag{2.133}$$

and we operate on both sides by $\mathbf{F}$, obtaining an analytic integral transport equation,

$$\mathbf{F}\psi = \frac{1}{k}\mathbf{F}(\mathbf{T}-\mathbf{S})^{-1}\chi\mathbf{F}\psi \quad . \tag{2.134}$$

Equivalently,

$$f = \frac{1}{k}\mathbf{L}f \quad , \tag{2.135}$$

where

$$f = f(\mathbf{r}) = \mathbf{F}\psi = \text{fission source} \quad , \tag{2.136}$$

$$\mathbf{L} = \mathbf{F}(\mathbf{T}-\mathbf{S})^{-1}\chi = \text{integral fission operator} \quad . \tag{2.137}$$

The integral fission operator is represented in discrete space by the fission matrix $\hat{\mathbf{L}}$.

The *Source Iteration* method is represented by introducing iteration indices to Equation 2.135,

$$f^{(i+1/2)} = \frac{1}{k^{(i)}}\mathbf{L}f^{(i)} \quad , \tag{2.138}$$

$$f^{(i+1)} = f^{(i+1/2)} \quad , \tag{2.139}$$

$$k^{(i+1)} = \frac{\int \mathbf{L}f^{(i)}dr}{\int f^{(i)}dr} = k^{(i)}\frac{\int f^{(i+1/2)}dr}{\int f^{(i)}dr} \quad . \tag{2.140}$$

This satisfies

$$f^{(n)} = \prod_{i=0}^{n-1} \frac{1}{k^{(i)}} \mathbf{L}^n f^{(0)} \quad . \tag{2.141}$$

The integral fission operator $\mathbf{L}$ has distinct eigenvalue solutions,

$$f_m = \frac{1}{k_m} \mathbf{L} f_m \quad , \quad k = k_1 > k_2 > k_3 > \cdots \quad . \tag{2.142}$$

Suppose the initial source guess for the source iteration, Equations 2.138 to 2.140, is a linear combination of the distinct solution eigenvectors [Lew84],

$$f^{(0)} = \sum_{\ell} \alpha_\ell f_\ell \quad . \tag{2.143}$$

Then, from Equation 2.142,

$$\mathbf{L}^n f^{(0)} = \sum_{\ell} \alpha_\ell k_\ell^n f_\ell = \alpha_1 k_1^n f_1 + \alpha_2 k_2^n f_2 + \sum_{\ell>2} \alpha_\ell k_\ell^n f_\ell \quad . \tag{2.144}$$

We see see that as $n \rightarrow \infty$, $k^{(n)}$ converges to the dominant eigenvalue,

$$k^{(n+1)} = \frac{\int (\alpha_1 k_1^{n+1} f_1 + \sum_{\ell>1} \alpha_\ell k_\ell^{n+1} f_\ell) dr}{\int (\alpha_1 k_1^n f_1 + \sum_{\ell>1} \alpha_\ell k_\ell^n f_\ell) dr} \tag{2.145}$$

$$= \frac{k_1^{n+1} \int \left(\alpha_1 f_1 + \sum_{\ell>1} \alpha_\ell \left(\frac{k_\ell}{k_1} \right)^{n+1} f_\ell \right) dr}{k_1^n \int \left(\alpha_1 f_1 + \sum_{\ell>1} \alpha_\ell \left(\frac{k_\ell}{k_1} \right)^{n} f_\ell \right) dr} \tag{2.146}$$

$$\rightarrow k_1 \text{ as } n \rightarrow \infty \quad . \tag{2.147}$$

Also, the fission source converges to the dominant eigenfunction,

$$\left(\frac{1}{k_1} \mathbf{L} \right)^n f^{(0)} = \alpha_1 f_1 + \alpha_2 (\rho)^n f_2 + \sum_{\ell>2} \alpha_\ell \left(\frac{k_\ell}{k_1} \right)^n f_\ell \tag{2.148}$$

$$\rightarrow \alpha_1 f_1 \text{ as } n \rightarrow \infty \quad , \tag{2.149}$$

where

$$\rho = \frac{k_2}{k_1} \tag{2.150}$$

is the *dominance ratio.* Reducing an error of order 1 in Equation 2.148 to order $\epsilon \ll 1$ requires

$$N = \frac{\log \epsilon}{\log \rho} \tag{2.151}$$

iterations. For example, reducing an error by three orders of magnitude in a system with dominance ratio 0.99 requires 688 iterations.

False Convergence

With a dominance ratio near unity, the source iteration method converges so slowly that it may appear to be converged, when in fact it really is not. A typical measure of convergence is the vector norm–say the ℓ_∞ norm, the maximum value–of the difference between two successive fission source iterates. Then, from Equations 2.148 and 2.149, the *apparent error* at iteration n, a_n, is

$$a_n = f^{(n)} - f^{(n-1)} \tag{2.152}$$

$$= \rho^{n-1}(\rho - 1)\alpha_2 f_2 + \sum_{\ell>2} \left[\left(\frac{k_\ell}{k_1}\right)^{(n)} - \left(\frac{k_\ell}{k_1}\right)^{(n-1)} \right] \alpha_\ell f_\ell \quad , \tag{2.153}$$

whereas the *real error* at iteration n, r_n, is

$$r_n = \alpha_1 f_1 - f^{(n)} = -\rho^n \alpha_2 f_2 - \sum_{\ell>2} \left(\frac{k_\ell}{k_1}\right)^n \alpha_\ell f_\ell \quad . \tag{2.154}$$

Considering only the leading terms of r_n and a_n and taking the vector norms, we see that, for dominance ratios near unity, the real error may be significantly greater than the apparent error:

$$\frac{||r_n||}{||a_n||} = \frac{\rho}{1-\rho} \gg 1 \qquad \text{for} \quad 1 - \rho \ll 1 \quad . \tag{2.155}$$

Two types of systems that tend to have dominance ratios near unity are large thermal nuclear reactors and isolated arrays of barrels of nuclear waste. We shall demonstrate how the dominance ratio approaches unity as a reactor becomes larger, and as elements of an array are increasingly separated.

Large Thermal Reactors

The dominance ratio is an indicator of the neutron communication between distant regions of the systems: the higher the dominance ratio, the weaker the communication. In general geometry, the diffusion equation for a homogeneous multiplying medium, V, with zero scalar flux at the extrapolated boundary δV is

$$-D \bigtriangledown^2 \phi(\mathbf{r}) + \Sigma_a \phi(\mathbf{r}) = \frac{\nu \Sigma_f}{k} \phi(\mathbf{r}) \ , \ \mathbf{r} \in V \ , \tag{2.156}$$

$$\phi(\mathbf{r}) = 0 \ , \ \mathbf{r} \in \delta V \ , \tag{2.157}$$

where

$$D = \frac{1}{3\Sigma_{tr}} = \text{diffusion coefficient} \ , \tag{2.158}$$

$$\Sigma_{tr} = \Sigma_t - \bar{\mu}_0 \Sigma_s = \text{macroscopic transport cross section} \ , \tag{2.159}$$

$$\bar{\mu}_0 = \text{average scattering angle cosine} \ . \tag{2.160}$$

Let us consider, as a solution of Equation 2.156, the solution $\psi_n(\mathbf{r})$ of the homogeneous differential equation [Dud76]

$$\bigtriangledown^2 \psi_n(\mathbf{r}) + B_n^2 \psi_n(\mathbf{r}) = 0 \ , \ \mathbf{r} \in V \ , \tag{2.161}$$

$$\psi_n(\mathbf{r}) = 0 \ , \ \mathbf{r} \in \delta V \ , \tag{2.162}$$

where the eigenvalues are arranged as $B_1 < B_2 < B_3 < \cdots$, and the eigenvectors are orthonormal:

$$\int \psi_n(\mathbf{r}) \psi_m(\mathbf{r}) d^3r = \delta_{nm} \ . \tag{2.163}$$

Comparing Equations 2.162 and 2.157, we observe that $\psi_n(\mathbf{r})$ satisfies the boundary condition of the diffusion equation, Equation 2.156, and, upon substitution, becomes

$$-D \bigtriangledown^2 \psi_n(\mathbf{r}) + \Sigma_a \psi_n(\mathbf{r}) = \frac{\nu \Sigma_f}{k_n} \psi_n(\mathbf{r}) \ . \tag{2.164}$$

From Equation 2.161, we see that

$$-D\nabla^2\psi_n(\mathbf{r}) = DB_n^2\psi_n(\mathbf{r}) \quad , \tag{2.165}$$

so Equation 2.164 becomes

$$DB_n^2\psi_n(\mathbf{r}) + \Sigma_a\psi_n(\mathbf{r}) = \frac{\nu\Sigma_f}{k_n}\psi_n(\mathbf{r}) \quad . \tag{2.166}$$

From Equation 2.166 we have that the k-eigenvalues are

$$k_n = \frac{\nu\Sigma_f}{DB_n^2 + \Sigma_a} \quad . \tag{2.167}$$

The two largest k_n's occur for the two smallest bucklings, B_n^2 (the eigenvalues of the homogeneous differential equation). Therefore, the dominance ratio ρ is

$$\rho = \frac{k_2}{k_1} = \frac{\Sigma_a + DB_1^2}{\Sigma_a + DB_2^2} \quad . \tag{2.168}$$

For a one-dimensional homogeneous slab of extrapolated width L, the eigenfunctions of the homogeneous differential equation are [Dud76]

$$\psi_n(x) = \cos B_n x \quad , \tag{2.169}$$

with corresponding eigenvalues

$$B_n^2 = \left(\frac{n\pi}{L}\right)^2 \quad . \tag{2.170}$$

Substituting these homogeneous equation eigenvalues (bucklings) into the general geometry expression for the dominance ratio, Equation 2.168, we obtain

$$\rho = \frac{\Sigma_a + D\left(\frac{\pi}{L}\right)^2}{\Sigma_a + D\left(\frac{2\pi}{L}\right)^2} = \frac{L^2\Sigma_a + D\pi^2}{L^2\Sigma_a + D4\pi^2} \quad . \tag{2.171}$$

Suppose $\Sigma_t = 1.0$, $\Sigma_a = 0.7$ (including fission), $\Sigma_s = 0.3$ (isotropic scattering), and $\nu\Sigma_f = 0.8$. Then Figure 2.4 shows, as the slab width increases, how k_{eff} increases toward k_∞ and how the dominance ratio asymptotically increases toward unity.

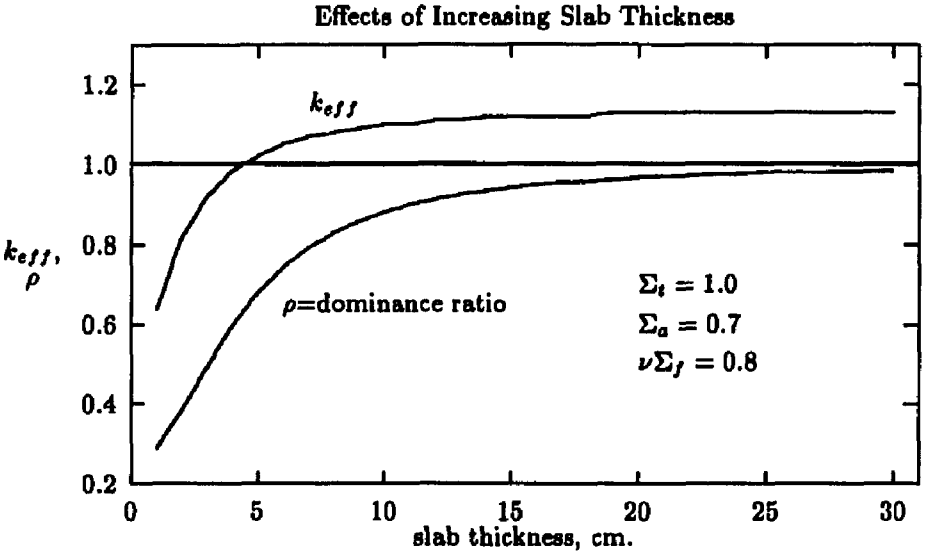

Figure 2.4: Diffusion theory expressions of the dominance ratio and k_{eff} show how k_{eff} approaches k_∞ and how the dominance ratio approaches unity as the homogeneous slab width increases.

Arrays of Isolated Fissionable Materials

Another type of system that typically has a dominance ratio near unity is an array of components, such as separated cans of nuclear waste. Using a one-dimensional discrete ordinates code, we consider the effects of increasingly separating array components on the dominance ratio. Consider two identical 2 cm slabs of fissionable material, each with $\Sigma_t = 1.0$, $\Sigma_s = 0.7$ (isotropic scattering), and $\nu\Sigma_f = 0.8$. Figure 2.5 shows that as the slabs are separated by an increasing width of scattering material, communication weakens, the dominance ratio approaches unity, and (in this case) k_{eff} decreases. The very high dominance ratio problems proved to be difficult for the code. When the dominance ratio is near one, the first and second eigenvalues are nearly the same. In this case, the first two eigenstates become less distinct, and the code may try to converge to some linear combination of the first two eigenstates.

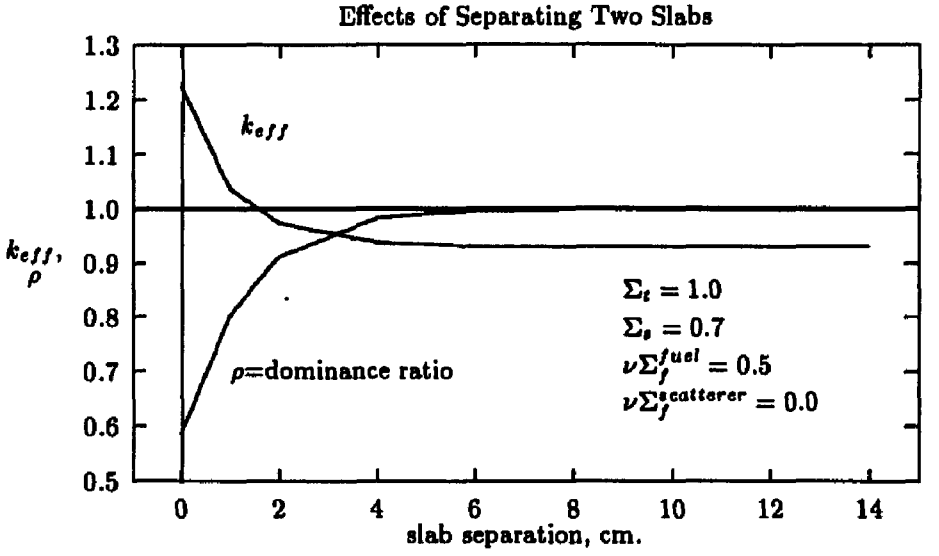

Figure 2.5: Several deterministic discrete-ordinates calculations show that as two slabs are separated by an increasing width of scattering material, k_{eff} approaches that of a single slab and the dominance ratio approaches unity.

2.4 The Fission Matrix

The fission matrix, $\hat{\mathbf{L}}$, may be estimated in different ways, for instance, by a Monte Carlo calculation, a set of diffusion calculations, or a set of discrete-ordinates transport calculations.

A fission matrix obtained from a Monte Carlo calculation is merely a matter of bookkeeping. When a fission source particle is born, its cell of origin is logged, say, cell j. After transport, suppose this particle produces a subsequent fission source particle in cell i. This production would be accumulated for element (i,j). After all the particles in the cycle are completed, each element is divided by the source in cell j, such that each element (i,j) is the probability that a particle born in cell j produces a subsequent fission source particle in cell i,

$$\hat{\mathbf{L}}_{ij} = \frac{\text{fission weight produced in } i \text{ due to a source in } j}{\text{source in } j} \quad . \tag{2.172}$$

The numerator of $\hat{\mathbf{L}}_{ij}$ does not directly contain source normalization. It is the fission weight from which source neutrons are sampled, not the actual simulated particles. Therefore, an element (i,j) of the fission matrix may have a nonzero contribution, but because of sampling, no simulated fission neutrons are actually produced in cell i. The fission weight is equivalent to the incremental contributions made to the k_{eff} estimator. Succinctly, then, the numerators of the fission matrix elements are the k_{eff} estimates in cell i due to a particle originating in cell j. Thus, we may have as many different types of fission matrices as we have k_{eff} estimator types. We may have a collision fission matrix, an absorption fission matrix, and a track length fission matrix.

Accumulating Monte Carlo data for a single cycle produces a *cycle fission matrix.* From the cycle fission matrix comes the dominant cycle eigenvector and cycle eigenvalue. One may obtain an average cycle eigenvalue over many cycles. The problem with the cycle fission matrix is that it is based only upon the number of histories per cycle. The number of histories per cycle may be enough for the M cells in the modeled system, but not enough for good statistics in the M^2 elements of the fission matrix. Additionally, the bias in the fission matrix elements, and hence the eigenvalue, is more prevalent when the number of histories is small. The bias is a manifestation of each fission matrix element being the ratio of the average of the numerator and the average of the denominator. Generally, the average of a ratio is not equal to the ratio of the average numerator to the average denominator [Elp85]. Experience has shown that this bias is usually positive, that is, the cycle fission matrix dominant eigenvalue is higher than the true eigenvalue.

The *cumulative fission matrix* diminishes the bias in its elements more so than does the cycle fission matrix. Instead of accumulating numerator and denominator

data over just a single cycle, the data are accumulated over all the cycles up to that point. The better statistics in the numerator and denominator result in reduced bias in the fission matrix elements. Even if the fission source is not converged, the data accumulated for the fission matrix is expected to be accurate since the fission matrix elements are probabilities. The validity of this statement is diminished when the fission source is not adequately sampled. The disadvantage of the eigenvalue of the cumulative fission matrix is that it is difficult to estimate its error in a simple, traditional manner. Eigenvalues from successive cycles are not independent. An attempt to propagate the errors through the source iteration determination of the dominant eigenstate seem cumbersome. However, some propagated error estimates have been proposed [Kap58].

The fission matrix is also deterministically obtainable. Instead of bookkeeping, though, this approach requires a separate fixed source calculation for each cell in the system. For a single calculation, a unit source is placed in one cell. If the calculation is a cell-edge diffusion calculation, it may require distributing the source between two cell-edges. Upon completion, there is a system-wide response to that unit source in the one cell. Scaled by the fission cross section, this response provides one column of the fission matrix. Then the calculation is repeated for each cell in the system. In this thesis, we use diffusion calculations instead of discrete-ordinates transport calculations, because our ultimate intended use is acceleration and the diffusion calculations are faster. Also, in practice, most criticality problems tend to have fairly isotropic scattering.

Because the fission matrix resides on a spatially discretized system, it suffers from a discretization error. For example, with vacuum boundary conditions, the fission matrix's flat fission source in the boundary cell overestimates the leakage. Therefore,

the eigenvalue of the fission matrix is not equal to the true eigenvalue.

CHAPTER III

Fourier Analysis and Damped Acceleration

3.1 Motivation

A Fourier Analysis is a way to determine the stability and speed of convergence of an iteration method. If the error for any particular mode, or frequency, grows with each iteration, the method is unstable. The rate at which the most dominant error mode decays gives the speed of convergence. The analysis requires an infinite, homogeneous medium and is only applicable to a linear method.

We will find that our fission source acceleration methods are unstable, or highly oscillatory, if the full additive correction is made at each cycle or iteration. Thus we damp the additive correction, adding only a portion of it. Unfortunately, since criticality calculations are nonlinear, we do not have the luxury of using a Fourier analysis to see the stabilizing effects of damping. Instead, we turn to fixed source acceleration methods, namely Diffusion Synthetic Acceleration (DSA). If the DSA method is discretized in an "inconsistent" way, it may suffer instabilities [Ree71]. We will show that *damping* the DSA additive correction can alleviate these instabilities. The discretization that causes the DSA instabilities is similar to the discretization we are forced to use in Monte Carlo fission source convergence acceleration. Therefore, we use the DSA results as a theoretical foundation for damping the Monte Carlo

fission source acceleration correction.

3.2 Transport Equation

The fixed-source, monoenergetic transport equation with isotropic scattering in one-dimensional homogeneous slab geometry is

$$\mu\frac{\partial\psi(x,\mu)}{\partial x}+\Sigma_t\psi(x,\mu)=\frac{1}{2}\Sigma_s\phi(x)+\frac{1}{2}Q(x) \quad , \tag{3.1}$$

where $\phi(x)$ is the scalar flux. Since the Fourier Analysis requires an infinite, homogeneous medium, we will not concern ourselves with boundary conditions.

3.3 Source Iteration

The Source Iteration method comes from introducing iteration indices to Equation 3.1. Its two steps are

$$\mu\frac{\partial}{\partial x}\psi^{(\ell+1/2)}(x,\mu)+\Sigma_t\psi^{(\ell+1/2)}(x,\mu)=\frac{1}{2}\Sigma_s\phi^{(\ell)}(x)+\frac{1}{2}Q(x) \quad , \tag{3.2}$$

$$\phi^{(\ell+1)}(x)=\phi^{(\ell+1/2)}(x)\equiv\int_{-1}^{1}\psi^{(\ell+1/2)}(x,\mu)d\mu \quad , \tag{3.3}$$

We want to Fourier-analyze the errors in the Source Iteration method. Denoting the error $E(x,\mu)$ as the difference between the ψ of successive iterations,

$$E^{(\ell+1/2)}(x,\mu)=\psi^{(\ell+1/2)}(x,\mu)-\psi^{(\ell-1/2)}(x,\mu) \quad , \tag{3.4}$$

and subtracting Equation 3.2 at iteration ℓ-1/2 from Equation 3.2 at iteration ℓ+1/2, we obtain

$$\mu\frac{\partial}{\partial x}E^{(\ell+1/2)}(x,\mu)+\Sigma_tE^{(\ell+1/2)}(x,\mu)=\frac{1}{2}\Sigma_s\int_{-1}^{1}E^{(\ell-1/2)}(x,\mu) \quad , \tag{3.5}$$

where we have assumed constant cross sections. Equation 3.5 tells us that we may interpret ψ and ϕ in Equation 3.2 and 3.3 as the iteration errors so long as

$$Q(x)=0 \quad . \tag{3.6}$$

Recognizing that $e^{i\lambda x}$ is the eigenfunction of the errors and ω the eigenvalue, we introduce into Equations 3.2 and 3.3 the following Fourier separation of variables ansatz

$$Q(x) = 0 \quad , \tag{3.7}$$

$$\phi^{(\ell)} = \omega^{\ell} e^{i\lambda x} \quad , \tag{3.8}$$

$$\psi^{(\ell+1/2)} = \omega^{\ell} a(\mu) e^{i\lambda x} \quad , \tag{3.9}$$

and obtain

$$a(\mu) = \frac{\Sigma_s}{2(\Sigma_t + i\lambda\mu)} \quad , \tag{3.10}$$

$$\omega = \int_{-1}^{1} a(\mu)\, d\mu \quad . \tag{3.11}$$

Substituting Equation 3.10 into 3.11, multiplying and dividing by the complex conjugate, and dividing numerator and denominator by Σ_t^2, we obtain an expression for the eigenvalue ω of the method,

$$\omega = \int_{-1}^{1} \frac{\Sigma_s}{2(\Sigma_t + i\lambda\mu)}\, d\mu = \int_{-1}^{1} \frac{\Sigma_s(\Sigma_t - i\mu\lambda)}{2(\Sigma_t^2 + \mu^2\lambda^2)}\, d\mu \tag{3.12}$$

$$= \frac{c}{2} \int_{-1}^{1} \frac{d\mu}{1 + \mu^2\lambda^2} \quad , \tag{3.13}$$

where λ is in units of cm^{-1} in Equation 3.12 and, in Equation 3.13, λ is in units of mfp^{-1} and

$$c = \frac{\Sigma_s}{\Sigma_t} = \text{scattering ratio} \quad . \tag{3.14}$$

The maximum eigenvalue, called the *spectral radius*, of the method measures the decay (or growth) of the dominant error mode. A spectral radius greater than unity implies error growth, or instability, and a spectral radius less than unity dictates the slowest error decay. For Source Iteration,

$$\sup_{\lambda} |\omega| = c \quad , \tag{3.15}$$

so it is stable since $c \leq 1$, but extremely slow for c near 1 and $\lambda \approx 0$.

3.4 Diffusion Synthetic Acceleration

The idea behind the Diffusion Synthetic Acceleration (DSA) Method is to calculate an approximation to the exact correction to the angular flux at each iteration. To that end, the exact correction at iteration ℓ is

$$g^{(\ell+1)}(x,\mu) = \psi(x,\mu) - \psi^{(\ell+1/2)}(x,\mu) \quad , \tag{3.16}$$

where $\psi(x,\mu)$ is the exact angular flux satisfying the transport equation in a homogeneous medium,

$$\mu\frac{\partial}{\partial x}\psi(x,\mu) + \Sigma_t\psi(x,\mu) = \frac{1}{2}\Sigma_s\phi(x) + \frac{1}{2}Q(x) \quad , \tag{3.17}$$

$$\phi(x) = \int_{-1}^{1}\psi(x,\mu)d\mu \quad . \tag{3.18}$$

Subtracting Equation 3.2 from Equation 3.17 yields an equation for the exact correction,

$$\mu\frac{\partial}{\partial x}g^{(\ell+1)}(x,\mu) + \Sigma_t g^{(\ell+1)}(x,\mu) - \frac{1}{2}\Sigma_s\int_{-1}^{1} g^{(\ell+1)}(x,\mu)d\mu = \frac{1}{2}\Sigma_s\left(\phi^{(\ell+1/2)}(x) - \phi^{(\ell)}(x)\right) \quad , \tag{3.19}$$

where

$$\phi^{(\ell+1/2)}(x) = \int_{-1}^{1}\psi^{(\ell+1/2)}(x,\mu)d\mu \quad . \tag{3.20}$$

Solving Equation 3.19 for $g^{(\ell+1)}(x,\mu)$ and adding it to the most recent angular flux results in the exact angular flux:

$$\psi(x,\mu) = \psi^{(\ell+1/2)}(x,\mu) + g^{(\ell+1)}(x,\mu) \quad , \tag{3.21}$$

and the calculation is finished. Unfortunately, Equation 3.19 is just as difficult to solve as the original Source Iteration problem, Equation 3.2. Therefore, we take the

diffusion approximation of Equation 3.19. First, we define

$$f_n^{(\ell+1)}(x) \equiv \int_{-1}^{1} \mu^n g^{(\ell+1)}(x,\mu)d\mu \tag{3.22}$$

and assume that the exact correction is linear in angle,

$$g^{(\ell+1)}(x,\mu) \approx \frac{1}{2}\left(f_0^{(\ell+1)}(x) + 3\mu f_1^{(\ell+1)}(x)\right) \quad . \tag{3.23}$$

Operating on Equation 3.19 by

$$\int_{-1}^{1}(\cdot)d\mu \tag{3.24}$$

and

$$\int_{-1}^{1}\mu(\cdot)d\mu \quad , \tag{3.25}$$

we obtain

$$\begin{aligned}\frac{\partial}{\partial x}f_1^{(\ell+1)}(x) + \Sigma_t f_0^{(\ell+1)}(x) - \Sigma_s f_0^{(\ell+1)}(x) \\ = \Sigma_s\left(\phi^{(\ell+1/2)}(x) - \phi^{(\ell)}(x)\right) \quad ,\end{aligned} \tag{3.26}$$

and

$$\frac{\partial}{\partial x}\int_{-1}^{1}\mu^2 g^{(\ell+1)}(x,\mu)d\mu + \Sigma_t f_1^{(\ell+1)}(x) = 0 \quad . \tag{3.27}$$

Using the linear approximation of g, Equation 3.23, in Equation 3.27 produces an expression for f_1,

$$f_1^{(\ell+1)}(x) = -\frac{1}{3\Sigma_t}\frac{\partial}{\partial x}f_0^{(\ell+1)}(x) \quad , \tag{3.28}$$

which, when substituted into Equation 3.26, yields the diffusion approximation to Equation 3.19, the acceleration equation,

$$\begin{aligned}-\frac{\partial}{\partial x}\frac{1}{3\Sigma_t}\frac{\partial}{\partial x}f_0^{(\ell+1)}(x) + \Sigma_a f_0^{(\ell+1)}(x) \\ = \Sigma_s\left(\phi^{(\ell+1/2)}(x) - \phi^{(\ell)}(x)\right) \quad .\end{aligned} \tag{3.29}$$

The DSA method, without considering boundary conditions, consists of a transport source iteration, Equation 3.2; calculating the most recent scalar flux,

$$\phi^{(\ell+1/2)}(x) = \int_{-1}^{1} \psi^{(\ell+1/2)}(x,\mu)d\mu \quad ; \tag{3.30}$$

calculating the correction from Equation 3.29; then applying it to the most recent scalar flux

$$\phi^{(\ell+1)}(x) = \phi^{(\ell+1/2)}(x) + f_0^{(\ell+1)} \quad ; \tag{3.31}$$

and continuing this sequence until convergence.

As was performed for the Source Iteration method, we may Fourier analyze the DSA method (assuming constant cross sections) and obtain [Lar84]

$$\omega = \left[\frac{c\lambda^2}{\lambda^2 + 3(1-c)}\right] \int_{-1}^{1} \frac{P_2(\mu)}{1+\lambda^2\mu^2} d\mu \tag{3.32}$$

$$= \left[\frac{\Sigma_s\lambda^2}{\Sigma_t\lambda^2 + 3\Sigma_a}\right] \int_{-1}^{1} \frac{P_2(\mu)}{1+\lambda^2\mu^2} d\mu \quad . \tag{3.33}$$

Here $P_2(\mu)$ is the second Legendre polynomial,

$$P_2(\mu) = \frac{3\mu^2 - 1}{2} \quad . \tag{3.34}$$

The spectral radius of the DSA method is less than or equal to $0.2247c$ [Lar84], so it is stable and converges for all c. The eigenvalues of both the Source Iteration and DSA methods are shown in Figure 3.1. One can see that DSA entirely removes the low order ($\lambda = 0$) error modes. These are the modes with which Source Iteration has the most difficulty. Additionally, the DSA eigenvalue is always less than the Source Iteration eigenvalue for all ω, so DSA will always converge faster.

3.5 Consistently Discretized DSA

The analytic equations for the Source Iteration and DSA methods are useful only to a certain degree. Systems more complicated in the way of materials and geom-

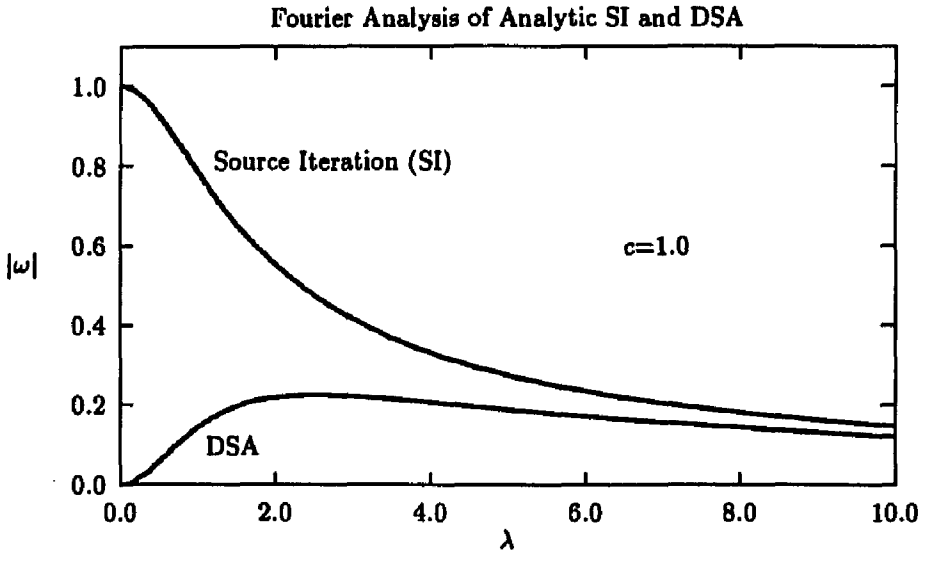

Figure 3.1: Eigenvalues of the Source Iteration and DSA methods for c=1.0.

etry require discretizing the analytic equations and solving them on a computer. How does one go about discretizing the transport and diffusion equations in DSA? It turns out that independently discretizing each equation, using one's favorite discretization schemes, may lead to instability when the mesh sizes are greater than about 1 mfp. In 1977, Alcouffe [Alc77] showed that DSA is unconditionally stable for the diamond-differenced S_N if the diffusion equation is discretized *consistently* with the transport equation. Instead of deriving the analytic DSA equations and independently discretizing the transport and diffusion equations, the diffusion part of the DSA equation is derived from the discretized transport equation. Larsen devised a four-step method of consistently deriving the discretized DSA equations for other transport differencing schemes [Lar82]. The spectral radius of the consistently discretized DSA schemes are the same as the analytical DSA, namely $0.2247c$, for all mesh sizes.

3.6 Inconsistently Discretized DSA

With the previous paragraph having little good to say about inconsistently discretized DSA, why on earth would anyone use it? There are at least two good reasons:

- The system being modeled is complicated such that the consistently discretized DSA equations are simply not practical, or
- A deterministic method is being used to accelerate a Monte Carlo transport method and the equations are *inherently* inconsistent.

The last item suggests that instabilities may exist when trying to accelerate Monte Carlo with a deterministic correction. We show here that this damning quality of inconsistently discretized DSA is stemmed by damping the DSA correction.

Analytically, the damped DSA equations are

$$\mu\frac{\partial}{\partial x}\psi^{(\ell+1/2)}(x,\mu)+\Sigma_t\psi^{(\ell+1/2)}(x,\mu)=\frac{1}{2}\Sigma_s\phi^{(\ell)}(x)+\frac{1}{2}Q(x) \quad , \tag{3.35}$$

$$\phi^{(\ell+1/2)}(x)=\int_{-1}^{1}\psi^{(\ell+1/2)}(x,\mu)d\mu \quad , \tag{3.36}$$

$$-\frac{\partial}{\partial x}\frac{1}{3\Sigma_t}\frac{\partial}{\partial x}f_0^{(\ell+1)}(x)+\Sigma_a f_0^{(\ell+1)}(x)=\Sigma_s\left(\phi^{(\ell+1/2)}(x)-\phi^{(\ell)}(x)\right) \quad , \tag{3.37}$$

$$\phi^{(\ell+1)}(x)=\phi^{(\ell+1/2)}(x)+\beta f_0^{(\ell+1)} \quad , \tag{3.38}$$

where β in Equation 3.38 is the damping factor that defines the method:

$$\beta = 0 \quad \text{Source Iteration} \quad , \tag{3.39}$$

$$0 < \beta < 1 \quad \text{Damped DSA} \quad , \tag{3.40}$$

$$\beta = 1 \quad \text{DSA} \quad . \tag{3.41}$$

Now we spatially discretize our system such that x_j are the centers and $x_{j+1/2}$ are the edges of uniform cells of width h. The angular variable is discretized using the S_N (N even) Gauss-Legendre quadrature set such that

$$\int_{-1}^{1} \mu d\mu \approx \sum_{m=1}^{N} \mu_m w_m \quad , \tag{3.42}$$

$$\mu_n = -\mu_{N-n+1} \quad , \tag{3.43}$$

$$w_m = w_{N-n+1} \quad , \tag{3.44}$$

$$2 = \sum_{m=1}^{N} w_m \quad , \tag{3.45}$$

where w_m is the weight (approximating $d\mu$) and μ_m approximates μ in the m^{th} angular bin. Discretization of the transport equation requires auxiliary equations to relate the cell edge angular fluxes to the cell center angular fluxes. These auxiliary equations constitute a differencing scheme. Many differencing schemes exist, but we will look solely at the Diamond Differencing scheme, where the cell center angular fluxes are the average of the two cell edge fluxes. The diffusion equation is centrally differenced. The inconsistently differenced, damped DSA equations for a homogeneous medium are as follows:

$$\frac{\mu_m}{h}\left(\psi_{m,j+1/2}^{(\ell+1/2)} - \psi_{m,j-1/2}^{(\ell+1/2)}\right) + \Sigma_t \psi_{m,j}^{(\ell+1/2)} = \frac{\Sigma_s}{2}\phi_j^{(\ell)} + \frac{1}{2}Q_j \quad , \tag{3.46}$$

$$\psi_{m,j}^{(\ell+1/2)} = \frac{1}{2}\left(\psi_{m,j+1/2}^{(\ell+1/2)} + \psi_{m,j-1/2}^{(\ell+1/2)}\right) \quad , \tag{3.47}$$

$$\phi_j^{(\ell+1/2)} = \sum_{n=1}^{N} \psi_{n,j}^{(\ell+1/2)} w_n \quad , \tag{3.48}$$

$$-\frac{1}{3\Sigma_t h^2}\left(f_{j+1}^{(\ell+1)} - 2f_j^{(\ell+1)} + f_{j-1}^{(\ell+1)}\right) + \Sigma_a f_j^{(\ell+1)} = \Sigma_s\left(\phi_j^{(\ell+1/2)} - \phi_j^{(\ell)}\right) \quad , \tag{3.49}$$

$$\phi_j^{(\ell+1)} = \phi_j^{(\ell+1/2)} + \beta f_j^{(\ell+1)} \quad . \tag{3.50}$$

Into Equations 3.46 through 3.50 we introduce the Fourier separation of variables ansatz,

$$Q_j = 0 \quad , \tag{3.51}$$

$$\phi_j^{(\ell)} = \omega^\ell e^{i\lambda x_j} \quad , \tag{3.52}$$

$$\psi_{m,j}^{(\ell+1/2)} = \omega^\ell a_m e^{i\lambda x_j} \quad , \tag{3.53}$$

$$\psi_{m,j+1/2}^{(\ell+1/2)} = \omega^\ell b_m e^{i\lambda x_{j+1/2}} \quad , \tag{3.54}$$

$$\phi_j^{(\ell+1/2)} = \omega^\ell u e^{i\lambda x_j} \quad , \tag{3.55}$$

$$f_j^{(\ell+1)} = \omega^\ell v e^{i\lambda x_j} \quad , \tag{3.56}$$

(where the zero source appears because the fluxes are interpreted as flux *errors*), and dividing by

$$\omega^\ell e^{i\lambda x_j} \quad , \tag{3.57}$$

we obtain

$$\frac{\mu_m}{h} b_m \left(e^{i\lambda h/2} - e^{-i\lambda h/2} \right) + \Sigma_t a_m = \frac{\Sigma_s}{2} \quad , \tag{3.58}$$

$$a_m = \frac{1}{2} b_m \left(e^{i\lambda h/2} + e^{-i\lambda h/2} \right) \quad , \tag{3.59}$$

$$u = \sum_{n=1}^{N} a_n w_n \quad , \tag{3.60}$$

$$-\frac{1}{3\Sigma_t h^2} v \left(e^{i\lambda h} - 2 + e^{-i\lambda h} \right) + \Sigma_t v = \Sigma_s (u - 1) \quad , \tag{3.61}$$

$$\omega = u + \beta v \quad . \tag{3.62}$$

Setting

$$\theta = \lambda h / 2 \tag{3.63}$$

and making use of the identities

$$\sin\theta = \frac{e^{i\theta} - e^{-i\theta}}{2i} \quad , \tag{3.64}$$

$$\cos\theta = \frac{e^{i\theta} + e^{-i\theta}}{2} \quad , \tag{3.65}$$

we find that

$$u = \frac{\Sigma_s}{2\Sigma_t} \sum_{m=1}^{N} \frac{\cos^2\theta}{\cos^2\theta + \frac{4}{\Sigma_t^2 h^2}\mu_m^2 \sin^2\theta} w_m \tag{3.66}$$

and

$$\omega = \frac{\left(\Sigma_a + \beta\Sigma_s + \frac{4}{3\Sigma_t h^2}\sin^2\theta\right) u - \beta\Sigma_s}{\Sigma_a + \frac{4}{3\Sigma_t h^2}\sin^2\theta} \quad . \tag{3.67}$$

Unlike the analytic eigenvalue, the damped DSA eigenvalue is periodic with period

$$T = \frac{2\pi}{h} \quad , \tag{3.68}$$

so we consider $|\lambda| \leq \frac{\pi}{h}$, or $0 \leq \lambda \leq \frac{\pi}{h}$. At the lowest frequency, $\lambda = 0$, the eigenvalue ω, from Equation 3.67, varies linearly with β,

$$\omega|_{\lambda=0} = (1-\beta)\frac{\Sigma_s}{\Sigma_t} \quad , \tag{3.69}$$

from $\omega = 0$ for DSA and $\omega = c = \frac{\Sigma_s}{\Sigma_t}$ for Source Iteration. At the highest, most oscillating frequency, we find

$$|\omega|_{\lambda=\frac{\pi}{h}} = \frac{\beta\Sigma_s}{\Sigma_a + \frac{4}{3\Sigma_t h^2}} \quad . \tag{3.70}$$

In order for the method to be stable, we must have the spectral radius less than or equal to 1. This stipulation limits the mesh size according to the following equation:

$$h^2\Sigma_t^2\left((\beta+1)\frac{\Sigma_s}{\Sigma_t} - 1\right) < \frac{4}{3} \quad . \tag{3.71}$$

We delightfully see from Equation 3.71 that damping the DSA allows stability with larger mesh sizes.

Figure 3.2 shows that, for a mesh size of 4/3 and $c = \frac{\Sigma_s}{\Sigma_t}$=1.0, the Source Iteration method ($\beta = 0$) converges slowly for the low frequencies and that DSA ($\beta = 1.0$) becomes unstable at the high frequencies. Damping eliminates the instability at the high frequencies for β =0.2, 0.4, and 0.6. Stability has the compromising price of

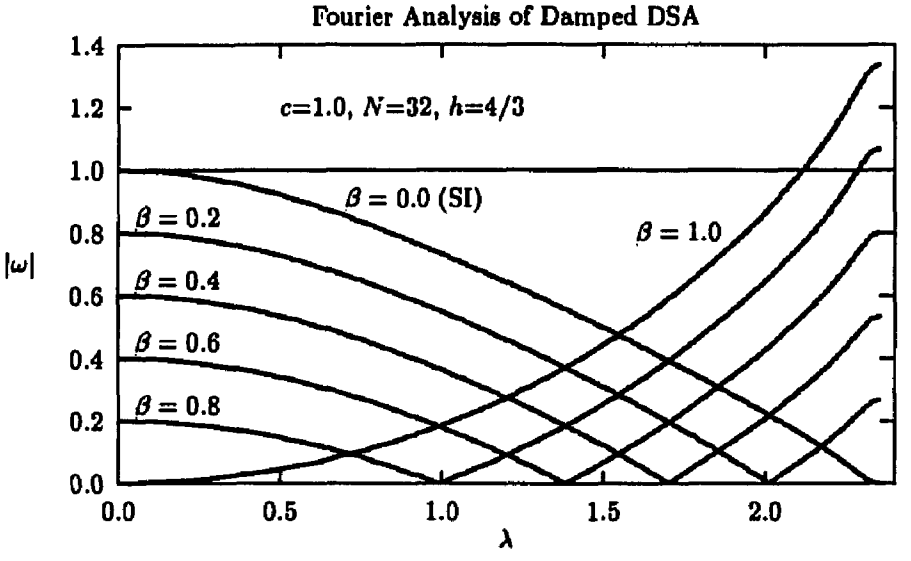

Figure 3.2: The inconsistently discretized, damped DSA eigenvalues for various frequencies λ and damping factors β.

reduced acceleration. The optimal β accelerates the most without going unstable. Figure 3.3 shows the DSA spectral radius from the Fourier analysis. The optimal beta–the beta for which the spectral radius is minimized–is about 0.429.

Figure 3.4 shows how, at the highest frequency $\lambda = \frac{\pi}{h}$, increasing the mesh size h for $\beta = 1.0$ will induce instability at a little over a mean free path thick. Damping (decreasing β) allows larger mesh sizes. For comparison, Figure 3.5 shows that the threshold mesh size is more advantageously sensitive to the scattering ratio (with β=1.0) than to β. That is, assuming the scattering ratio is variable, the method stabilizes faster for decreasing c than for decreasing β. This behavior is verified by Equation 3.71.

3.7 Numerical Results

To verify the results of the Fourier analysis, we demonstrate, as a function of mesh size, the stability of the following methods using Diamond Differencing:

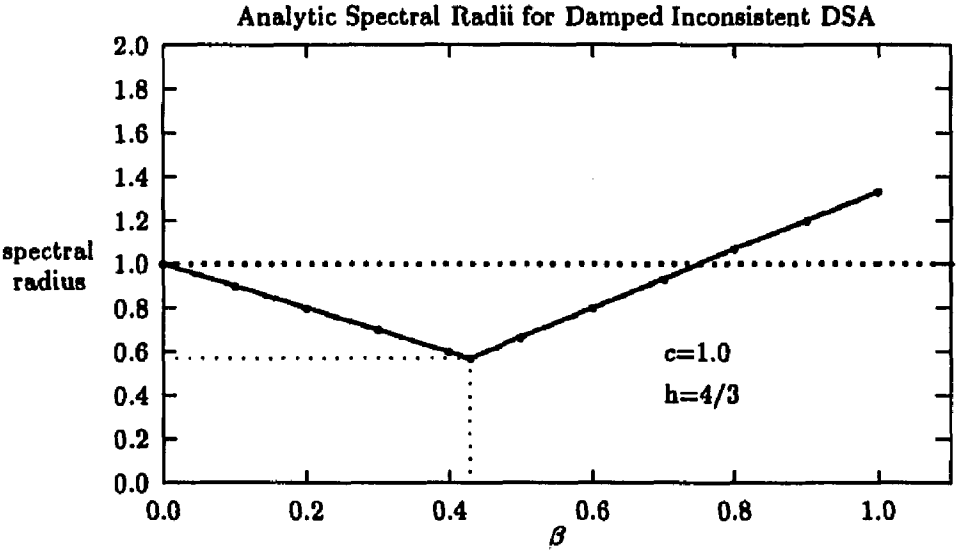

Figure 3.3: The spectral radii for inconsistently discretized, damped DSA eigenvalues for various values of β. The optimal beta is depicted at about 0.429.

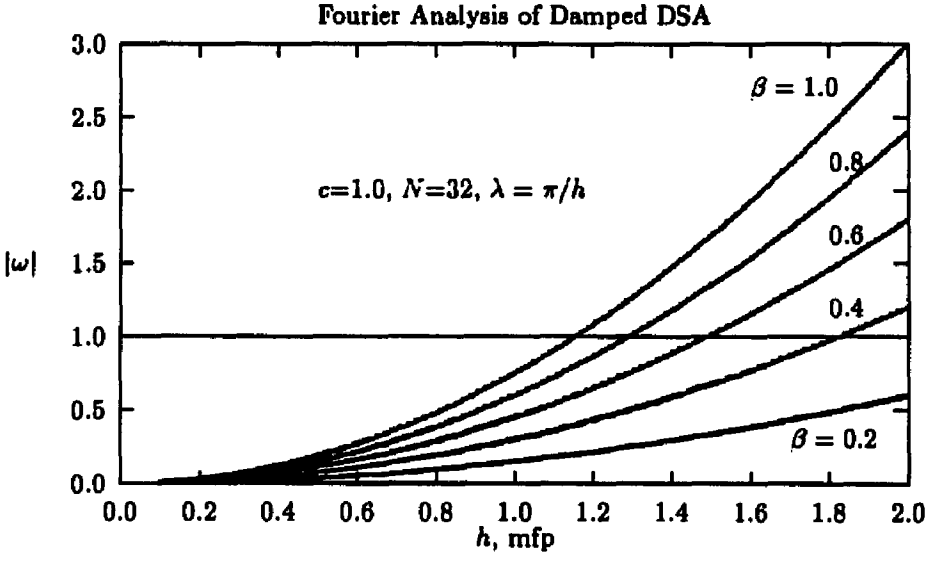

Figure 3.4: Damping the inconsistently discretized DSA allows for larger mesh size before instability sets in.

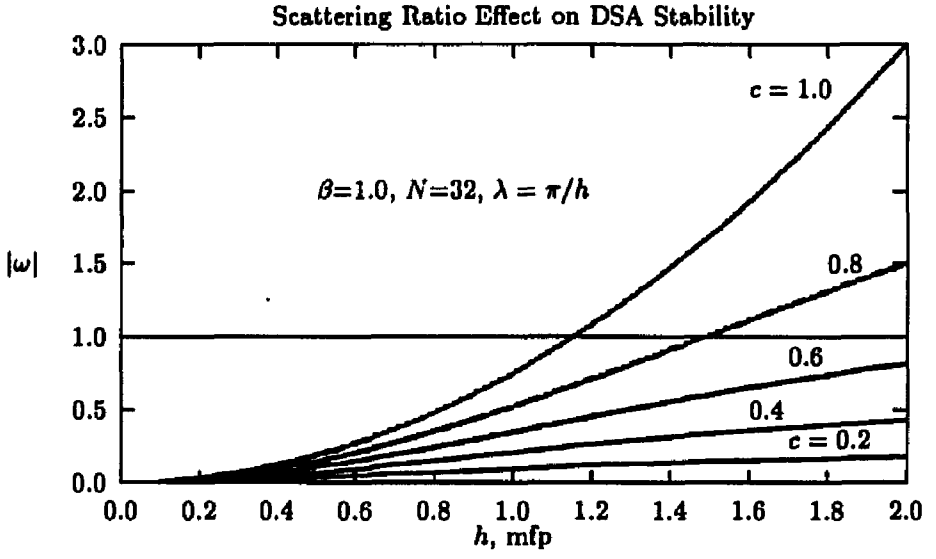

Figure 3.5: For inconsistently differenced DSA (β=1.0), the scattering ratio has a larger effect on the threshold (to instability) mesh size than does β.

- unaccelerated Source Iteration,
- accelerated with consistently differenced DSA, and
- accelerated with inconsistently differenced DSA,
  - $\beta = 1.0$
  - $\beta = 0.6$
  - $\beta = 0.4$.

We analyze a 40 mfp homogeneous slab with a nearly normal incident beam on the left edge. Using an S_{32} quadrature set, the incident angular flux, $\psi_{0,m}$ is

$$\psi_{0,m} = \frac{\delta_{m,32}}{\mu_{32} w_{32}}, \tag{3.72}$$

such that the current is unity. The right edge of the slab is a vacuum. The scattering ratio of the slab is 1.0. Using a convergence criterion of 10^{-6} for the relative error, we

use mesh sizes of 0.0625 cm, 0.125 cm, and so on, doubled, up to 8.0 cm, for a total of 8 cases. The unaccelerated source iteration took approximately 3080 iterations to converge for all cases, except for the 8.0 cm mesh size, where it required 3400 iterations to converge. Figure 3.6 shows the experimental spectral radii for both the consistently and inconsistently discretized DSA. The expression for estimating the spectral radius is

$$\rho = \frac{||\phi^{(n)} - \phi^{(n-1)}||_2}{||\phi^{(n-1)} - \phi^{(n-2)}||_2} \quad , \tag{3.73}$$

where $||\cdot||_2$ denotes the ℓ_2 norm. For the full correction, $\beta = 1.0$, the inconsistently discretized DSA is unstable for mesh sizes of 1.15 cm and larger. For larger mesh sizes, damping instills stability, whereas it diminishes the gain for smaller mesh sizes.

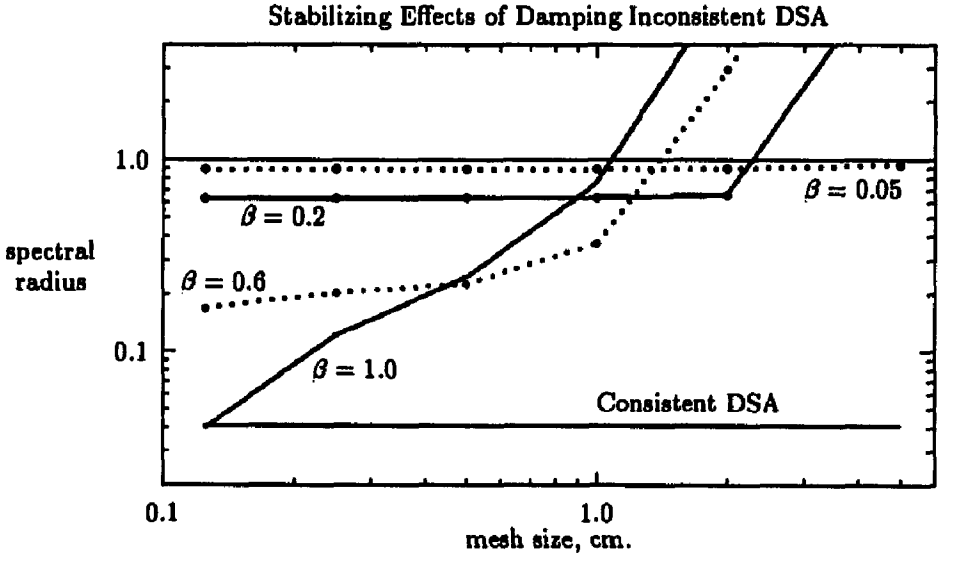

Figure 3.6: The experimental spectral radii for inconsistently discretized, damped DSA for increasing mesh size and for various values of β.

For a specific mesh size, there is an optimal β that results in the minimum spectral radius. Figure 3.7 indicates that the optimal β is about 0.4. This figure generally agrees with the plot of the optimal β from the analytic Fourier analysis, Figure 3.3.

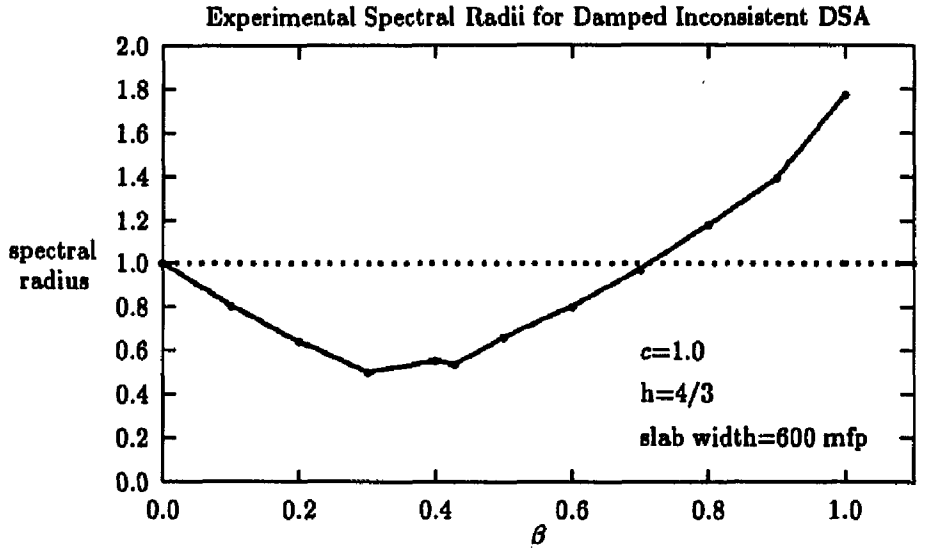

Figure 3.7: For a mesh size of 4/3 mfp, an optimal β exists such that the spectral radius is a minimum for inconsistently discretized DSA.

We conclude by noting that if a cell-edge differencing scheme was used for the diffusion equation in DSA instead of a cell-center differencing scheme, the method would have a wider range of stability. To apply the DSA correction, the cell-edge corrections are averaged before adding to the transport flux, which reside on the cell centers for diamond-differencing. The result of averaging the corrections is the reduction of the high order errors, those that cause the method's instability.

CHAPTER IV

Experimental Fourier Analysis Tool

We have demonstrated the analytic Fourier Analysis applied to Diffusion Synthetic Acceleration. The analytic Fourier Analysis is not directly applicable to real problems because it requires an infinite, homogeneous medium. Moreover, it requires a linear method. These reasons exclude it from application to criticality problems.

We present an *experimental Fourier analysis* that, in the vein of the analytic analysis, indicates the stability and convergence of the various modes of the solution. In one-dimensional slab geometry, the fission source $f(x)$, $0 \leq x \leq 2L$, may be represented by the Fourier series [Spi68]

$$f(x) = \frac{a_0}{2} + \sum_{n=1}^{\infty} \left(a_n \cos \frac{n\pi x}{L} + b_n \sin \frac{n\pi x}{L} \right) \quad , \tag{4.1}$$

where the series converges to $f(x)$ where $f(x)$ is continuous, and to the average of $f(x)$ where $f(x)$ is discontinuous; $f(x)$ is periodic on the interval, such that $f(x + 2L) = f(x)$; and the coefficients are

$$a_n = \frac{1}{L} \int_0^{2L} f(x) \cos \frac{n\pi x}{L} dx \quad , \tag{4.2}$$

$$b_n = \frac{1}{L} \int_0^{2L} f(x) \sin \frac{n\pi x}{L} dx \quad . \tag{4.3}$$

In Equation 4.1, the $n = 1$ terms represent the fundamental mode, and $n \geq 2$ represent the higher modes. Note that, for each n, the sine and cosine may be

written as [Kap84]

$$A_n \sin\left(\frac{n\pi x}{L} + \gamma\right) \quad , \tag{4.4}$$

where

$$A_n = \sqrt{a_n^2 + b_n^2} \quad , \tag{4.5}$$

$$a_n = A_n \sin\gamma \quad , \tag{4.6}$$

$$b_n = A_n \cos\gamma \quad . \tag{4.7}$$

Computationally, to gauge the convergence of the various modes of the fission source, we extract the individual Fourier coefficients of the fission source in a fashion similar to that of Equations 4.2 and 4.3, utilizing Equation 4.5. Let us consider a one-dimensional slab of width X with M cells, each of width Δx, and discrete values $f_m^{(\ell)}$ of the fission source in cell m at iteration, or cycle, ℓ. The Fourier coefficient for the n^{th} mode at iteration, or cycle, ℓ is

$$F^{(\ell)}(n\pi) = \frac{1}{X}\sum_{m=1}^{M} f_m^{(\ell)} \sin\frac{n\pi(m-\frac{1}{2})}{M}\,\Delta x \tag{4.8}$$

$$\approx \frac{1}{X}\int_0^X f^{(\ell)}(x)\sin\frac{n\pi x}{X}dx, \tag{4.9}$$

where $n = 1, 2, \ldots, M$.

Plotting the Fourier coefficient of a particular mode as a function of iteration, or cycle, we observe the convergence of that mode when the plot levels off. The slope of the plot as it is converging gives an idea of the speed of convergence. However, unlike the usual Fourier analysis for an infinite medium, the boundary effects here keep the modes from being entirely independent.

We will use the experimental Fourier analysis to gauge the convergence of both deterministic and Monte Carlo criticality methods, and to show the effects of accelerating the fission source convergence.

CHAPTER V

Diffusion-Simulated Monte Carlo Calculations

It is no secret that the statistical noise is the main culprit plaguing a potential Monte Carlo criticality acceleration method [Swa72]. Pedagogically then, let us investigate potential Monte Carlo criticality acceleration methods using diffusion theory to simulate the transport theory. This was the route taken by Carter and McCormick [Car69] to examine their proposed Monte Carlo acceleration method. Diffusion theory possesses no statistical noise, but the success of an acceleration scheme in diffusion theory gives an indication of potential success in transport (Monte Carlo) theory.

Realizing the success of Mihalczo [Mih67] with the fission matrix approach (that is, simply using the eigenvalue of the fission matrix), Carter and McCormick incorporated this information into the actual criticality calculation. After each iteration, they adjusted the newly acquired source in each cell by the ratio of that cell's fission matrix eigenvectors from successive iterations. We will explain their method, propose a modification to their method, and compare both to the unaccelerated case.

Carter and McCormick present the continuous, analytic, integral transport equation as

$$S(\mathbf{r}) = \frac{1}{k} \int K(\mathbf{r}, \mathbf{r}') S(\mathbf{r}')\, d^3r' \quad , \tag{5.1}$$

where $S(\mathbf{r})$ is the fission source, $\hat{k}$ is the eigenvalue, and $K(\mathbf{r},\mathbf{r}')$ is the number of fission source particles produced per unit volume about $\mathbf{r}$ due to a particle born at $\mathbf{r}'$ [Car69] Introducing iteration indices produces an analytic source iteration scheme representing the Monte Carlo method,

$$S^{(n)}(\mathbf{r}) = \frac{1}{\hat{k}^{(n)}} \int K(\mathbf{r},\mathbf{r}') S^{(n-1)}(\mathbf{r}')\, d^3r' \quad . \tag{5.2}$$

The kernel $K(\mathbf{r},\mathbf{r}')$ is approximated in discrete form by the fission matrix $\mathbf{L}^{(n)}$ whose (i,j)th element, at iteration n, is

$$L_{ij}^{(n)} = \frac{\int_i \int_j K(\mathbf{r},\mathbf{r}') S^{(n-1)}(\mathbf{r}')\, d^3r'\, d^3r}{\int_j S^{(n-1)}(\mathbf{r}')\, d^3r'} \quad , \tag{5.3}$$

where the indices on the integrals indicate the volume of cell i or j. The fission matrix $\mathbf{L}^{(n)}$ depends on the fission source at iterations n and $n-1$, so it, too, is iteration dependent. $\mathbf{L}^{(n)}$ is analogous to the cycle fission matrix in Monte Carlo. The eigenstate of $\mathbf{L}^{(n)}$ satisfies

$$f^{(n)} = \frac{1}{k^{(n)}} \mathbf{L}^{(n)} f^{(n)} \quad . \tag{5.4}$$

Here $f^{(n)}$ is the dominant eigenvector and $k^{(n)}$ is the dominant eigenvalue of $\mathbf{L}^{(n)}$ at iteration n.

Carter and McCormick proposed, without derivation, the following acceleration method:

$$S^{(n)}(\mathbf{r}) = \frac{1}{\hat{k}^{(n)}} \sum_j \left(\frac{f_j^{(n)}}{f_j^{(n-1)}} \right) \int_j K(\mathbf{r},\mathbf{r}') S^{(n-1)}(\mathbf{r}')\, d^3r' \quad . \tag{5.5}$$

We propose a slight variation to Carter and McCormick's method by replacing the correcting ratio in Equation 5.5 with

$$\left(\frac{f_j^{(n)}}{S_j^{(n-1)}} \right) \quad , \tag{5.6}$$

to obtain

$$S^{(n)}(\mathbf{r}) = \sum_j \left(\frac{f_j^{(n)}}{S_j^{(n-1)}} \right) \int_j K(\mathbf{r},\mathbf{r}') S^{(n-1)}(\mathbf{r}')\, d^3r' \quad , \tag{5.7}$$

where

$$S_j^{(n-1)} = \int_j S^{(n-1)}(\mathbf{r}')\, d^3r' \tag{5.8}$$

is the cell-averaged source in cell j at iteration n. This modification ties the acceleration more closely to the source being accelerated. The correcting ratio modifies the magnitude of the fission source in each cell and the transport kernel K controls the shape of the fission source within each cell.

The kernel $K(\mathbf{r},\mathbf{r}')$ represents Monte Carlo or deterministic, say discrete ordinates, neutron transport. Numerically, let us represent $K(\mathbf{r},\mathbf{r}')$ by a fine-grid fission matrix, $\mathbf{K}$, whose elements are K_{ij}. We calculate $\mathbf{K}$ by a series of fixed-source diffusion calculations. Each calculation has a unit source in one cell. The response to that unit source is converted from a scalar flux to a fission source by multiplying by $\nu\sigma_f$. One calculation with the source in cell j produces the jth column of $\mathbf{K}$. If there are N cells in the system, N calculations are required. The unaccelerated source iteration method is represented by

$$S_i^{(n)} = \frac{1}{\hat{k}^{(n)}} \sum_j K_{ij} S_j^{(n-1)} \quad . \tag{5.9}$$

We effectively normalize the source iteration by dividing the right hand side of Equation 5.9 by $\hat{k}^{(n)}$, given recursively by

$$\hat{k}^{(n)} = \hat{k}^{(n-1)} \frac{\int S^{(n)}(\mathbf{r}')\, d^3r'}{\int S^{(n-1)}(\mathbf{r}')\, d^3r'} \quad . \tag{5.10}$$

The coarse-grid fission matrix is obtained from Equation 5.3 as a fission source-weighted collapse of the fine-grid fission matrix,

$$L_{kl}^{(n)} \;=\; \frac{\sum_{j\in l} \left[\sum_{i\in k} K_{ij} S_j^{(n-1)} \right]}{\sum_{j\in l} S_j^{(n-1)}} \quad . \tag{5.11}$$

For instance, if there are 4 fine cells and 2 coarse cells, with coarse cell 1 containing fine cells 1 and 2, and coarse cell 2 containing fine cells 3 and 4, the first row of L is

$$L_{11}^{(n)} = \frac{(K_{11}+K_{21})S_1^{(n-1)} + (K_{12}+K_{22})S_2^{(n-1)}}{S_1^{(n-1)} + S_2^{(n-1)}} \quad , \tag{5.12}$$

$$L_{12}^{(n)} = \frac{(K_{13}+K_{23})S_3^{(n-1)} + (K_{14}+K_{24})S_4^{(n-1)}}{S_3^{(n-1)} + S_4^{(n-1)}} \quad . \tag{5.13}$$

We investigated these two acceleration methods on a one-group, one-dimensional slab of thickness 60.0 cm with vacuum boundaries. The physical parameters, with isotropic scattering, are

$$\Sigma_t = 1.0 \text{ cm}^{-1} \quad , \tag{5.14}$$

$$\Sigma_a = 0.3 \text{ cm}^{-1} \quad , \tag{5.15}$$

$$\nu\Sigma_f = 0.30713574 \text{ cm}^{-1} \quad . \tag{5.16}$$

This constitutes a critical system when the slab is 20 mfp thick [Kap74]. The slab was made larger so as to incur a larger dominance ratio of about 0.991. To make the acceleration more visible, we began with a very poor initial fission source distribution: flat in the left half of the slab and zero in the right half. The convergence requirement was 1.0×10^{-5} and false convergence was taken into account, by multiplying the convergence requirement by $(1-\rho)$, where ρ is the spectral radius, estimated by

$$\rho \approx \frac{||S^{(n+1)} - S^{(n)}||_\infty}{||S^{(n)} - S^{(n-1)}||_\infty} \quad . \tag{5.17}$$

The fine-grid fission matrix is calculated on 0.5 mfp cells, or 120 cells total.

Figure 5.1 shows the number of iterations required for convergence for varying numbers of coarse-grid cells. For too few coarse-grid cells, there is not enough resolution to provide significant acceleration. For too many coarse-grid cells, the poor initial fission source guess makes more of a significant impact on the coarse-grid

fission matrix and inhibits acceleration. The modified method has a much greater range of effectiveness over the number of coarse-grid cells. With the number of com-

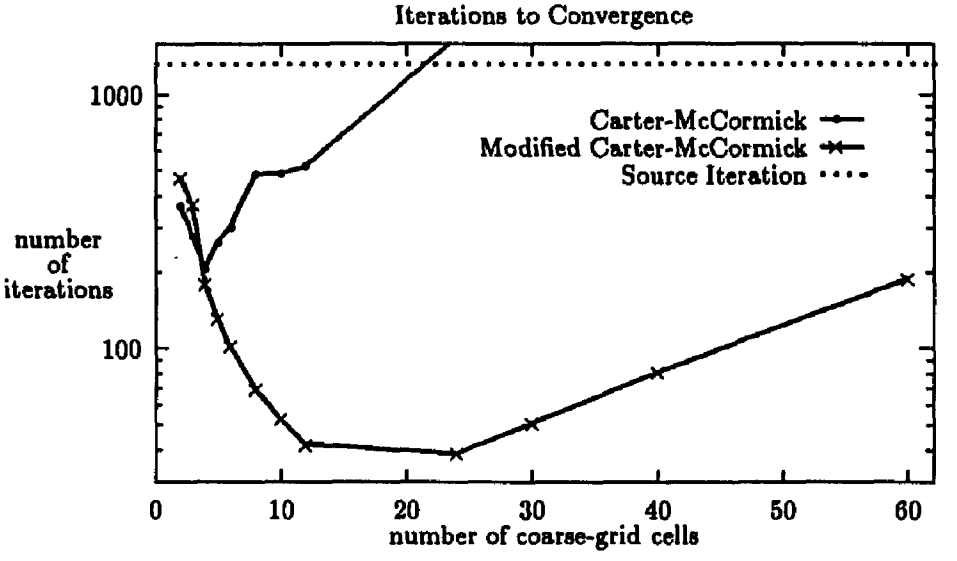

Figure 5.1: Acceleration behavior (iterations to converge) for the Carter-McCormick and Modified Carter-McCormick methods with varying number of coarse-grid cells.

putational operations going up as N^3 with the number of coarse-grid cells, N, fewer iterations with a larger matrix may take more computer time. The computer times on a Sun SPARC20 workstation are shown in Figure 5.2.

We shall also look at the experimental Fourier mode convergence for the unaccelerated case, the Carter-McCormick method with 4 coarse-grid cells, and the Modified Carter-McCormick method with 10 coarse-grid cells. Figures 5.3, 5.4, and 5.5 show the convergence of the first three experimental Fourier modes. They show that the Carter-McCormick method is wildly oscillatory before it converges. The Modified Carter-McCormick method is also oscillatory, but to a lesser degree.

In the next chapter, we discuss *damping*, or *reducing* an additive correction to keep an acceleration method from becoming unstable. If it should become necessary

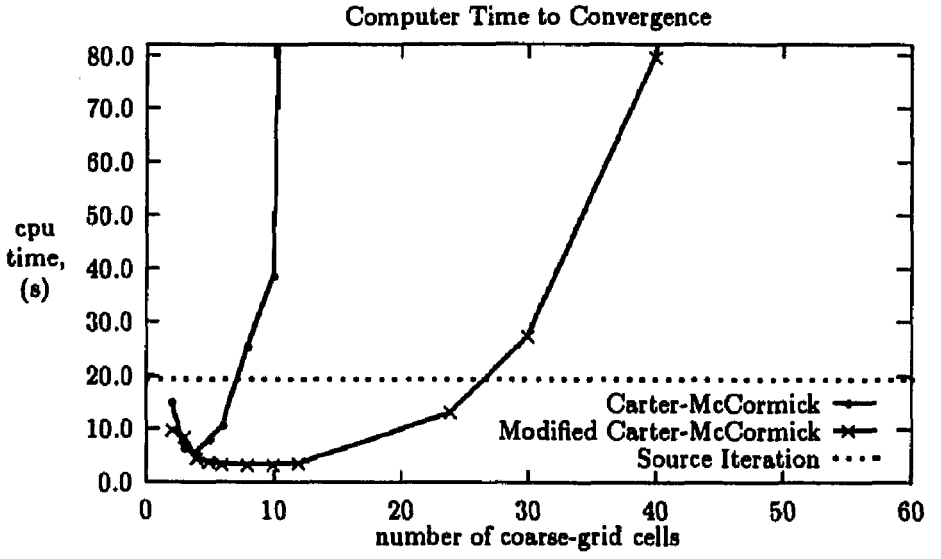

Figure 5.2: Acceleration behavior (computer time) for the Carter-McCormick and Modified Carter-McCormick methods with varying number of coarse-grid cells.

for stability reasons to damp a *multiplicative* correction γ, we note that it may be damped, or made closer to unity, by the following operation:

$$\gamma \leftarrow \frac{r+\gamma}{r+1} \quad , \tag{5.18}$$

where $r > 0$.

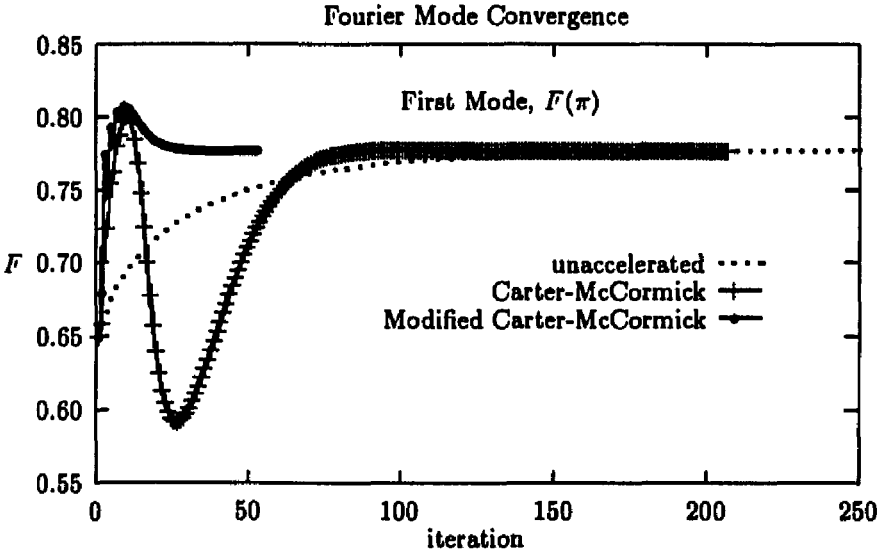

Figure 5.3: Convergence of the first experimental Fourier mode for the unaccelerated, Carter-McCormick, and Modified Carter-McCormick methods.

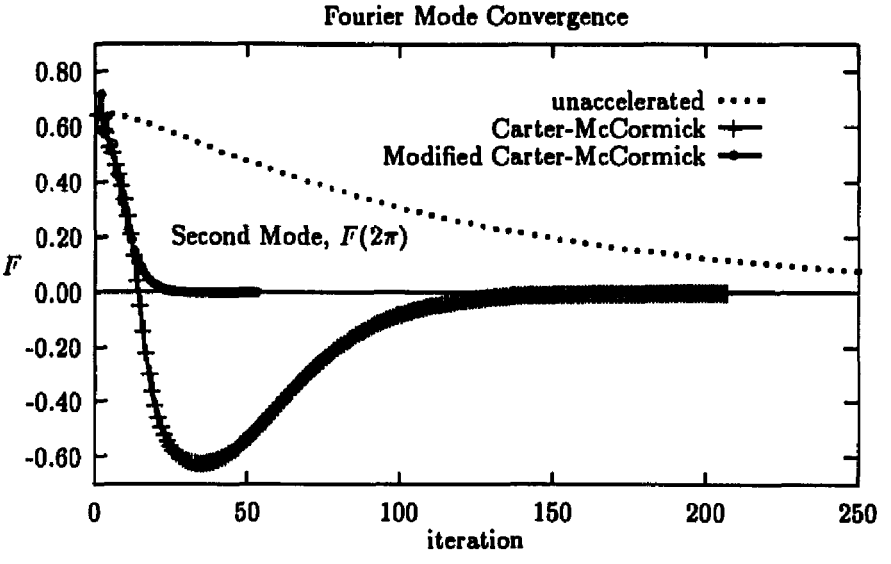

Figure 5.4: Convergence of the second experimental Fourier mode for the unaccelerated, Carter-McCormick, and Modified Carter-McCormick methods.

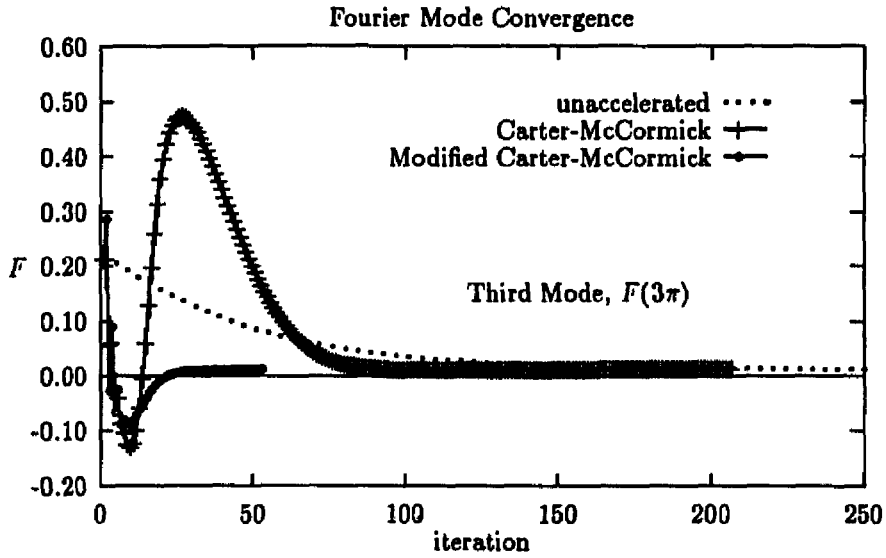

Figure 5.5: Convergence of the third experimental Fourier mode for the unaccelerated, Carter-McCormick, and Modified Carter-McCormick methods.

CHAPTER VI

Fission Matrix Acceleration Method

Criticality calculations utilizing unaccelerated source iteration require many iterations or cycles to converge the fission source for high dominance ratio problems. We wish to remedy this downside of source iteration by devising a method to accelerate the fission source convergence. The approach we take is to derive equations for the *exact* corrections to the fission source at any iteration or cycle. After adding the exact correction to the fission source, we arrive, in one iteration or cycle, at the exact solution, and the calculation is finished. However, realizing that solving for the exact correction is just as difficult as the original problem, the equations for the correction are approximated in some fashion so that they are much simpler to solve. With an approximate correction, the overall method will not converge in one iteration, but it can accelerate convergence and overcome the extra time spent computing the correction. This procedure is common. Diffusion Synthetic Acceleration is an example of this approach.

6.1 Derivation of the Fission Matrix Method

For clarity and continuity, we repeat the steps for obtaining the integral transport equation. We begin with the monoenergetic, one-dimensional integro-differential

transport equation with isotropic scattering. We consider a slab of width L with vacuum boundaries,

$$\mu\frac{\partial\psi(x,\mu)}{\partial x}+\Sigma_t(x)\psi(x,\mu)=\frac{1}{2}\left(\Sigma_s(x)+\frac{\nu\Sigma_f(x)}{k}\right)\int\psi(x,\mu)d\mu \quad , \tag{6.1}$$

$$\psi(0,\mu)=0\ , \quad \mu>0 \quad , \tag{6.2}$$

$$\psi(L,\mu)=0\ , \quad \mu<0 \quad . \tag{6.3}$$

For simplification, we define the transport operator $\mathbf{T}$ as the leakage and collision terms,

$$\mathbf{T}\psi(x,\mu) \;=\; \mu\frac{\partial\psi(x,\mu)}{\partial x}+\Sigma_t(x)\psi(x,\mu) \quad , \tag{6.4}$$

the scattering operator $\mathbf{S}$ as the inscattering term,

$$\mathbf{S}\psi(x,\mu) \;=\; \frac{1}{2}\Sigma_s(x)\int\psi(x,\mu)d\mu \quad , \tag{6.5}$$

and the fission operator $\mathbf{F}$ as the fission source,

$$\mathbf{F}\psi(x,\mu) \;=\; \frac{1}{2}\frac{\nu\Sigma_f(x)}{k}\int\psi(x,\mu)d\mu \quad . \tag{6.6}$$

We manipulate the transport equation, first by moving the inscattering term to the left hand side,

$$(\mathbf{T}-\mathbf{S})\psi(x,\mu)=\frac{1}{k}\mathbf{F}\psi(x,\mu) \quad , \tag{6.7}$$

then operating on both sides by $(\mathbf{T}-\mathbf{S})^{-1}$, to obtain

$$\psi(x,\mu)=\frac{1}{k}(\mathbf{T}-\mathbf{S})^{-1}\mathbf{F}\psi(x,\mu) \quad . \tag{6.8}$$

Operating on both sides of Equation 6.8 by the fission operator $\mathbf{F}$, we obtain an integral transport equation,

$$f(x)=\frac{1}{k}\mathbf{L}f(x) \quad , \tag{6.9}$$

where

$$f(x) = \mathbf{F}\psi(x,\mu) \tag{6.10}$$

is the fission source, and

$$\mathbf{L} = \mathbf{F}(\mathbf{T} - \mathbf{S})^{-1} \tag{6.11}$$

is an integral operator acting only on the spatial variable. (We approximate **L** by the fission matrix, as we shall see later.) The integral form of the transport equation in Equation 6.9 best describes the Monte Carlo criticality method. It is also fitting for a type of diffusion calculation where the operator **L** is approximated by a matrix whose elements are estimated by diffusion theory.

The analytic form of the source iteration method is represented by introducing iteration indices to Equation 6.9, the integral transport equation,

$$f^{(\ell+\frac{1}{2})} = \frac{1}{k^{(\ell)}}\mathbf{L}f^{(\ell)} \quad , \tag{6.12}$$

$$f^{(\ell+1)} = f^{(\ell+\frac{1}{2})} \quad . \tag{6.13}$$

We desire the exact additive correction, $g^{(\ell+1)}$, to the most recent source iteration fission source, $f^{(\ell+\frac{1}{2})}$, that results in the exact fission source. Using Equations 6.9 and 6.12, we formulate $g^{(\ell+1)}$ as follows:

$$g^{(\ell+1)} \equiv f - f^{(\ell+\frac{1}{2})} \tag{6.14}$$

$$= \frac{1}{k}\mathbf{L}f - f^{(\ell+\frac{1}{2})} \tag{6.15}$$

$$= \frac{1}{k}\mathbf{L}(f - f^{(\ell+\frac{1}{2})}) + \frac{1}{k}\mathbf{L}f^{(\ell+\frac{1}{2})} - f^{(\ell+\frac{1}{2})} \quad . \tag{6.16}$$

Collecting the $g^{(\ell+1)}$ terms on the left and rearranging the right hand side, we obtain

$$(\mathbf{I}-\frac{1}{k}\mathbf{L})g^{(\ell+1)} = \frac{1}{k}\mathbf{L}f^{(\ell+\frac{1}{2})}-f^{(\ell+\frac{1}{2})} \quad (6.17)$$

$$= (\frac{1}{k}\mathbf{L}-\mathbf{I})f^{(\ell+\frac{1}{2})} \quad (6.18)$$

$$= (\frac{1}{k}\mathbf{L}-\mathbf{I})\frac{1}{k^{(\ell)}}\mathbf{L}f^{(\ell)} \quad (6.19)$$

$$= \frac{1}{k^{(\ell)}}\mathbf{L}\left(\frac{1}{k}\mathbf{L}f^{(\ell)}-f^{(\ell)}\right) \quad (6.20)$$

$$= \mathbf{L}\left(\frac{1}{k}f^{(\ell+\frac{1}{2})}-\frac{1}{k^{(\ell)}}f^{(\ell)}\right) \quad . \quad (6.21)$$

This is an exact equation for $g^{(\ell+1)}$, the additive correction to the most recent fission source estimate, $f^{(\ell+\frac{1}{2})}$. This equation is as complicated and difficult to solve as the original problem in Equations 6.12 and 6.13. Therefore, we shall approximate it.

We must approximate the analytic quantities in Equation 6.21. The quantities $f^{(\ell)}(x)$, $f^{(\ell+\frac{1}{2})}(x)$, and $g^{(\ell+1)}(x)$ are all densities of fission source particles at x. (The correction g is more appropriately a fission source correction density.) We convert the fission source particle densities to vectors of cell-average quantities by discretizing the system, operating on them by the projection operator $\mathbf{P}$, and normalizing, such that, in cell j,

$$\hat{f}_j^{(\ell)} = \mathbf{P}_j f^{(\ell)}(x) \quad , \quad (6.22)$$

$$\hat{f}_j^{(\ell+1/2)} = \mathbf{P}_j f^{(\ell+1/2)}(x) \quad . \quad (6.23)$$

The projection operator $\mathbf{P}$ in a deterministic calculation amounts to integrating in space over cell j,

$$\hat{f}_j^{(\ell)} = \mathbf{P}_j^{Det} f^{(\ell)}(x) = \int_{x\in j} f^{(\ell)}(x)dx \quad . \quad (6.24)$$

In a Monte Carlo calculation, the quantities $f^{(\ell)}(x)$ and $f^{(\ell+\frac{1}{2})}(x)$ are collections of particles whose discrete locations are represented by $x_i^{(\ell)}$ and $x_i^{(\ell+1/2)}$. The Monte

Carlo projection operator amounts to summing up the fission source particles in cell j,

$$\hat{f}_j^{(\ell)} = \mathbf{P}_j^{MC} f^{(\ell)}(x) = \sum_i \gamma_{x_{i,j}^{(\ell)}} \quad , \tag{6.25}$$

where

$$\gamma_{x_{i,j}^{(\ell)}} = \begin{cases} 1 \quad , & x_i^{(\ell)} \in \text{cell } j \\ 0 \quad , & \text{otherwise} \quad . \end{cases} \tag{6.26}$$

The operator $\mathbf{L}$ is approximated by the fission matrix, $\hat{\mathbf{L}}$, whose (i,j)th element is the probability that a neutron born in cell j produces a subsequent source neutron in cell i. In a Monte Carlo calculation, $\hat{\mathbf{L}}$ may be estimated from the Monte Carlo data by mere bookkeeping during the calculation. Another way to estimate the fission matrix is through a series of diffusion calculations. Each diffusion calculation has a source in the jth cell and the fission production over the entire system produces the jth column of the fission matrix. Whatever way it is calculated, the fission matrix has dominant eigenvalue $\hat{k}$ and eigenvector $\hat{f}$, such that

$$\hat{f} = \frac{1}{\hat{k}} \hat{\mathbf{L}} \hat{f} \quad . \tag{6.27}$$

We will also find the adjoint eigenvector useful. It is obtained from the adjoint fission matrix, which is the transposed fission matrix, since the elements of the fission matrix are all real. Therefore, we have

$$\hat{f}^* = \frac{1}{\hat{k}} \hat{\mathbf{L}}^* \hat{f}^* \quad . \tag{6.28}$$

Substituting the aforementioned approximations for their analytic counterparts, Equation 6.21 becomes

$$(\mathbf{I} - \frac{1}{\hat{k}} \hat{\mathbf{L}}) \hat{g}^{(\ell+1)} = \hat{\mathbf{L}} \left(\frac{1}{k^{(\ell+1)}} \hat{f}^{(\ell+\frac{1}{2})} - \frac{1}{k^{(\ell)}} \hat{f}^{(\ell)} \right) \quad , \tag{6.29}$$

where $\hat{g}^{(\ell+1)} = \hat{f}^{(\ell+1)} - \hat{f}^{(\ell+\frac{1}{2})}$ is the cell-averaged correction. Since $\hat{f}^{(\ell+\frac{1}{2})}$ is known, solving for $\hat{g}^{(\ell+1)}$ is equivalent to solving for $\hat{f}^{(\ell+1)}$, the updated fission source.

Unfortunately, Equation 6.29 does not automatically have a solution. Utilizing the Fredholm-Alternative Theorem [Kre78], we obtain a solvability condition by taking the inner product of both sides of Equation 6.29 with the adjoint eigenvector, $\hat{f}^*$. The left hand side is, by Equation 6.28, identically zero,

$$\left(\hat{f}^*, (\mathbf{I} - \frac{1}{\hat{k}}\hat{\mathbf{L}})(\hat{f}^{(\ell+1)} - \hat{f}^{(\ell+\frac{1}{2})})\right) = \left((\mathbf{I} - \frac{1}{\hat{k}}\hat{\mathbf{L}}^*)\hat{f}^*, (\hat{f}^{(\ell+1)} - \hat{f}^{(\ell+\frac{1}{2})})\right) \quad (6.30)$$

$$= 0 \quad , \quad (6.31)$$

giving us the solvability condition,

$$k^{(\ell+1)} = k^{(\ell)} \frac{\left(\hat{f}^*, \hat{\mathbf{L}}\hat{f}^{(\ell+\frac{1}{2})}\right)}{\left(\hat{f}^*, \hat{\mathbf{L}}\hat{f}^{(\ell)}\right)} \quad (6.32)$$

$$= k^{(\ell)} \frac{\left(\hat{\mathbf{L}}^*\hat{f}^*, \hat{f}^{(\ell+\frac{1}{2})}\right)}{\left(\hat{\mathbf{L}}^*\hat{f}^*, \hat{f}^{(\ell)}\right)} \quad (6.33)$$

$$= k^{(\ell)} \frac{\left(\hat{f}^*, \hat{f}^{(\ell+\frac{1}{2})}\right)}{\left(\hat{f}^*, \hat{f}^{(\ell)}\right)} \quad . \quad (6.34)$$

For arbitrary discrete vectors a and b, we define the inner product as

$$(a, b) = \sum_{i=1}^{J} a_i b_i \quad . \quad (6.35)$$

Using the value of $k^{(\ell+1)}$ from Equation 6.34 in Equation 6.29, we solve for $\hat{g}^{(\ell+1)}$, the additive correction. The value of the additive correction is not unique, since any multiple of the fission matrix eigenvector, $\hat{f}$, added to the correction is also a solution of Equation 6.29. Therefore, we make $\hat{g}^{(\ell+1)}$ unique by requiring it to be orthogonal to the adjoint fission matrix eigenvector. Operationally, this condition is satisfied by setting the additive correction to $\hat{g}_o^{(\ell+1)}$, where

$$\hat{g}_o^{(\ell+1)} = \hat{g}^{(\ell+1)} - \frac{(\hat{f}^*, \hat{g}^{(\ell+1)})}{(\hat{f}^*, \hat{f}^*)}\hat{f}^* \quad , \quad (6.36)$$

such that

$$(\hat{f}^*, \hat{g}_o^{(\ell+1)}) = (\hat{f}^*, \hat{g}^{(\ell+1)}) - (\hat{f}^*, \hat{g}^{(\ell+1)}) \tag{6.37}$$

$$= 0 \quad . \tag{6.38}$$

The additive correction $\hat{g}_o^{(\ell+1)}$ is used to update, or accelerate, the most recent fission source. As explained in Chapter III, the correction is scaled by a "damping" factor β, $0 \leq \beta \leq 1$, to enhance stability. The resulting method is unaccelerated source iteration with $\beta = 0$, and full acceleration with $\beta = 1$. The additive correction is converted to a multiplicative correction by the following approximation,

$$f^{(\ell+1)} = f^{(\ell+\frac{1}{2})} + \beta \hat{g}_o^{(\ell+1)} \tag{6.39}$$

$$\approx f^{(\ell+\frac{1}{2})} \left(1 + \beta \frac{\hat{g}_o^{(\ell+1)}}{\hat{f}^{(\ell+\frac{1}{2})}}\right) \quad . \tag{6.40}$$

In a deterministic calculation, the fission source is multiplied by the multiplicative correction factor. In a Monte Carlo calculation, depending on the departure of the multiplicative correction factor from unity, the individual fission source particles are either killed, cloned, or left untouched.

The analytic fission matrix acceleration method is unbiased. It converges to the unaccelerated result since the right hand side of Equation 6.29, and hence the correction, go to zero as the source converges.

The steps for the fission matrix acceleration method are summarized as follows:

1. Perform a transport cycle, Equation 6.12,

$$f^{(\ell+\frac{1}{2})} = \frac{1}{k^{(\ell)}} \mathbf{L} f^{(\ell)} \quad . \tag{6.41}$$

2. Calculate the eigenstate of the fission matrix and adjoint fission matrix,

$$\hat{f} = \frac{1}{\hat{k}} \mathbf{L} \hat{f} \quad , \quad \hat{f}^* = \frac{1}{\hat{k}} \hat{\mathbf{L}}^* \hat{f}^* \quad . \tag{6.42}$$

3. Calculate $k^{(\ell+1)}$, the solvability condition from Equation 6.34,

$$k^{(\ell+1)} = k^{(\ell)} \frac{\left(\hat{f}^*, \hat{f}^{(\ell+\frac{1}{2})}\right)}{\left(\hat{f}^*, \hat{f}^{(\ell)}\right)} \quad . \tag{6.43}$$

4. Calculate the fission source correction using Equation 6.29,

$$(\mathbf{I} - \frac{1}{\hat{k}}\hat{\mathbf{L}})\hat{g}^{(\ell+1)} = \hat{\mathbf{L}}\left(\frac{1}{k^{(\ell+1)}}\hat{f}^{(\ell+\frac{1}{2})} - \frac{1}{k^{(\ell)}}\hat{f}^{(\ell)}\right) \quad . \tag{6.44}$$

5. Apply the correction using Equation 6.40 ,

$$f^{(\ell+1)} \approx f^{(\ell+\frac{1}{2})}\left(1 + \beta\frac{\hat{g}_o^{(\ell+1)}}{\hat{f}^{(\ell+\frac{1}{2})}}\right) \quad . \tag{6.45}$$

and return to step 1 for another cycle.

6.2 Obtaining and Using the Fission Matrix

The fission matrix, $\hat{\mathbf{L}}$, may be computationally obtained in a number of different ways as described in Section 2.4. We will focus on the Monte Carlo and diffusion fission matrices. Any type of fission matrix may be used to accelerate any type of criticality calculation. A Monte Carlo-obtained fission matrix may be used to accelerate a Monte Carlo calculation. A diffusion-obtained fission matrix may be used to accelerate a diffusion calculation or a Monte Carlo calculation. Other combinations, though not necessarily practical, are possible.

Using a cumulative Monte Carlo fission matrix results in a fission matrix, available while the calculation is in process, that statistically improves in accuracy each cycle. The Monte Carlo fission matrix is easily accumulated on the typically complicated Monte Carlo cells; it does not require a regular spatial grid.

If a series of diffusion calculations is used to estimate the fission matrix, that set of calculations need be performed only once at the beginning of the computation, thereby eliminating step 2 of the fission matrix method at every cycle. The diffusion fission matrix has the advantage of containing no statistical noise.

6.3 Filtering the Monte Carlo Statistical Noise

Implementing fission matrix acceleration in a Monte Carlo calculation may also require "filtering" the statistical noise, whether the fission matrix is from Monte Carlo or diffusion. The statistical noise occurs in the driving term–the residual of successive fission sources–of the correction equation, Equation 6.40. The statistical noise tends to have a high frequency which can affect lower frequencies through the acceleration and induce instability. We discuss three ways to filter the statistical noise:

- diffusion filter
- looping
- chopping
  - local
  - global .

The *diffusion filter* (for Monte Carlo) selectively smooths the high frequency fluctuations in a function, say, $\rho(x)$. The strength of the filter depends on a user-chosen parameter α^2 and produces the smoothed function, say, $\gamma(x)$. The filter equation is a second-order, diffusion-like equation:

$$-\alpha^2 \frac{d^2}{dx^2}\gamma(x) + \gamma(x) = \rho(x) \quad , \tag{6.46}$$

$$\gamma(0) = \gamma(L) = 0 \quad . \tag{6.47}$$

The filter behaves like the diffusion equation. It smooths out high-order fluctuations in a function while leaving the low-order components untouched. It preserves the

zeroth moment of the function (or, conserves the neutrons). An assumed form of $\rho(x)$,

$$\rho(x) = e^{i\lambda x} \quad , \tag{6.48}$$

demonstrates how the smoothed function $\gamma(x)$, the solution of Equation 6.46, has damped high frequencies:

$$\gamma(x) = \frac{\rho(x)}{1 + (\alpha\lambda)^2} \quad . \tag{6.49}$$

The filter allows low frequencies ($\lambda \approx 0$) of $\rho(x)$ to pass by unscathed, whereas the filter suppresses high frequencies of $\rho(x)$.

The smoothing operation defined by Equation 6.46 is applied to $\hat{f}^{(\ell+\frac{1}{2})}$ and $\hat{f}^{(\ell)}$ on the right side of Equation 6.29. Note that to apply the diffusion filter, we must impose a spatial grid and discretize Equation 6.46.

There are many, many other kinds of filters similar in spirit to the diffusion filter. One filter might simply consist of replacing a value at a point with the average of it and all the surrounding values.

The other two filters, looping and chopping, are more specific to our acceleration methods. *Looping* is an attempt to filter the driving term of the acceleration equation, Equation 6.29, by multiplying it by the fission matrix n times. The acceleration equation then becomes

$$(\mathbf{I} - \frac{1}{\hat{k}}\hat{\mathbf{L}})\hat{g}^{(\ell+1)} = \left(\frac{1}{\hat{k}}\hat{\mathbf{L}}\right)^n \hat{\mathbf{L}} \left(\frac{1}{k^{(\ell+1)}}\hat{f}^{(\ell+\frac{1}{2})} - \frac{1}{k^{(\ell)}}\hat{f}^{(\ell)}\right) \quad . \tag{6.50}$$

The effect of multiplying the right hand side by the fission matrix is to damp out the high frequencies, just as the hyperbolic transport equation does. However, larger values of n produce more filtering, or damping, and, adversely, less gain in acceleration. More than likely, there are problematic optimal values of n. We did not make

a lot of use of this filter, because, in one-dimensional slab geometries, the diffusion filter seemed more effective. Looping is attractive in problems with complicated geometries because it does not require a regular spatial grid.

Local chopping is the simple task of limiting the multiplicative correction, $\hat{g}^{(\ell+1)}$, to below a ceiling of a and above a floor of $1/a$, where a is real and $a > 1$. Local chopping may produce a bias because it does not preserve any qualities of the correction; portions of the correction may be limited according to a, while other portions are not limited. Note that, even when local chopping is not employed, zero always acts as a floor because we do not keep track of negative particles.

Global chopping is similar to local chopping, except that it determines the damping factor, β, that keeps the most offending multiplicative correction (the smallest or largest) above the floor or below the ceiling. Then it recalculates the entire correction with this value of β. While global chopping does not instill the bias that local chopping may, its acceleration gain may be seriously diminished.

Whatever type of filtering is used, it is not independent of the damping factor β. In Equation 6.40, β damps out the correction for all frequency modes. If filtering is absent, a lower value of β may damp the offending high frequencies, but it also cuts back the low-order gain in acceleration. If filtering does its job and smooths the high frequency noise, β may be increased, resulting in stability and greater acceleration. It is evident that there are, interdependently, optimal degrees of filtering and values of damping.

6.4 Test Problems

We consider three different monoenergetic, one-dimensional slab geometry problems, each with isotropic scattering. All three have vacuum boundaries. The first

is a 60 mfp homogeneous slab with Σ_t=1.0, Σ_s=0.7, and $\nu\Sigma_f$ = 0.30713574 cm^{-1}, as shown in Figure 6.1. These physical parameters are such that the slab is critical

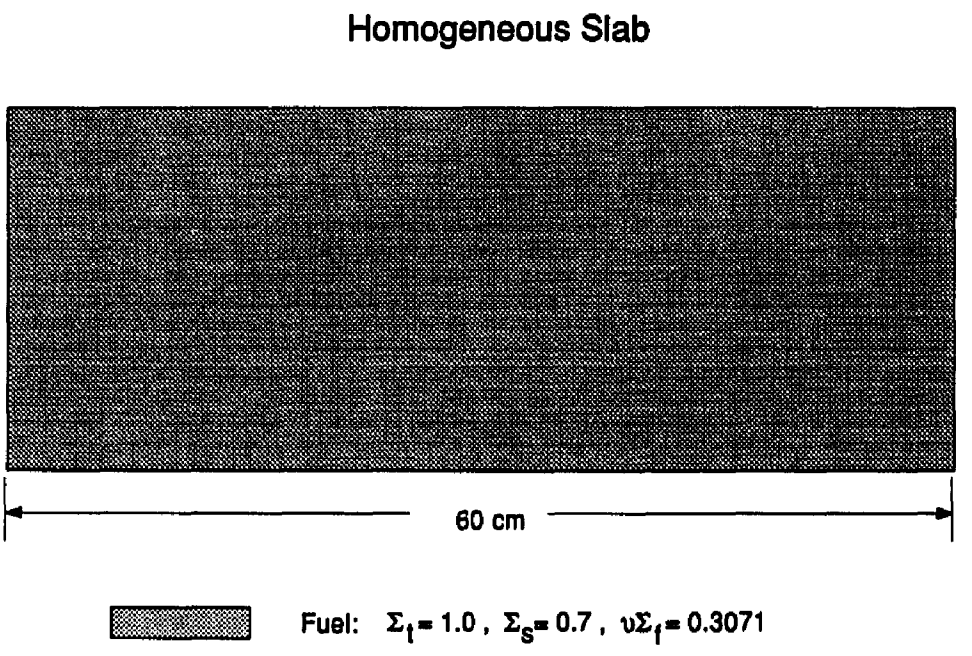

Figure 6.1: Homogeneous slab test problem: 60 mean free paths thick with a scattering ratio of 0.7 and dominance ratio of about 0.991.

when it is 20 mfp thick [Kap74]. We consider a thicker slab so that the dominance ratio is closer to unity. The dominance ratio is about 0.991. The k_{eff} of the system is about 1.02082. Both these values were obtained from a fine mesh, S_{32} calculation.

The second test problem is a uniform lattice. The fissionable fuel regions are made up of the same material as in the homogeneous slab. The fuel regions are each 2 cm thick and are separated by 1 cm thick regions of absorbing material with a scattering ratio of 0.001. The material at the boundaries is another 1 cm slab of absorber material. There are 19 fuel elements as shown in Figure 6.2. The dominance ratio of this problem is about 0.996, according to a fine-mesh S_{32} calculation. k_{eff} is about 0.59852.

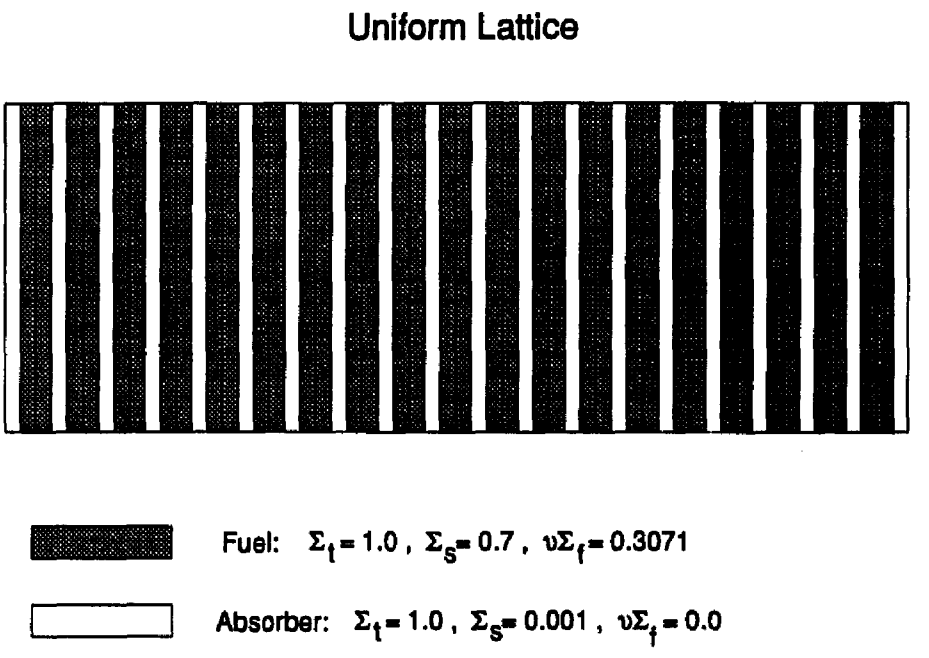

Figure 6.2: Uniform lattice test problem: 58 cm thick system with alternating 2 cm fuel regions and 1 cm absorber regions, for a total of 19 fuel elements.

The third test problem is a one-dimensional representation of the "k_{eff} of the world" problem [Whi71]. The "k_{eff} of the world" problem is a 9x9x9 array of subcritical plutonium spheres, except for the middle critical sphere. The problem is a difficult one for Monte Carlo calculations since the sampling is inevitably poor due to the small percentage of *important* fissionable material, located in the center sphere. Also, the usual initial flat source is very far from the converged source, which is peaked at the center critical sphere. Our one-dimensional slab representation of the "k_{eff} of the world" consists of replacing the center element of the uniform lattice in the previous test problem with hotter fuel. This representation is shown in Figure 6.3. The k_{eff} of the system is 0.72400 and the dominance ratio is 0.82318. For reference, a single regular fuel element surrounded by 1 cm slabs of absorbing material has a k_{eff} of about 0.4436. A hot fuel element surrounded by absorber has

a k_{eff} of about 0.5881.

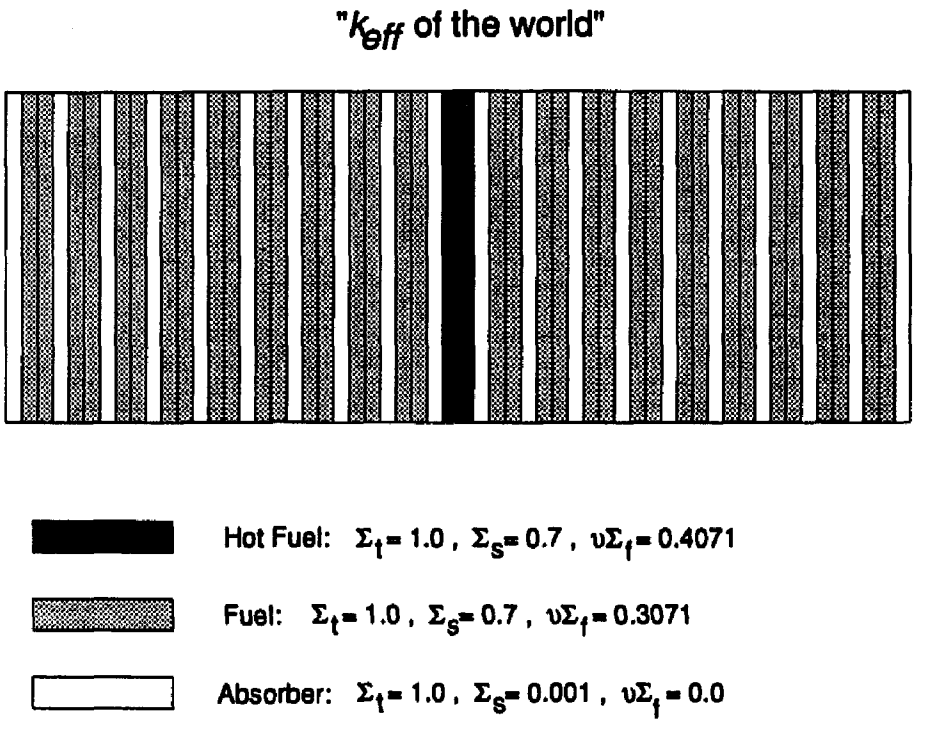

Figure 6.3: One-dimensional representation of the "k_{eff} of the world," consisting of the uniform lattice with the center element replaced by material with $\nu\Sigma_f = 0.4071$

6.5 Fission Matrix Acceleration Results

We present results using different variations of the fission matrix acceleration method. First we use a diffusion fission matrix on a coarse grid to accelerate a fine-grid diffusion fission matrix calculation in the homogeneous slab problem. This is a setup similar to that used for the Carter-McCormick method. These results give us an idea of what to expect for more sophisticated castings of the acceleration equation. Second, we present the results of using a diffusion fission matrix to accelerate S_N transport calculations for all three test problems. Third is a demonstration of a Monte Carlo calculation accelerated with a Monte Carlo fission matrix. In the next

section, we show the results of implementing Monte Carlo fission matrix acceleration into the production Monte Carlo code MCNP^{TM} [Bri94] and performing a calculation on a model of the actual 3-dimensional "k_{eff} of the world" problem.

6.5.1 Diffusion Fission Matrix-Accelerated Diffusion

We use a fine-grid diffusion fission matrix to simulate transport source iteration. Acceleration is delivered through a coarse-grid diffusion fission matrix. There are (at least) two ways of obtaining the coarse-grid diffusion fission matrix. The first is to simply estimate it through a series of diffusion calculations on the coarse grid. Therefore the diffusion fission matrix is *precalculated*–calculated before the source iteration begins. The adaptation of this type of diffusion acceleration to discrete-ordinates and Monte Carlo is straightforward. The second way to obtain the coarse-grid diffusion fission matrix is by a source-weighted collapse of the fine-grid fission matrix at each iteration. This was the method used in the chapter investigating Carter and McCormick's method. The analogous fission matrix in a purely Monte Carlo calculation is the cycle fission matrix. Effectively, though, it behaves like the cumulative fission matrix because it becomes more accurate each iteration (cycle). Nevertheless, we will call this the "cycle" diffusion fission matrix.

Unlike the Carter-McCormick and Modified Carter-McCormick methods, the diffusion fission matrix-accelerated diffusion calculations are stable over all coarse-grid cell sizes. The iterations and computing time required for convergence using the diffusion fission matrix are shown in Figure 6.4 for the homogeneous system. As the coarse grid becomes finer, fewer iterations are necessary. However, more computing time is required for the larger matrices in the acceleration equation. The optimal number of coarse mesh cells for 120 fine mesh cells is 20, resulting in a speedup of

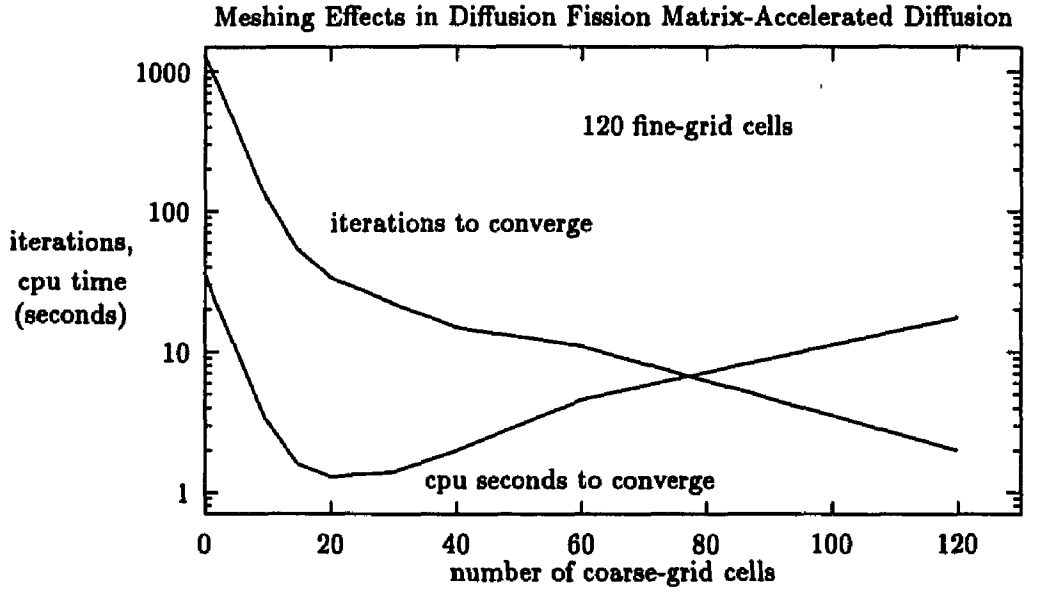

Figure 6.4: The iterations and time required for convergence of a diffusion criticality calculation when the coarse-grid diffusion fission matrix is precalculated.

28.

The iterations and computing time required for convergence when using the "cycle" diffusion fission matrix are shown in Figure 6.5. Again, the necessary number of iterations for convergence decreases for increasing number of coarse mesh cells. The minimum time necessary for convergence occurs for 10 coarse mesh cells, for a speedup of 10.5. Compared to the precalculated diffusion fission matrix, the "cycle" diffusion fission matrix acceleration requires fewer iterations to converge, but each iteration requires calculating the fission matrix and its eigenstate, so computing times are longer.

Figure 6.6 shows the convergence of the first and second Fourier modes for unaccelerated diffusion, precalculated diffusion fission matrix acceleration, and "cycle" diffusion fission matrix acceleration. The accelerated cases are for the optimal coarse mesh cell size. The expected value of the second Fourier mode coefficient is zero because the system is symmetric.

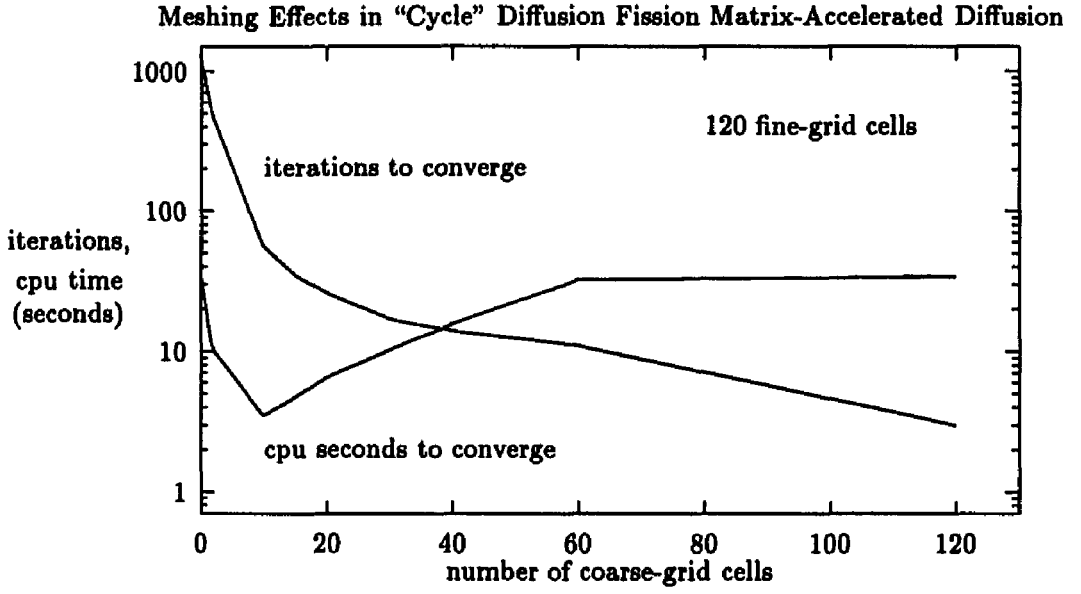

Figure 6.5: The iterations and time required for convergence of a diffusion criticality calculation when the coarse-grid diffusion fission matrix each cycle by the source-weighted collapse of the fine-grid fission matrix.

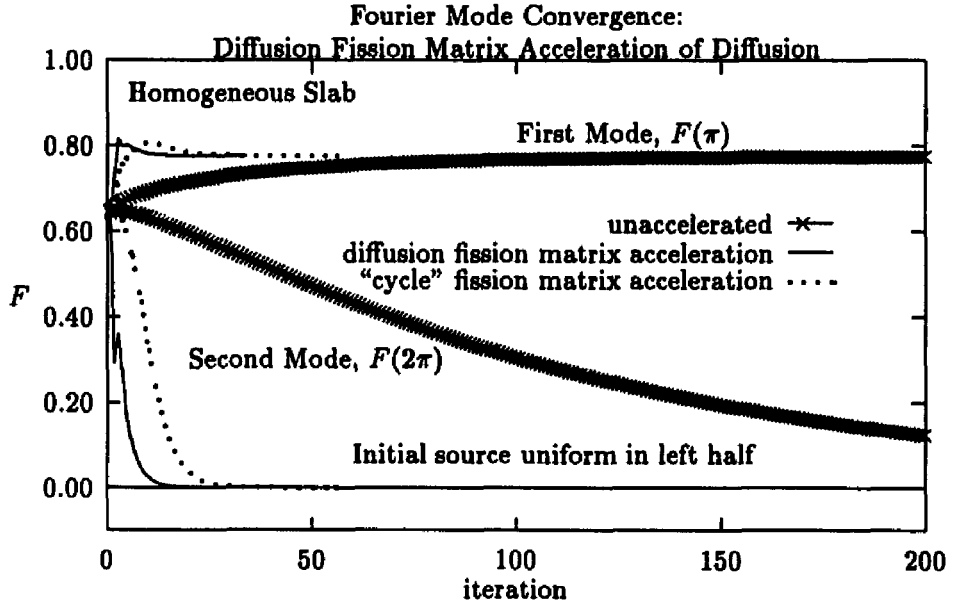

Figure 6.6: The convergence of the first and second Fourier modes for unaccelerated diffusion source iteration, precalculated diffusion fission matrix acceleration, and "cycle" diffusion fission matrix acceleration.

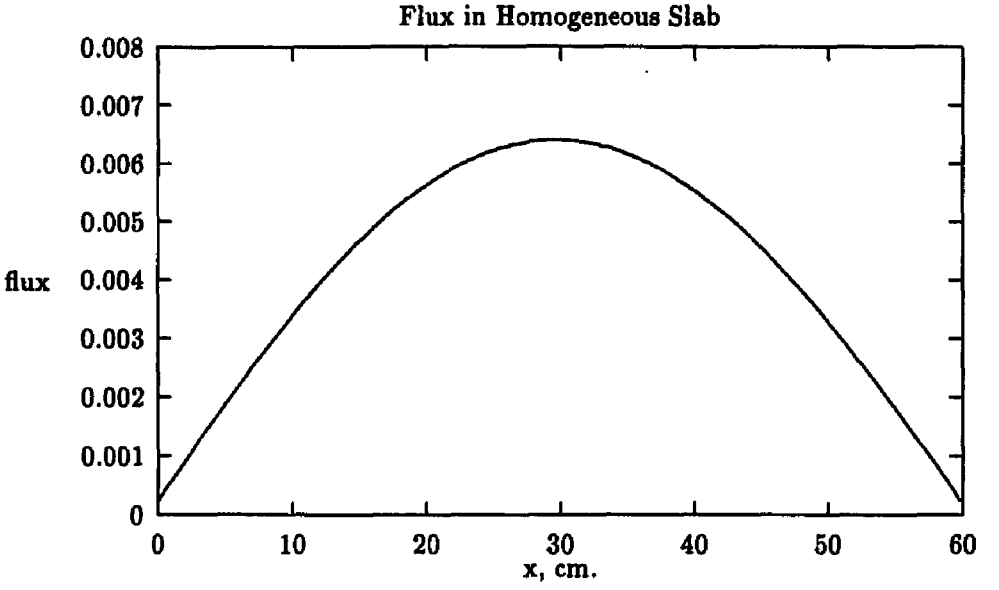

Figure 6.7: The converged flux for the homogeneous slab problem.

6.5.2 Diffusion Fission Matrix-Accelerated Discrete Ordinates Transport

The converged flux corresponding to the converged fission source for the homogeneous slab is shown in Figure 6.7. We use an S_{32} quadrature set for this problem and break the system into 240 uniform fine mesh cells. The convergence criterion for the fission source (ℓ_∞ norm) is 10^{-4}. We begin with an initial source containing 2/3 of the source in the left half and 1/3 in the right half with each half distributed uniformly. This is a deliberately bad source guess, chosen to demonstrate the efficacy of the method. We calculate the diffusion fission matrix on a coarse grid with anywhere from two cells up to the number of fine mesh cells. As the number of coarse grid cells decreases, the amount of material smearing, or homogenization, increases, which may or may not be beneficial. Note that if the initial source was flat for this symmetric problem, two coarse cells would provide no acceleration. As we increase the number of coarse cells (more resolution), the acceleration requires fewer iterations to converge, as shown in Figure 6.8. However, acceleration work for N coarse

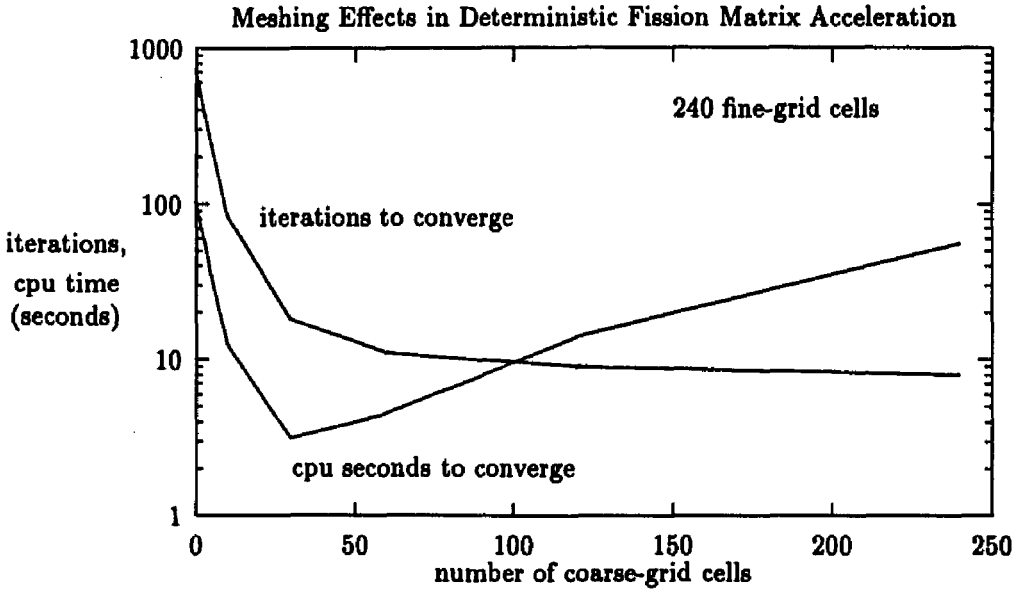

Figure 6.8: Effect of the number of coarse mesh cells in the Diffusion Fission Matrix Acceleration of discrete ordinates transport. Although the number of iterations required for convergence decreases with more coarse mesh cells, more cells require more work and an optimal exist such that the computing time is minimized.

cells increases as N^3, so, as Figure 6.8 also shows, an optimal number of coarse mesh cells exists, such that the computation time is minimized. We found for all three test problems that the optimal coarse mesh cell contained eight (2^3) fine mesh cells. Also, damping was not required for these deterministic problems; reducing β decreased the acceleration.

Figure 6.9 shows the convergence of the Fourier coefficients for the first and second modes. For 30 coarse mesh cells, the accelerated case requires 18 iterations to converge, whereas the unaccelerated case requires 723 iterations. Since the problem is symmetric, the expected value of the second Fourier mode coefficient is zero upon convergence. Comparing the running times on a Sun SPARC20 of 106 and 3.15 seconds, the acceleration realized a speedup of 33.7.

The second test problem is the uniform lattice. This is a very difficult problem

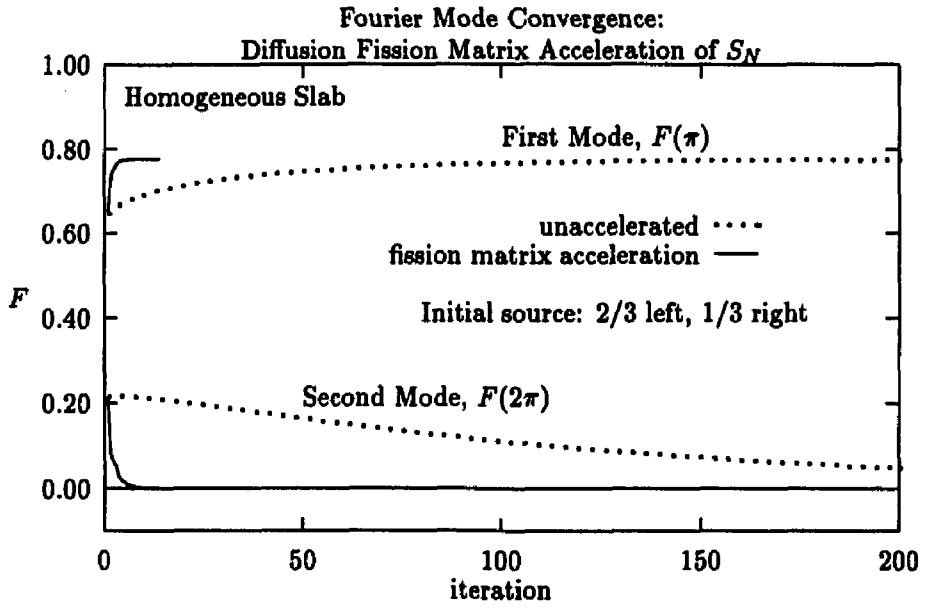

Figure 6.9: The first and second Fourier mode coefficients for unaccelerated and diffusion fission matrix accelerated discrete ordinates for the homogeneous problem.

with dominance ratio 0.996. Beginning with a flat initial source and 464 fine mesh cells, the unaccelerated discrete ordinates required 434 iterations (227 seconds) to converge. The converged flux is shown in Figure 6.10. Using 58 coarse mesh cells, the fission matrix acceleration method required only 18 iterations (12.6 seconds) to converge, giving a speedup factor of 18. The Fourier mode coefficient convergence is shown in Figure 6.11 for the first and third modes.

The third problem is the one-dimensional "k_{eff} of the world" problem. The converged flux for this problem is shown in Figure 6.12. For an initial flat source, Figure 6.13 shows the convergence of the first and third Fourier mode coefficients. The unaccelerated calculation took 66 iterations and 35.5 seconds to converge, and the diffusion fission matrix accelerated S_{32} with 58 coarse mesh cells and $\beta = 1$ took 15 iterations and 9.3 seconds for a speedup of 3.8.

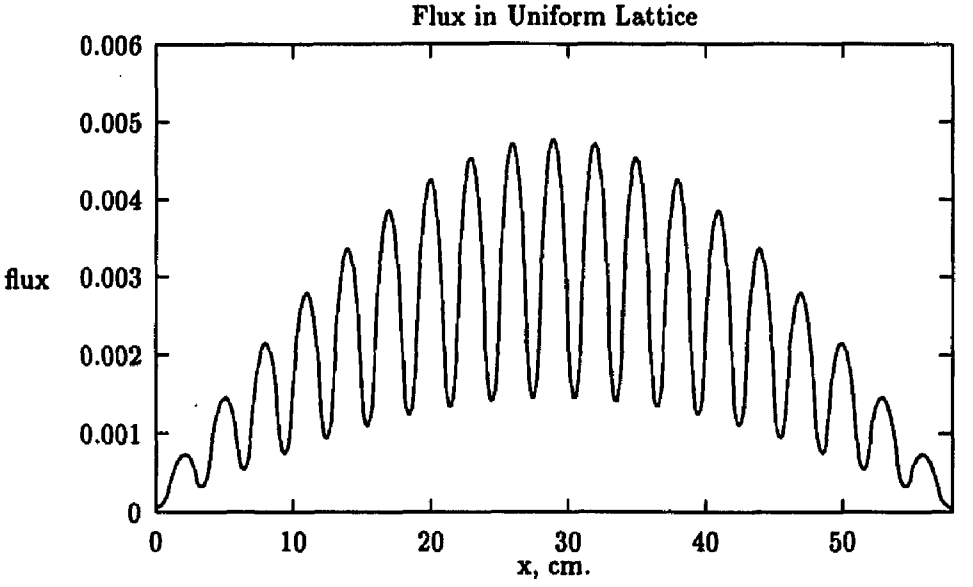

Figure 6.10: The converged flux for the uniform lattice test problem.

6.5.3 Fission Matrix Accelerated Monte Carlo

If Monte Carlo contained no statistical noise, the results of accelerating Monte Carlo criticality calculations would be similar to those of accelerating deterministic criticality calculations. Unfortunately, the statistical noise, which is high-order, is propagated by the acceleration into low-order errors. This undesirable phenomenon is not overcome even when using a diffusion fission matrix instead of a Monte Carlo fission matrix. The driving term of the acceleration equation is the primary source of the noise. We use the diffusion filter in the cases presented here. Increasing the density of particles in important regions of a system reduces the statistical noise and therefore reduces the need for filtering. Validity of this statement is found by comparing the Monte Carlo results for the homogeneous slab and the one-dimensional "k_{eff} of the world" problem later in this subsection. The latter calculation appears nearly deterministic in nature due to the small important fissionable component.

We first apply the Monte Carlo fission matrix acceleration method to the 60 cm

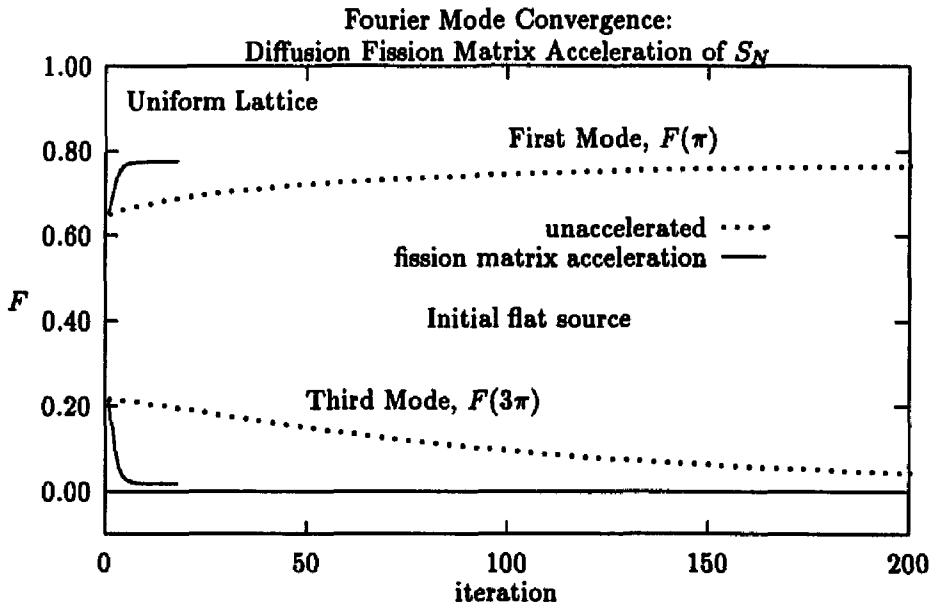

Figure 6.11: The first and third Fourier mode coefficients for unaccelerated and diffusion fission matrix accelerated discrete ordinates for the uniform lattice.

homogeneous slab. Figure 6.14 shows the convergence of the first and second Fourier modes for both the unaccelerated and accelerated cases. For both cases, the initial source had 2/3 of the particles in the left half and 1/3 of the particles in the right half of the slab. There were 60 uniform 1 cm cells and 5000 histories per cycle. For this symmetric system, the second Fourier mode has expected value zero. The unaccelerated case takes approximately 110 cycles to converge. The diffusion filter parameter was held constant over the cycles, $\alpha^2 = 5.0$. Since the fission source is smooth and slowly varying over space, a relatively higher value of α^2 is possible. For heterogeneous problems, the filter could undesirably smooth out actual physical fluctuations in the fission source. The all-mode damping (β) of the correction is held at a constant 0.2 for the first three cycles, then it drops off exponentially. Convergence of the accelerated case takes about 20 cycles. Comparing the computer times at this cycle and the unaccelerated cycle 110 gives a speedup of 5.0.

The second problem is the one-dimensional simulation of Whitesides' "k_{eff} of

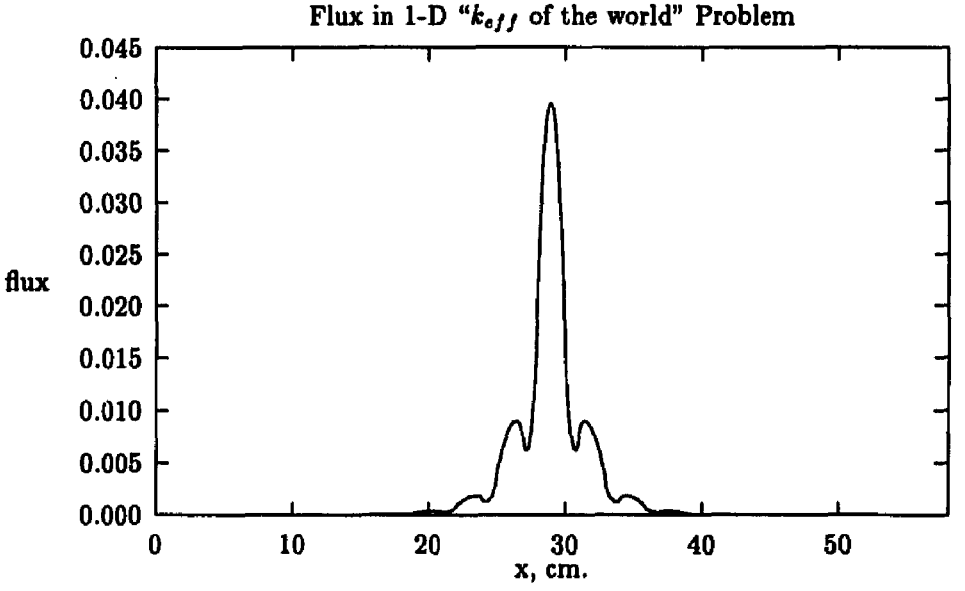

Figure 6.12: The converged flux for the one-dimensional "k_{eff} of the world" test problem.

the world" problem [Whi71]. For 5000 histories per cycle in 58 mesh cells, the initial source was flat across the entire system. The driving terms of the acceleration equation were filtered by the diffusion filter with $\alpha^2 = 5n/(n+10)$. Thus, the filter parameter starts out at about 1/2, then approaches 5. If the filter parameter is too large, the combined filtering and acceleration will not sufficiently overcome the artificial discontinuity at the center of the slab in the initial fission source. In some underdamped cases, the fission source oscillates about the initial artificial discontinuity. Because eventually and effectively there was a high density of particles in the important fissionable regions, the calculations appeared nearly deterministic. Therefore the full correction ($\beta = 1.0$) was possible. Figure 6.15 shows that unaccelerated Monte Carlo converges on the hot component in about 35 cycles, whereas the accelerated Monte Carlo takes about 6 cycles. The computational time speedup is about 4.8.

Compared to the second problem, the acceleration in the first problem is more

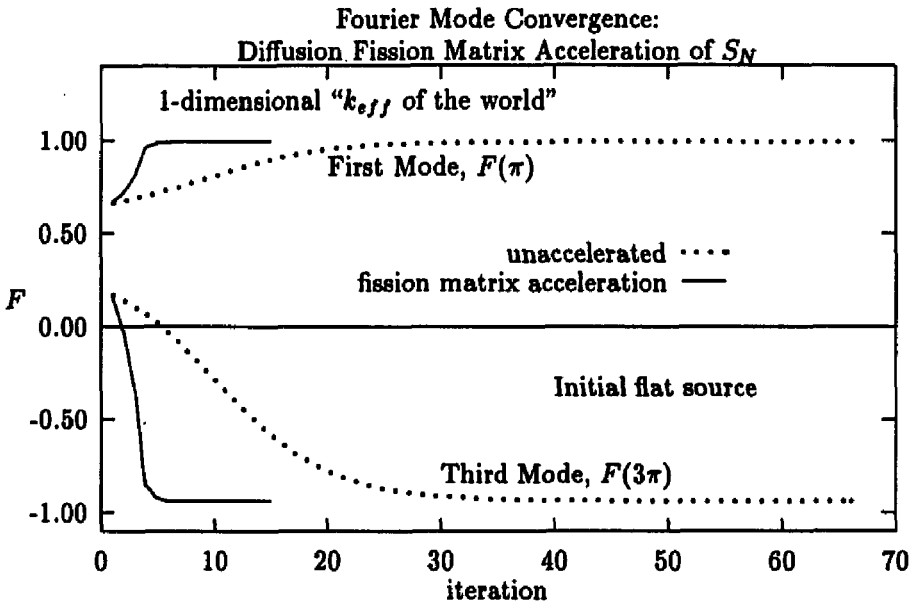

Figure 6.13: The first and third Fourier mode coefficients for unaccelerated and diffusion fission matrix accelerated discrete ordinates for the one-dimensional "k_{eff} of the world" problem.

sensitive to the damping and filtering parameters, β and α^2. The difference occurs due to the different particle densities in the important fissionable volumes. The "k_{eff} of the world" simulation, upon convergence, has a very large particle density in the hot component and a low particle density elsewhere, and appears almost deterministic. (In a deterministic calculation, filtering is not required and, unless it is severely heterogeneous, neither is damping.) The large homogeneous system has more statistical noise, so the filtering becomes very important. The filter may not smooth the fission source optimally, and the noise that the filter does not remove must be damped out. Therefore, the parameters α^2 and β are not independent.

Accelerating the Monte Carlo source convergence in the uniform lattice test problem is a very difficult task. Acceleration with this geometry is definitely possible as evidenced by the deterministic test problems. The acceleration method is unbiased, meaning that it yields the same converged solution as the unaccelerated method,

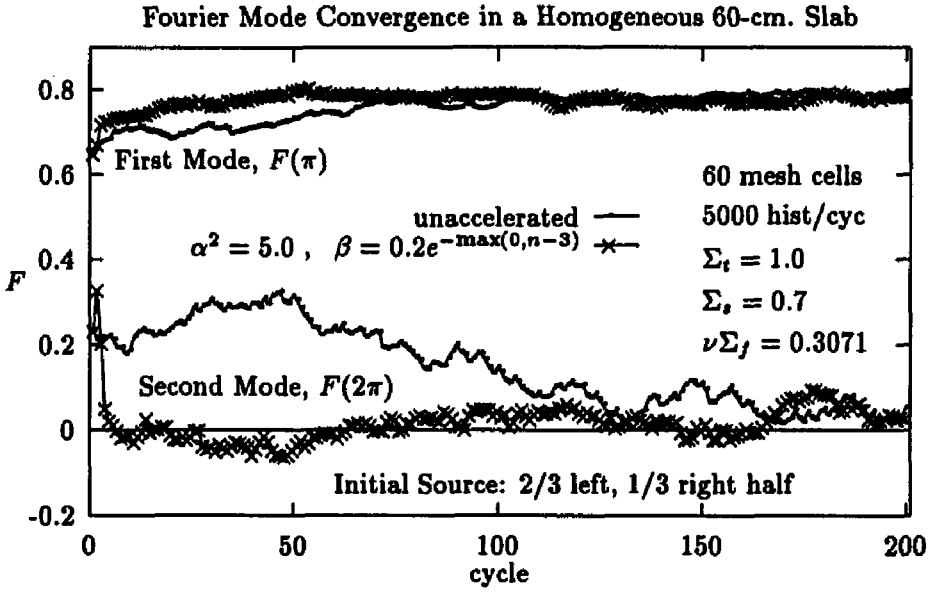

Figure 6.14: Convergence of the first and second Fourier modes for unaccelerated Monte Carlo and filtered and damped accelerated Monte Carlo in a homogeneous slab.

only faster. However, unaccelerated Monte Carlo has inherent difficulties converging the source for high dominance ratio problems consisting of a lattice of identical components. For example, if there were two identical critical reactors separated by a large distance, all the particles in a Monte Carlo simulation would eventually end up in one of the reactors. (This example is attributable to Tom Booth of Los Alamos National Laboratory.) The basis for this comment lies in the fact that the two-reactor example has a dominance ratio very near unity. Each reactor is expected to have the same number of particles. However, because of statistical noise, one reactor will almost always have more particles than the other. Furthermore, in a high dominance ratio problem, regions that have a population of particles higher than expected will tend to maintain that high population. The end result, after many cycles, is that one reactor is depleted of Monte Carlo particles.

The uniform lattice problem possesses similarities to the two-reactor example.

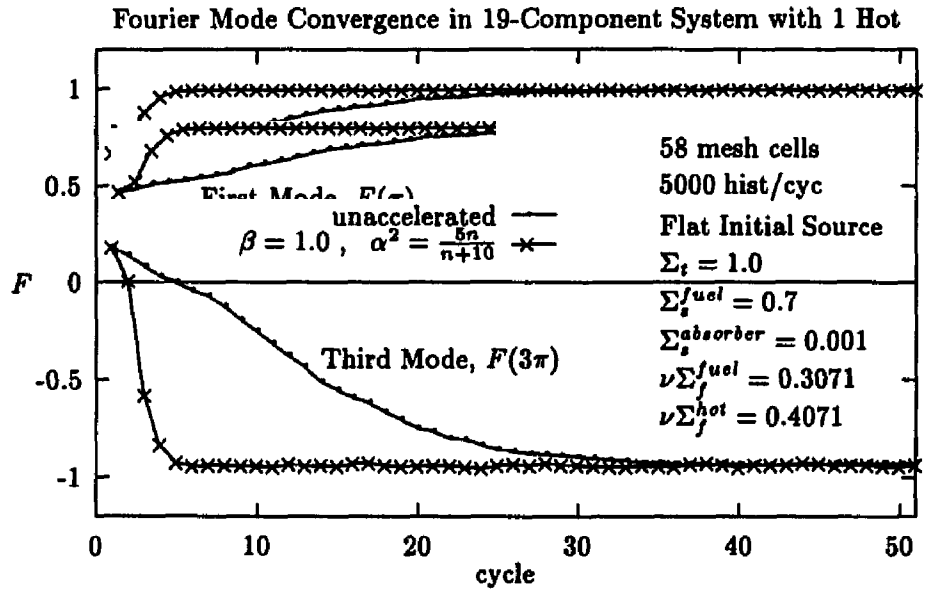

Figure 6.15: Convergence of the first and third Fourier modes for unaccelerated Monte Carlo and filtered and accelerated Monte Carlo in a one-dimensional "k_{eff} of the world" simulation.

The absorber regions in our uniform lattice are fairly thin, so all the particles will not collect in a single fuel element. Still, we see collections of adjacent fuel elements persistently maintaining their too large or too small populations. In an unaccelerated case, we ran 5000 histories per cycle, began with a flat source guess, skipped 30 (inactive) cycles, and ran 200 active cycles. The flux, which is still not converged after 200 active cycles, is shown in Figure 6.16 at that cycle. The very small error bars indicate that the population in each fuel element is not changing very much. Over 10's or 100's of cycles, the fission source would appear converged, when, in fact, it really is not.

Accelerating the Monte Carlo calculation for the uniform lattice meets with little success. Filtering this system is different than filtering a homogeneous system. Here, it is as if there are two frequencies that the filtering should target: the high frequencies due to the statistical noise within the fuel elements, and the low frequen-

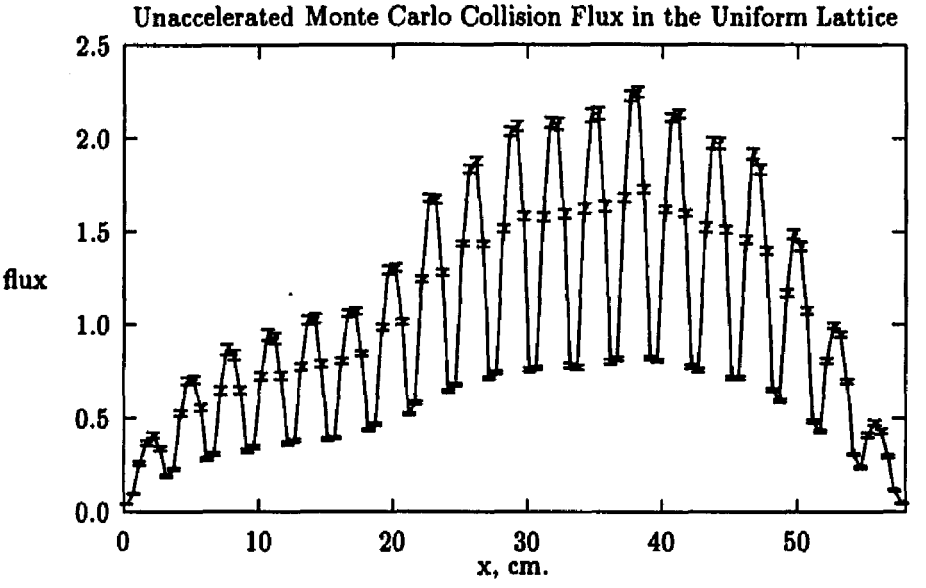

Figure 6.16: The Monte Carlo collision flux in the uniform lattice after 200 active cycles.

cies describing the global shape. The accelerated method essentially arrives at the state of incorrect populations faster, although it may not arrive at the same state as the unaccelerated method because of statistical noise. So, for this system, the acceleration appears unable to overcome the inherent shortcomings of Monte Carlo.

6.6 Fission Matrix Acceleration in MCNP

The fission matrix acceleration method is extendible to more complicated Monte Carlo simulations. We demonstrate the acceleration method as implemented in MCNP, a general-purpose production Monte Carlo code. MCNP is able to model complicated three-dimensional geometries, and simulates transport with continuous energy.

The modified version of MCNP uses only the Monte Carlo fission matrix. The Monte Carlo fission matrix is obtainable on the typically complicated cells that make up an MCNP geometry and is fully self-contained in the code. Using a diffusion

fission matrix would require a grid, as opposed (or in addition) to complicated Monte Carlo cells, and linking to a production diffusion theory code. The grid would not necessarily have to be involved in the particles tracking; it could simply overlay the complicated Monte Carlo cells. So, a diffusion fission matrix in a production Monte Carlo code is possible, but much more complicated than a self-contained Monte Carlo fission matrix. These same arguments apply to not being able to practically use the diffusion-like filter. Instead, we employ the looping filter, where the driving term of the acceleration equation is multiplied by the fission matrix to reduce some of the statistical noise. Although not employed, chopping is certainly possible, too.

The test problem we consider for the modified version of MCNP is the "k_{eff} of the world" problem, a 9x9x9 array of subcritical plutonium spheres with center sphere critical and the whole array surrounded by a water reflector. A three-dimensional rendering of the system without the inner surface of the water reflector is shown in Figure 6.17. Notice the larger, critical sphere in the center. This rendering was done by Ken Van Riper of Los Alamos National Laboratory using Sabrina^{TM} [2] [Van93][Lee94]. MCNP also does two-dimensional geometry plotting; a two-dimensional cross section through the center of the geometry is shown in Figure 6.18.

The problem used 5000 histories per cycle with the initial source locations at points in the center of each of the 729 spheres. Twenty cycles were allotted to converge the source, followed by 100 active cycles. Twenty cycles is not nearly enough to converge the source, but it is a typical number used by criticality safety people running Monte Carlo codes. The onset of fission matrix acceleration was deferred 20 cycles just to make sure that sampling would have no adverse effects on the fission matrix elements. Each fission matrix element contained one sphere. The

[2] Sabrina is a trademark of the Regents of the University of California, Los Alamos National Laboratory

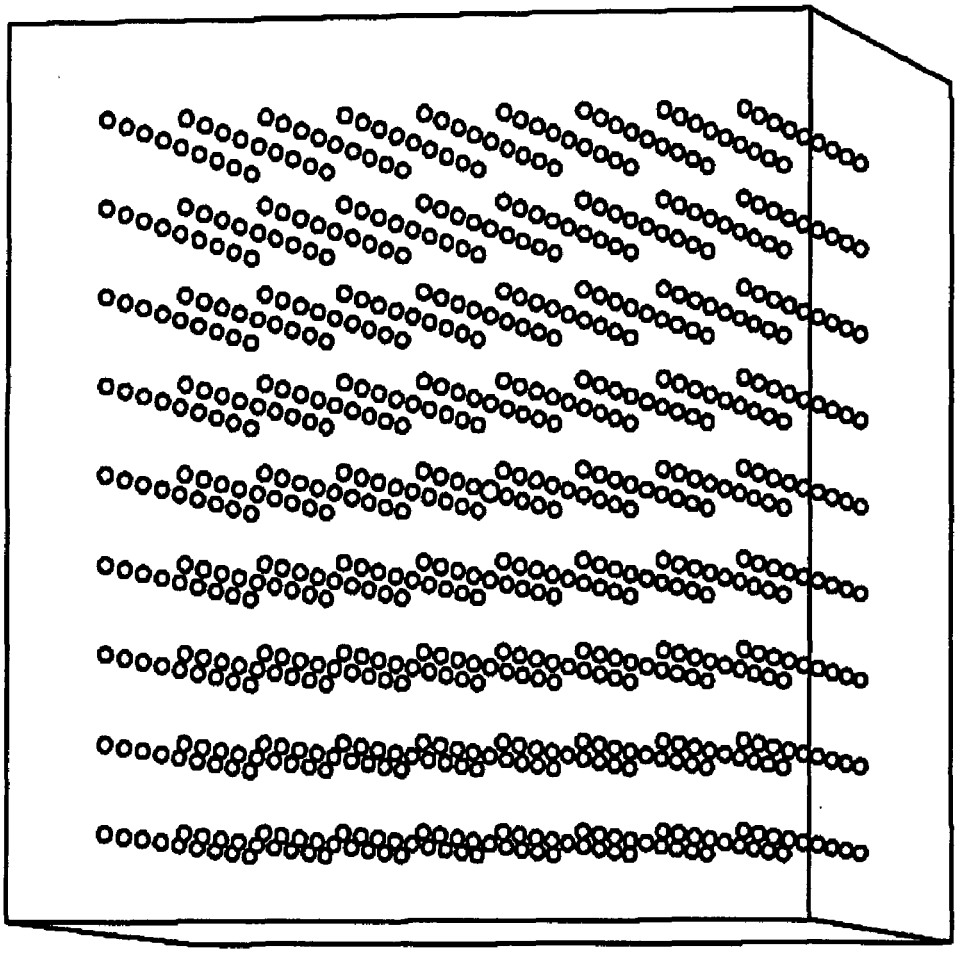

Figure 6.17: Three-dimensional rendering of the "k_{eff} of the world" problem without the inner water reflector surface by Sabrina. The larger critical sphere is located in the center.

value of 20 was probably conservatively large. We employed no filtering and set the damping factor to

$$\beta = 0.9e^{-\frac{1}{2}(n-20)} \quad , \quad n > 20 \quad , \tag{6.51}$$

so that, on the first cycle that was acceleration, cycle 21, the damping factor was $0.9e^{-1/2}$ and dropped off exponentially. Since we do not have a regular grid, we do not have the luxury of using the informative experimental Fourier analysis to gauge convergence. Other measures exist, though. Figure 6.19 shows the cycle value of the collision k_{eff} estimator at each cycle. After cycle 20, engaging the acceleration

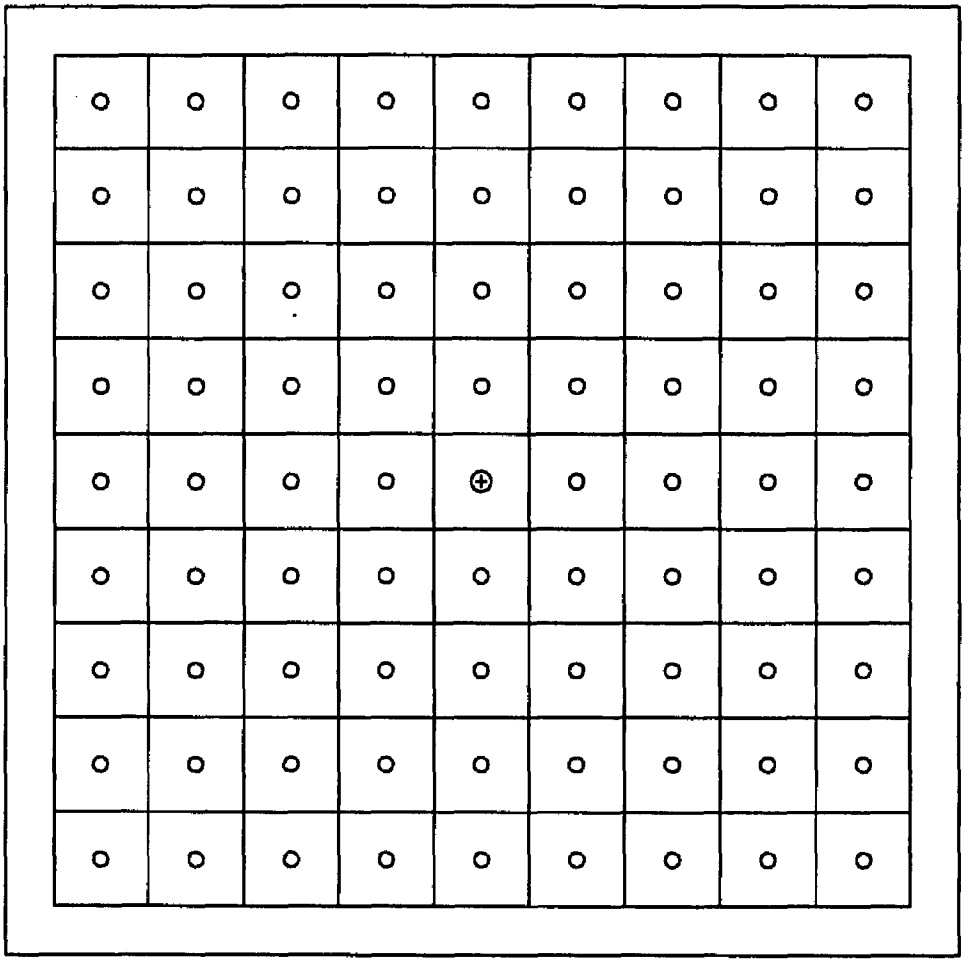

Figure 6.18: MCNP plot of a 2-D cross section of the water-reflected array problem with the larger, critical sphere in the center.

very quickly puts more particles into the important center sphere. The collision k_{eff} jumps immediately to critical and oscillates around 1.0. By cycle 43, β was small enough so that no additional particles would be killed or cloned, and the acceleration automatically shut itself off. It takes unaccelerated MCNP about 90 cycles to converge. Figure 6.20 shows the number of particles in the center critical sphere as a function of cycle. The acceleration may have overshot the correction a little at first, and, since β was decreasing, it could not as quickly correct the overshoot.

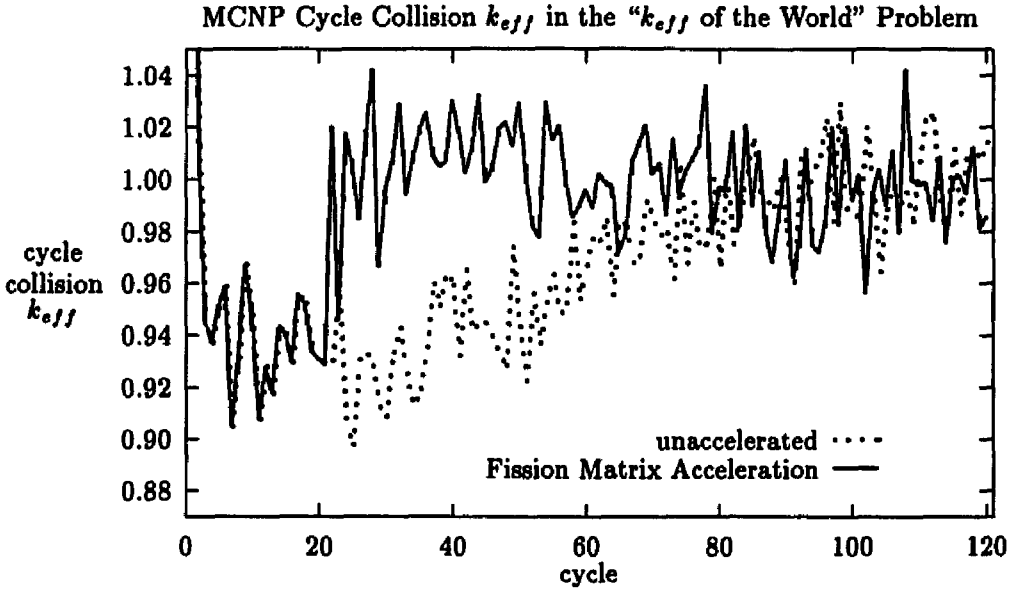

Figure 6.19: The cycle collision k_{eff} estimator for unaccelerated and fission matrix acceleration MCNP on the "k_{eff} of the world" problem.

The three-combined k_{eff} estimator is a linear least squares combination of the average collision, absorption, and track length estimators [Urb95]. The average k_{eff} estimators equally weight the cycle k_{eff} estimates from each active cycle. Therefore, in the unaccelerated case, the poorly converged k_{eff} estimates in the early active cycles contaminate the average, and hence, the three-combined, k_{eff} estimators throughout the entire run. Figure 6.21, when compared to Figure 6.19, shows the contamination on the three-combined k_{eff} estimator due to the unconverged source.

MCNP contains statistical checks that help the user assess the quality of the calculation [For94]. The unaccelerated case alerted the user that the first and second half three-combined k_{eff} estimates did not agree at the 99% confidence level, indicating a drift due to an unconverged source. In the fission matrix accelerated case, the cycle track length k_{eff} estimates did not pass the normality check. This failed test is understandable since the the acceleration began at the beginning of the

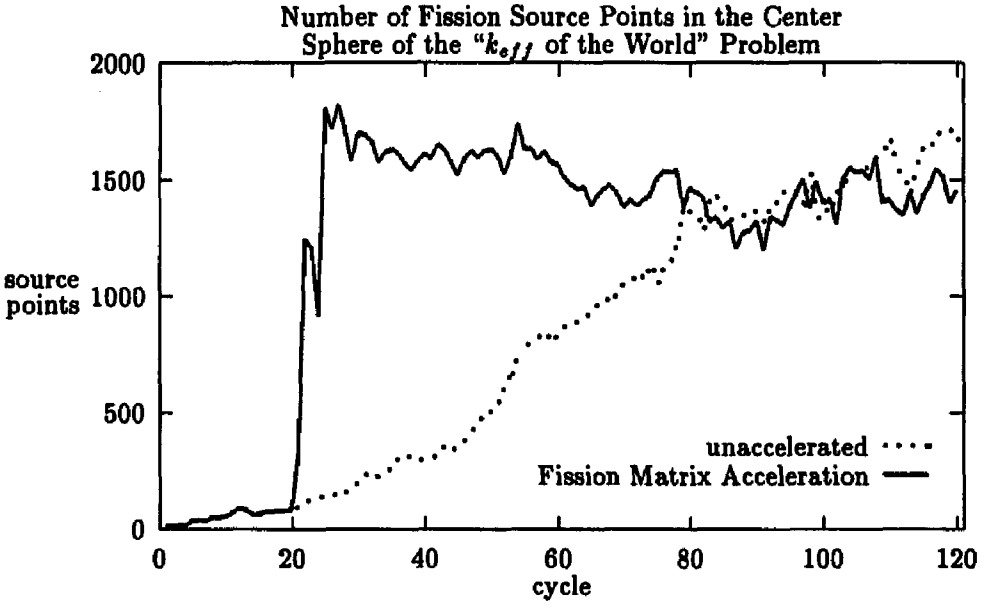

Figure 6.20: The number of source points in the center critical sphere of the "k_{eff} of the world" problem for unaccelerated and fission matrix accelerated MCNP.

active cycles. Ideally the acceleration should converge the source before the active cycles. Fortunately, MCNP gives the results for any number of cycles skipped. For the accelerated case, the minimum standard deviation occurred at 23 cycles skipped, giving a 95% confidence interval of [0.9972,1.0033], meaning that the precise value of k_{eff} lies within this range with 95% confidence. The minimum standard deviation for the unaccelerated case occurred at 116 inactive cycles and 4 active cycles, giving a 95% confidence interval of [0.9854,1.0247]. However, four cycles is nowhere near enough cycles to consider in the averaging. This statistical check is another indication to the user that the unaccelerated case has problems. The three-combined k_{eff} estimate by cycles skipped is shown in Figure 6.22.

6.7 Summary and Discussion

The Fission Matrix Acceleration method is obtained by deriving an exact correction to the fission source from an integral form of the transport equation. Applying

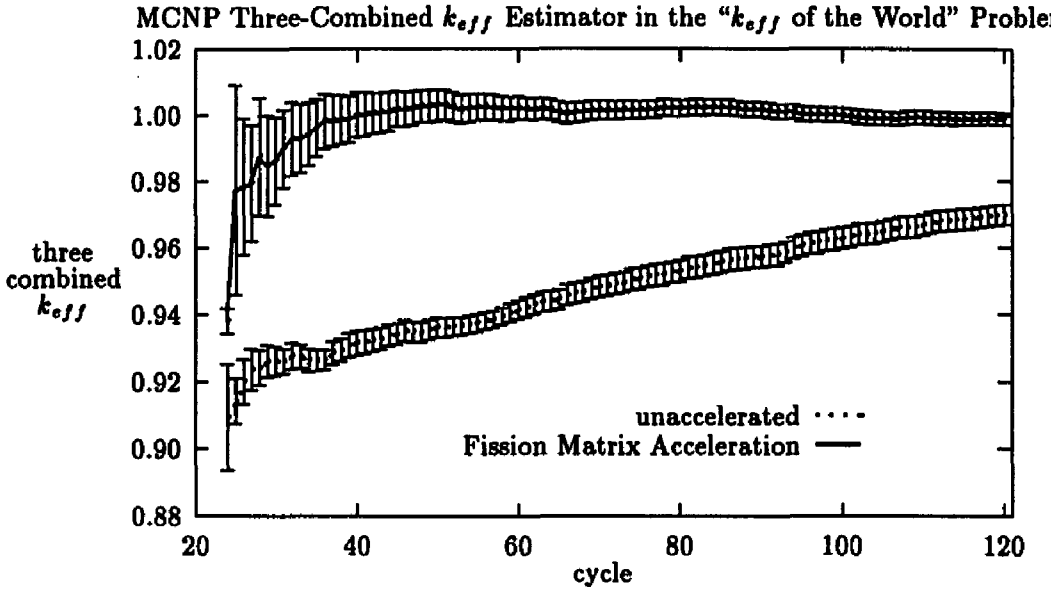

Figure 6.21: The three-combined k_{eff} estimator for unaccelerated and fission matrix acceleration MCNP on the "k_{eff} of the world" problem.

the exact correction yields the exact solution and concludes the calculation in one cycle or iteration. If not impossible, obtaining the the exact correction is impractical. The fission matrix, on the discretized system, provides an approximation to the exact kernel and makes the method practical.

The Fission Matrix Acceleration method is designed to reduce the number of deterministic iterations, or Monte Carlo inactive cycles–those required to converge the fission source. It works best when the initial assumed fission source is far from the true fission source. This method is also efficient for systems with high dominance ratios. These are systems for which unaccelerated Monte Carlo would require many inactive cycles to converge the source.

We first posed the acceleration in the form where a coarse-grid diffusion fission matrix was used in accelerating a fine-grid diffusion fission matrix. Two different ways of obtaining the coarse-grid fission matrix resulted in speedups of 11 and 28 for the homogeneous slab test problem.

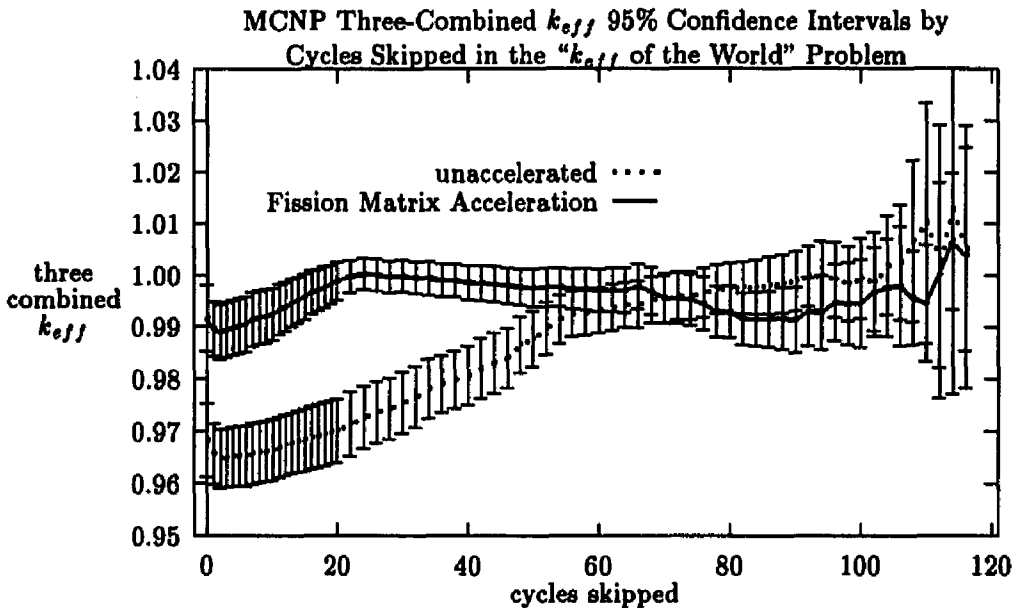

Figure 6.22: The three-combined k_{eff} estimator for unaccelerated and fission matrix acceleration MCNP as a function of cycles skipped for the "k_{eff} of the world" problem.

Next we used the diffusion fission matrix to accelerate discrete ordinates transport calculations. Speedups ranged from 3.8 for the "k_{eff} of the world" problem to 34 for the homogeneous slab.

Applying fission matrix acceleration to Monte Carlo calculations is yet another example of trying to make a Monte Carlo calculation behave like a deterministic calculation. The major deterrence to success is Monte Carlo's statistical noise. The perfect example is the Monte Carlo criticality calculation itself, where Monte Carlo is made to adhere to source iteration. One repercussion is a bias in the eigenvalue. Luckily, the bias is inversely proportional to the number of histories per cycle, and usually negligible [Gas75][Bow83][Bri86][Gel90][Gel91][Gel94]. Asaoka, et al. had some success applying coarse-mesh rebalancing to Monte Carlo eigenvalue calculations [Asa74]. Accumulating data over coarser meshes implies more particles and less statistical noise. Swaja accelerated Monte Carlo source convergence through

Chebyshev extrapolation [Swa73]. However, Swaja found it necessary to filter the statistical noise with a Kalman filter.

If it was possible to totally eliminate the statistical noise in a Monte Carlo criticality calculation, Fission Matrix Acceleration applied to Monte Carlo would behave similarly as in a deterministic calculation. Otherwise, the acceleration magnifies the high-order noise. In practice, we eliminate as much of the statistical noise as possible, so as to approach the deterministic characteristics. Some type of filter is used to reduce the high-order fluctuations in the driving term of the acceleration equation. Additionally, a damping factor β damps *all* frequencies of the additive correction. The selection of filtering and damping parameters is not automated. Acceleration success can be quite sensitive to these parameters for some problems. The parameters are not independent. If the filtering does not adequately rid the calculation of statistical noise, the damping will need increasing (lower β). Unfortunately, the damping also reduces the low-order acceleration gain. Too much filtering could introduce artificial and incorrect trends in the calculation that would manifest themselves in large oscillations.

For Monte Carlo, the resulting speedups for the homogeneous test problem and the one-dimensional "k_{eff} of the world" problem were about 5. Monte Carlo criticality code users traditionally perceive source convergence in terms of inactive cycles instead of computer time. They are accustomed to performing, say, 10 to 30 inactive cycles, so even a modest speedup of 5.0 is very beneficial in obtaining accurate solutions for these types of systems.

The Fission Matrix Acceleration method cannot, however, overcome some inherent deficiencies in Monte Carlo criticality calculations. The Fission Matrix Acceleration method is essentially unbiased–it arrives at the same solution as the unacceler-

ated calculation, only faster. Due to statistical noise, unaccelerated Monte Carlo has difficulties with the uniform lattice problem in that it may not converge to the correct source. In this case, the acceleration simply finds an incorrect source quicker. In Chapter VIII, we present a hybrid method that, since it is not unbiased, overcomes these difficulties.

6.8 Related Techniques for An Improved Initial Source

When the variations of the fission matrix acceleration are in place in a computer code, there exist other easy ways to obtain an initial source. For instance, the source can be started according to the diffusion solution. A drawback of this technique is that the diffusion solution may not adequately describe a system with many transport effects. In fact, for a system similar to the uniform lattice, except that it had much thicker absorber regions, the diffusion calculation would break down if the cells were not fine enough.

Another technique for an improved initial source is to use the eigenvector of the fission matrix. A diffusion fission matrix would provide an eigenvector immediately. A Monte Carlo fission matrix would have a suitable eigenvector after a few initial cycles. We implemented this type of source initialization by running a *head start cycle* that consisted of a very large number of histories. The initial source for the head start cycle would require at least a flat distribution so that all fissionable regions are sampled. The fission matrix should only have second order errors because the elements depend on the source shape over a cell instead of over the entire system [Car75]. After the head start cycle, the acceleration coding was used to sample from the very large number of source points according to the eigenvector of the fission matrix. After the head start cycle, each cycle contained a smaller, practical number

of histories. This type of source initialization fails if the eigenvector fails. An example of where the eigenvector fails is a system like the "k_{eff} of the world" problem except that, instead of one, two hot cells are present. Due to statistical noise and poor communication between the fuel cells, the eigenvector would not adequately detect both hot cells.

CHAPTER VII

Fission Diffusion Synthetic Acceleration Method

We now present a different form of the source convergence acceleration method, called Fission Diffusion Synthetic Acceleration (FDSA). FDSA involves a different form of the transport equation and a different low-order approximation than the fission matrix acceleration method. Instead of beginning the derivation with an analytic integral equation, we consider the integro-differential transport equation for the analytic and source iteration cases. We subtract these to obtain an equation for the exact correction to the angular flux. This equation is just as difficult as the source iteration problem, so we solve its diffusion approximation. Instead of using the fission matrix and its forward and adjoint eigenstates, this method requires a forward and adjoint diffusion calculation prior to the deterministic or Monte Carlo criticality calculation. Analytically, however, FDSA is equivalent to the diffusion fission matrix acceleration method.

7.1 Derivation of Fission Diffusion Synthetic Acceleration

We begin with the analytic integro-differential transport equation for a slab of width L, isotropic scattering, and vacuum boundary conditions. Using the operators

defined in Equations 6.4, 6.5, and 6.6, we have

$$\mathbf{T}\psi(x,\mu) = \mathbf{S}\psi(x,\mu) + \frac{1}{k}\mathbf{F}\psi(x,\mu) \quad , \tag{7.1}$$

$$\psi(0,\mu) = 0 \ , \quad \mu > 0 \quad , \tag{7.2}$$

$$\psi(L,\mu) = 0 \ , \quad \mu < 0 \quad . \tag{7.3}$$

The source iteration equations are obtained by introducing iteration indices to Equations 7.1, 7.2, and 7.3,

$$\mathbf{T}\psi^{(\ell+1/2)}(x,\mu) = \mathbf{S}\psi^{(\ell+1/2)}(x,\mu) + \frac{1}{k^{(\ell)}}\mathbf{F}\psi^{(\ell)}(x,\mu) \quad , \tag{7.4}$$

$$\psi^{(\ell+1/2)}(0,\mu) = 0 \ , \quad \mu > 0 \quad , \tag{7.5}$$

$$\psi^{(\ell+1/2)}(L,\mu) = 0 \ , \quad \mu < 0 \quad . \tag{7.6}$$

We desire the exact angular flux correction,

$$g^{(\ell+1)}(x,\mu) = \psi(x,\mu) - \psi^{(\ell+1/2)}(x,\mu) \quad . \tag{7.7}$$

Subtracting Equation 7.4 from Equation 7.1 yields an equation for the correction g,

$$\mathbf{T}g^{(\ell+1)}(x,\mu) - \mathbf{S}g^{(\ell+1)}(x,\mu) - \frac{1}{k}\mathbf{F}g^{(\ell+1)}(x,\mu) = \frac{1}{k}\mathbf{F}\psi^{(\ell+1/2)}(x,\mu) - \frac{1}{k^{(\ell)}}\mathbf{F}\psi^{(\ell)}(x,\mu) \quad , \tag{7.8}$$

and likewise for the boundary conditions,

$$g^{(\ell+1)}(0,\mu) = 0 \ , \quad \mu > 0 \quad , \tag{7.9}$$

$$g^{(\ell+1)}(L,\mu) = 0 \ , \quad \mu < 0 \quad . \tag{7.10}$$

Equation 7.8 is just as difficult to solve as Equation 7.4 ; therefore, we approximate it. First, we define

$$\phi_n^{(\ell+1)}(x) \equiv \int_{-1}^{1} \mu^n \psi^{(\ell+1)}(x,\mu) d\mu \quad , \tag{7.11}$$

where $\phi^{(\ell+1)}(x) = \phi_0^{(\ell+1)}(x)$ is the scalar flux, and

$$f_n^{(\ell+1)}(x) \equiv \int_{-1}^{1} \mu^n g^{(\ell+1)}(x,\mu)d\mu \quad , \tag{7.12}$$

and assume that the exact correction is linear in angle,

$$g^{(\ell+1)}(x,\mu) \approx \frac{1}{2}\left(f_0^{(\ell+1)}(x) + 3\mu f_1^{(\ell+1)}(x)\right) \quad . \tag{7.13}$$

Operating on Equation 7.8 by

$$\int_{-1}^{1}(\cdot)d\mu \tag{7.14}$$

and

$$\int_{-1}^{1}\mu(\cdot)d\mu \quad , \tag{7.15}$$

we obtain

$$\begin{aligned}\frac{\partial}{\partial x}f_1^{(\ell+1)}(x) + \Sigma_t(x)f_0^{(\ell+1)}(x) - \Sigma_s(x)f_0^{(\ell+1)}(x) - \frac{\nu\Sigma_f(x)}{k}f_0^{(\ell+1)} \\ = \frac{\nu\Sigma_f(x)}{k}\phi^{(\ell+1/2)}(x) - \frac{\nu\Sigma_f(x)}{k^{(\ell)}}\phi^{(\ell)}(x) \quad ,\end{aligned} \tag{7.16}$$

and

$$\frac{\partial}{\partial x}\int_{-1}^{1}\mu^2 g^{(\ell+1)}(x,\mu)d\mu + \Sigma_t(x)f_1^{(\ell+1)}(x) = 0 \quad . \tag{7.17}$$

Substituting the linear approximation of g, Equation 7.13, into Equation 7.17, we obtain an expression for f_1,

$$f_1^{(\ell+1)}(x) = -\frac{1}{3\Sigma_t(x)}\frac{\partial}{\partial x}f_0^{(\ell+1)}(x) \quad , \tag{7.18}$$

which, when substituted into Equation 7.16, yields the diffusion approximation to the acceleration equation, Equation 7.8:

$$\begin{aligned}-\frac{\partial}{\partial x}\frac{1}{3\Sigma_t(x)}\frac{\partial}{\partial x}f_0^{(\ell+1)}(x) + \left(\Sigma_a(x) - \frac{\nu\Sigma_f(x)}{k_d}\right)f_0^{(\ell+1)}(x) \\ = \frac{\nu\Sigma_f(x)}{k^{(\ell+1)}}\phi^{(\ell+1/2)}(x) - \frac{\nu\Sigma_f(x)}{k^{(\ell)}}\phi^{(\ell)}(x) \quad .\end{aligned} \tag{7.19}$$

The boundary conditions, called Marshak boundary conditions [Bel70], are obtained using the linear approximation, Equation 7.13, and Equation 7.18. On the left side,

$$0 = \int_0^1 \mu g^{(\ell+1)}(0,\mu)d\mu \tag{7.20}$$

$$= \frac{1}{2} f_0^{(\ell+1)}(0) \int_0^1 \mu d\mu + \frac{3}{2} f_1^{(\ell+1)}(0) \int_0^1 \mu^2 d\mu \tag{7.21}$$

$$= \frac{1}{4} f_0^{(\ell+1)}(0) + \frac{1}{2} f_1^{(\ell+1)}(0) \tag{7.22}$$

$$0 = f_0^{(\ell+1)}(0) - \frac{2}{3\Sigma_t(0)} \frac{\partial}{\partial x} f_0^{(\ell+1)}(0) \quad , \tag{7.23}$$

and on the right side,

$$0 = \int_{-1}^0 \mu g^{(\ell+1)}(L,\mu)d\mu \tag{7.24}$$

$$= \frac{1}{2} f_0^{(\ell+1)}(L) \int_{-1}^0 \mu d\mu + \frac{3}{2} f_1^{(\ell+1)}(L) \int_{-1}^0 \mu^2 d\mu \tag{7.25}$$

$$= -\frac{1}{4} f_0^{(\ell+1)}(L) + \frac{1}{2} f_1^{(\ell+1)}(L) \tag{7.26}$$

$$0 = f_0^{(\ell+1)}(L) + \frac{2}{3\Sigma_t(L)} \frac{\partial}{\partial x} f_0^{(\ell+1)}(L) \quad . \tag{7.27}$$

In Equation 7.19, k_d is the dominant eigenvalue from the adjoint diffusion equation (with vacuum boundaries),

$$-\frac{\partial}{\partial x} \frac{1}{3\Sigma_t(x)} \frac{\partial}{\partial x} \phi_d^*(x) + \Sigma_a(x)\phi_d^*(x) = \frac{\nu\Sigma_f(x)}{k_d} \phi_d^*(x) \quad . \tag{7.28}$$

Equation 7.19 does not automatically have a solution. We specify $k^{(\ell+1)}$ to satisfy the solvability condition, which is obtained by multiplying the acceleration equation, Equation 7.19, by the adjoint diffusion flux and integrating over space,

$$\int \phi_d^*(x) \left[-\frac{\partial}{\partial x} \frac{1}{3\Sigma_t(x)} \frac{\partial}{\partial x} f_0^{(\ell+1)}(x) + \left(\Sigma_a(x) - \frac{\nu\Sigma_f(x)}{k_d} \right) f_0^{(\ell+1)}(x) \right] dx$$

$$= \frac{1}{k^{(\ell+1)}} \int \phi_d^*(x) \left(\nu\Sigma_f(x) \phi^{(\ell+1/2)}(x) \right) dx - \frac{1}{k^{(\ell)}} \int \phi_d^*(x) \left(\nu\Sigma_f(x) \phi^{(\ell)}(x) \right) dx \quad . \tag{7.29}$$

The left side of Equation 7.29 is zero, giving us a value of $k^{(\ell+1)}$ for the solvability condition,

$$k^{(\ell+1)} = k^{(\ell)} \frac{\int \phi_d^*(x) \nu\Sigma_f(x) \phi^{(\ell+1/2)}(x) dx}{\int \phi_d^*(x) \nu\Sigma_f(x) \phi^{(\ell)}(x) dx} \quad . \tag{7.30}$$

After solving Equation 7.19, we see that $f_0(x)$ is not unique, since any multiple of the forward diffusion solution may be added to it,

$$f_0^{(\ell+1)}(x) = f_{0,particular}^{(\ell+1)}(x) + A\phi_d(x) \quad , \tag{7.31}$$

where ϕ_d is the solution of the forward diffusion equation,

$$-\frac{\partial}{\partial x}\frac{1}{3\Sigma_t(x)}\frac{\partial}{\partial x}\phi_d(x) + \Sigma_a(x)\phi_d(x) = \frac{\nu\Sigma_f(x)}{k_d}\phi_d(x) \quad . \tag{7.32}$$

Therefore, we make the correction unique by requiring that the additive correction be normal to the adjoint diffusion flux,

$$\int \phi_d^*(x) f_0^{(\ell+1)}(x)dx = 0 \quad . \tag{7.33}$$

As in the fission matrix acceleration method, we damp the additive correction, if necessary, and convert it to a multiplicative correction factor,

$$\begin{aligned} \nu\Sigma_f(x)\phi^{(\ell+1)} &= \nu\Sigma_f(x)\left(\beta f_0^{(\ell+1)}(x) + \phi^{(\ell+1/2)}(x)\right) & (7.34) \\ &\approx \nu\Sigma_f(x)\phi^{(\ell+1/2)}\left(1 + \beta\frac{\nu\Sigma_f(x)f_0^{(\ell+1)}(x)}{\hat{f}^{(\ell+1/2)}}\right) \quad , & (7.35) \end{aligned}$$

where $\hat{f}^{(\ell+1/2)}$ is the fission source $\nu\Sigma_f(x)\phi^{(\ell+1/2)}$ projected onto a cell. The projection causes the approximation between Equation 7.34 and Equation 7.35.

Let us summarize the steps for Fission Diffusion Synthetic Acceleration. Steps 1 and 2 are performed only once before the calculation begins. The iterations, or cycles, proceed over step 3 to 6:

1. Calculate the solution of the forward diffusion equation, Equation 7.32,

$$-\frac{\partial}{\partial x}\frac{1}{3\Sigma_t(x)}\frac{\partial}{\partial x}\phi_d(x) + \Sigma_a(x)\phi_d(x) = \frac{\nu\Sigma_f(x)}{k_d}\phi_d(x) \quad . \tag{7.36}$$

2. Calculate the solution of the adjoint diffusion equation, Equation 7.28,

$$-\frac{\partial}{\partial x}\frac{1}{3\Sigma_t(x)}\frac{\partial}{\partial x}\phi_d^*(x) + \Sigma_a(x)\phi_d^*(x) = \frac{\nu\Sigma_f(x)}{k_d}\phi_d^*(x) \quad . \tag{7.37}$$

3. Perform a transport iteration or cycle, Equation 7.4,

$$\mathbf{T}\psi^{(\ell+1/2)}(x,\mu) = \mathbf{S}\psi^{(\ell+1/2)}(x,\mu) + \frac{1}{k^{(\ell)}}\mathbf{F}\psi^{(\ell)}(x,\mu) \quad , \tag{7.38}$$

4. Calculate $k^{(\ell+1)}$, the solvability condition from Equation 7.30,

$$k^{(\ell+1)} = k^{(\ell)} \frac{\int \phi_d^*(x)\nu\Sigma_f(x)\phi^{(\ell+1/2)}(x)dx}{\int \phi_d^*(x)\nu\Sigma_f(x)\phi^{(\ell)}(x)dx} \quad . \tag{7.39}$$

5. Calculate the fission source correction using Equation 7.19 and 7.33,

$$-\frac{\partial}{\partial x}\frac{1}{3\Sigma_t(x)}\frac{\partial}{\partial x}f_0^{(\ell+1)}(x) + \left(\Sigma_a(x) - \frac{\nu\Sigma_f(x)}{k_d}\right) f_0^{(\ell+1)}(x)$$
$$= \frac{\nu\Sigma_f(x)}{k^{(\ell+1)}}\phi^{(\ell+1/2)}(x) - \frac{\nu\Sigma_f(x)}{k^{(\ell)}}\phi^{(\ell)}(x) \quad , \tag{7.40}$$

$$\int \phi_d^*(x) f_0^{(\ell+1)}(x)dx = 0 \quad . \tag{7.41}$$

6. Apply the correction using Equation 7.35 ,

$$\nu\Sigma_f(x)\phi^{(\ell+1)} \approx \nu\Sigma_f(x)\phi^{(\ell+1/2)}\left(1 + \beta\frac{\nu\Sigma_f(x)f_0^{(\ell+1)}(x)}{\hat{f}^{(\ell+1/2)}}\right) \quad , \tag{7.42}$$

and return to step 3 for another iteration or cycle.

7.2 Implementing FDSA

The Fission Diffusion Synthetic Acceleration method requires less computer storage since it does not require toting around fission matrices. FDSA has the advantage that its diffusion equation may be performed in multigroup, regardless of whether the transport is multigroup S_N or continuous energy Monte Carlo. The actual acceleration is collapsed to one energy group and is still dependent only on space, just as in the fission matrix method. Greater accuracy may be achieved from using a multigroup diffusion acceleration equation. The disadvantages are that it requires

more pre-calculation and requires a spatial grid on which to perform the diffusion-like acceleration calculation.

In the deterministic realm, we are faced with the same dilemma that occurs in DSA (Chapter III): How should we discretize the equations? Inconsistent discretization is the most straightforward procedure, where the transport equation and the diffusion-like acceleration equation are discretized any desired way. As in DSA, inconsistent discretization may induce instabilities for large mesh sizes. Consistent discretization arises when FDSA is derived from the already-discretized transport equation. While having more desirable features, consistent discretization is not always feasible in higher dimensioned, more complicated systems. Moreover, how exactly does one consistently discretize Monte Carlo FDSA? The concept appears to have no clear meaning.

7.2.1 Consistently Discretized FDSA

We consider a slab of width L divided into J cells that are not necessarily uniform. We use Diamond Differencing and S_N angular quadrature and consider vacuum boundaries. The discretized transport equation is

$$\frac{\mu_m}{h_j}\left(\psi_{m,j+1/2}^{(\ell+1/2)}-\psi_{m,j-1/2}^{(\ell+1/2)}\right)+\Sigma_{t_j}\psi_{m,j}^{(\ell+1/2)}-\frac{1}{2}\Sigma_{s_j}\sum_{n=1}^{N}\psi_{n,j}^{(\ell+1/2)}w_n=\frac{\nu\Sigma_{f_j}}{2k^{(\ell)}}\phi_j^{(\ell)} \quad , \tag{7.43}$$

$$\psi_{m,j}^{(\ell+1/2)} = \frac{1}{2}\left(\psi_{m,j+1/2}^{(\ell+1/2)}+\psi_{m,j-1/2}^{(\ell+1/2)}\right) \quad , \tag{7.44}$$

$$\psi_{m,1/2}^{(\ell+1/2)} = 0 \ , \ \mu_m > 0 \quad , \tag{7.45}$$

$$\psi_{m,J+1/2}^{(\ell+1/2)} = 0 \ , \ \mu_m < 0 \quad , \tag{7.46}$$

$$\phi_j^{(\ell+1/2)} = \sum_{m=1}^{N}\psi_{m,j}^{(\ell+1/2)}w_m \quad , \tag{7.47}$$

where, again, w_m are the angular quadrature weights such that

$$\sum_{m=1}^{N} w_m = 2 \quad , \tag{7.48}$$

and the $j \pm 1/2$ subscripts indicate cell-edge quantities and the j subscripts indicate cell-average quantities.

We begin the FDSA derivation by defining the transport corrections on the cell centers and cell edges,

$$g_{m,j}^{(\ell+1)} = \psi_{m,j} - \psi_{m,j}^{(\ell+1/2)} \quad , \tag{7.49}$$

$$g_{m,j+1/2}^{(\ell+1)} = \psi_{m,j+1/2} - \psi_{m,j+1/2}^{(\ell+1/2)} \quad , \tag{7.50}$$

such that adding g to the most recent angular fluxes results in the exact angular fluxes. Let us subtract Equations 7.43 to 7.47 from the exact problem (that is, Equations 7.43 to 7.47 without iteration indices). We obtain a problem for the exact angular flux corrections,

$$\frac{\mu_m}{h_j}\left(g_{m,j+1/2}^{(\ell+1)} - g_{m,j-1/2}^{(\ell+1)}\right) + \Sigma_{t_j} g_{m,j}^{(\ell+1)} - \frac{1}{2}\Sigma_{s_j}\sum_{n=1}^{N}\psi_{n,j}w_n + \frac{1}{2}\Sigma_{s_j}\sum_{n=1}^{N}\psi_{n,j}^{(\ell+1/2)}w_n$$
$$= \frac{\nu\Sigma_{f_j}}{2k}\phi_j - \frac{\nu\Sigma_{f_j}}{2k^{(\ell)}}\phi_j^{(\ell)} + \frac{\nu\Sigma_{f_j}}{2k}\sum_{n=1}^{N}\psi_{n,j}^{(\ell+1/2)}w_n - \frac{\nu\Sigma_{f_j}}{2k}\sum_{n=1}^{N}\psi_{n,j}^{(\ell+1/2)}w_n \quad , \tag{7.51}$$

where the last term was added and subtracted to easily get the equation in the following form:

$$\frac{\mu_m}{h_j}\left(g_{m,j+1/2}^{(\ell+1)} - g_{m,j-1/2}^{(\ell+1)}\right) + \Sigma_{t_j} g_{m,j}^{(\ell+1)} - \frac{1}{2}\Sigma_{s_j}\sum_{n=1}^{N} g_{n,j}^{(\ell+1)}w_n - \frac{\nu\Sigma_{f_j}}{2k}\sum_{n=1}^{N} g_{n,j}^{(\ell+1)}w_n$$
$$= \frac{\nu\Sigma_{f_j}}{2k}\sum_{n=1}^{N}\psi_{n,j}^{(\ell+1/2)}w_n - \frac{\nu\Sigma_{f_j}}{2k^{(\ell)}}\phi_j^{(\ell)} \quad , \tag{7.52}$$

$$g_{m,j}^{(\ell+1)} = \frac{1}{2}\left(g_{m,j+1/2}^{(\ell+1)} + g_{m,j-1/2}^{(\ell+1)}\right) \quad , \tag{7.53}$$

$$g_{m,1/2}^{(\ell+1)} = 0 \ , \ \mu_m > 0 \ , \tag{7.54}$$

$$g_{m,J+1/2}^{(\ell+1)} = 0 \ , \ \mu_m < 0 \ , \tag{7.55}$$

$$\phi_j^{(\ell+1/2)} = \sum_{m=1}^{N}\psi_{m,j}^{(\ell+1/2)}w_m \quad . \tag{7.56}$$

Adding the exact correction to the most recent angular flux yields the exact angular flux

$$\psi_{m,j} = \psi_{m,j}^{(\ell+1/2)} + g_{m,j}^{(\ell+1)} \quad , \tag{7.57}$$

or, integrated over angle, it yields the exact scalar flux,

$$\phi_j = \phi_j^{(\ell+1/2)} + \sum_{m=1}^{N} g_{m,j}^{(\ell+1)} w_m \quad . \tag{7.58}$$

Solving this problem gives the exact (discretized) result in one iteration. Not unexpectedly, we find that this problem is as difficult to solve as the original problem. Thus, at this point, we have gained nothing. The remedy is to take the diffusion approximation of the acceleration. We define

$$f_{0,j}^{(\ell+1)} = \sum_{m=1}^{N} g_{m,j}^{(\ell+1)} w_m \quad , \tag{7.59}$$

$$f_{1,j}^{(\ell+1)} = \sum_{m=1}^{N} \mu_m g_{m,j}^{(\ell+1)} w_m \quad , \tag{7.60}$$

and assume the angular flux correction is linear in angle,

$$g_{m,j}^{(\ell+1)} \approx \frac{1}{2}\left(f_{0,j}^{(\ell+1)} + 3\mu_m f_{1,j}^{(\ell+1)}\right) \quad . \tag{7.61}$$

Next, we operate on Equation 7.52 by

$$\sum_{m=1}^{N} (\cdot) w_m \tag{7.62}$$

and obtain

$$\frac{1}{h_j}\left(f_{1,j+1/2}^{(\ell+1)} - f_{1,j-1/2}^{(\ell+1)}\right) + \Sigma_{t_j} f_{0,j}^{(\ell+1)} - \Sigma_{s_j} f_{0,j}^{(\ell+1)} - \frac{\nu\Sigma_{f_j}}{k} f_{0,j}^{(\ell+1)}$$
$$= \frac{\nu\Sigma_{f_j}}{k}\phi_j^{(\ell+1/2)} - \frac{\nu\Sigma_{f_j}}{k^{(\ell)}}\phi_j^{(\ell)} \quad , \quad 1 \le j \le J \quad . \tag{7.63}$$

Operating on Equation 7.52 by

$$\sum_{m=1}^{N} \mu_m (\cdot) w_m \quad , \tag{7.64}$$

and using the linear approximation in Equation 7.61, we obtain

$$\frac{1}{3h_j}\left(f_{0,j+1/2}^{(\ell+1)} - f_{0,j-1/2}^{(\ell+1)}\right) + \Sigma_{t_j} f_{1,j}^{(\ell+1)} = 0 \ , \ 1 \le j \le J \ . \tag{7.65}$$

Operating on Equation 7.53 by the same two operators yields

$$f_{0,j}^{(\ell+1)} = \frac{1}{2}\left(f_{0,j+1/2}^{(\ell+1)} + f_{0,j-1/2}^{(\ell+1)}\right) \ , \tag{7.66}$$

$$f_{1,j}^{(\ell+1)} = \frac{1}{2}\left(f_{1,j+1/2}^{(\ell+1)} + f_{1,j-1/2}^{(\ell+1)}\right) \ . \tag{7.67}$$

Now we look to approximate the boundary conditions. Multiplying Equation 7.54 by $\mu_m w_m$ and integrating (summing) over positive μ_m, we find the partial incoming current for the left boundary, where we utilize the linear approximation for g,

$$0 = \sum_{\mu_m>0} g_{m,1/2}^{(\ell+1)} w_m \tag{7.68}$$

$$\approx \frac{1}{2}\sum_{\mu_m>0} \mu_m \left(f_{0,1/2}^{(\ell+1)} + 3\mu_m f_{1,1/2}^{(\ell+1)}\right) w_m \tag{7.69}$$

$$= \frac{1}{2}\left(\sum_{\mu_m>0} \mu_m w_m\right) f_{0,1/2}^{(\ell+1)} + \frac{1}{2} f_{1,1/2}^{(\ell+1)} \ , \tag{7.70}$$

since

$$\sum_{\mu_m>0} \mu_m^2 w_m = \frac{1}{2}\sum_{\text{all } \mu_m} \mu_m^2 w_m = \frac{1}{3} \ . \tag{7.71}$$

Setting

$$\gamma_N \equiv 2\sum_{\mu_m>0} \mu_m w_m \tag{7.72}$$

we have as the left boundary condition,

$$0 = \gamma_N f_{0,1/2}^{(\ell+1)} + 2 f_{1,1/2}^{(\ell+1)} \ . \tag{7.73}$$

Similarly, the right boundary condition is

$$0 = -\gamma_N f_{0,J+1/2}^{(\ell+1)} + 2 f_{1,J+1/2}^{(\ell+1)} \ . \tag{7.74}$$

The scalar flux is accelerated by

$$\phi_j^{(\ell+1)} = \phi_j^{(\ell+1/2)} + f_{0,j}^{(\ell+1)} \quad . \tag{7.75}$$

Equations 7.63, 7.65, 7.66, 7.67, 7.73, 7.74, and 7.75 constitute $4J+2$ equations in $4J+2$ unknowns. Now we want to eliminate $f_1^{(\ell+1)}$ from these equations. First, we substitute Equations 7.66 and 7.67 into Equations 7.63 and 7.65 so the corrections all reside on the cell edges. This substitution yields the following two equations,

$$\begin{aligned}\left(f_{1,j+1/2}^{(\ell+1)} - f_{1,j-1/2}^{(\ell+1)}\right) &= \frac{\Sigma_{a,j}h_j}{2}\left(f_{0,j+1/2}^{(\ell+1)} + f_{0,j-1/2}^{(\ell+1)}\right) + \frac{\nu\Sigma_{f,j}h_j}{2k}\left(f_{0,j+1/2}^{(\ell+1)} + f_{0,j-1/2}^{(\ell+1)}\right) \\ &\quad + \frac{\nu\Sigma_{f,j}h_j}{k}\phi_j^{(\ell+1/2)} - \frac{\nu\Sigma_{f,j}h_j}{k^{(\ell)}}\phi_j^{(\ell)} \quad , \; 1 \le j \le J \quad , \end{aligned} \tag{7.76}$$

$$\left(f_{1,j+1/2}^{(\ell+1)} + f_{1,j-1/2}^{(\ell+1)}\right) = \frac{-2}{3\Sigma_{t,j}h_j}\left(f_{0,j+1/2}^{(\ell+1)} - f_{0,j-1/2}^{(\ell+1)}\right) \quad , \; 1 \le j \le J \quad . \tag{7.77}$$

Adding and subtracting Equations 7.76 and 7.77 produces two different equations:

$$\begin{aligned}2f_{1,j+1/2}^{(\ell+1)} &= \left(\frac{\nu\Sigma_{f,j}h_j}{2k} - \frac{\Sigma_{a,j}h_j}{2}\right)\left(f_{0,j+1/2}^{(\ell+1)} + f_{0,j-1/2}^{(\ell+1)}\right) + \frac{\nu\Sigma_{f,j}h_j}{k}\phi_j^{(\ell+1/2)} \\ &\quad - \frac{\nu\Sigma_{f,j}h_j}{k^{(\ell)}}\phi_j^{(\ell)} - \frac{2}{3\Sigma_{t,j}h_j}\left(f_{0,j+1/2}^{(\ell+1)} - f_{0,j-1/2}^{(\ell+1)}\right) \quad , \; 1 \le j \le J \quad , \end{aligned} \tag{7.78}$$

$$\begin{aligned}2f_{1,j-1/2}^{(\ell+1)} &= \left(\frac{\Sigma_{a,j}h_j}{2} - \frac{\nu\Sigma_{f,j}h_j}{2k}\right)\left(f_{0,j+1/2}^{(\ell+1)} + f_{0,j-1/2}^{(\ell+1)}\right) - \frac{\nu\Sigma_{f,j}h_j}{k}\phi_j^{(\ell+1/2)} \\ &\quad + \frac{\nu\Sigma_{f,j}h_j}{k^{(\ell)}}\phi_j^{(\ell)} - \frac{2}{3\Sigma_{t,j}h_j}\left(f_{0,j+1/2}^{(\ell+1)} - f_{0,j-1/2}^{(\ell+1)}\right) \quad , \; 1 \le j \le J \quad . \end{aligned} \tag{7.79}$$

In order to eliminate $f_{1,j+1/2}^{(\ell+1)}$, we shift the indices in Equation 7.79 from $j-1/2$ to $j+1/2$ such that the range of applicable j is shifted to $0 \le j \le J-1$. Equating the expressions and rearranging yields the acceleration equation,

$$
\begin{aligned}
&-\frac{1}{3\Sigma_{t,j+1}h_{j+1}}\left(f_{0,j+3/2}^{(\ell+1)}-f_{0,j+1/2}^{(\ell+1)}\right)+\frac{1}{3\Sigma_{t,j}h_j}\left(f_{0,j+1/2}^{(\ell+1)}-f_{0,j-1/2}^{(\ell+1)}\right)\\
&\quad+\frac{1}{4}\left[\left(\Sigma_{a,j+1}h_{j+1}-\frac{\nu\Sigma_{f,j+1}h_{j+1}}{k_d}\right)\left(f_{0,j+3/2}^{(\ell+1)}+f_{0,j+1/2}^{(\ell+1)}\right)\right.\\
&\qquad\left.+\left(\Sigma_{a,j}h_j-\frac{\nu\Sigma_{f,j}h_j}{k_d}\right)\left(f_{0,j+1/2}^{(\ell+1)}+f_{0,j-1/2}^{(\ell+1)}\right)\right]\\
&\quad=\frac{1}{2}\left[\frac{1}{k^{(\ell+1)}}\left(\nu\Sigma_{f,j+1}h_{j+1}\phi_{j+1}^{(\ell+1/2)}+\nu\Sigma_{f,j}h_j\phi_j^{(\ell+1/2)}\right)\right.\\
&\left.-\frac{1}{k^{(\ell)}}\left(\nu\Sigma_{f,j+1}h_{j+1}\phi_{j+1}^{(\ell)}+\nu\Sigma_{f,j}h_j\phi_j^{(\ell)}\right)\right]\quad,\quad 1\le j\le J-1\quad, \qquad (7.80)
\end{aligned}
$$

Note that we introduced the diffusion eigenvalue, k_d, on the left side of Equation 7.80 and $k^{(\ell+1)}$, the eigenvalue satisfying the solvability condition, on the right side. Substituting Equations 7.78 and 7.79 into Equations 7.73 and 7.74, we obtain the left and right boundary conditions,

$$
\begin{aligned}
\gamma_N f_{0,1/2}^{(\ell+1)} &- \frac{2}{3\Sigma_{t,1}h_1}\left(f_{0,3/2}^{(\ell+1)}-f_{0,1/2}^{(\ell+1)}\right)+\frac{1}{2}\left(\Sigma_{a,1}h_1-\frac{\nu\Sigma_{f,1}h_1}{k_d}\right)\left(f_{0,3/2}^{(\ell+1)}+f_{0,1/2}^{(\ell+1)}\right)\\
&=\frac{\nu\Sigma_{f,1}h_1}{k^{(\ell+1)}}\phi_1^{(\ell+1/2)}-\frac{\nu\Sigma_{f,1}h_1}{k^{(\ell)}}\phi_1^{(\ell)}\quad, \qquad (7.81)\\
\gamma_N f_{0,J+1/2}^{(\ell+1)} &+ \frac{2}{3\Sigma_{t,J}h_J}\left(f_{0,J+1/2}^{(\ell+1)}-f_{0,J-1/2}^{(\ell+1)}\right)\\
&+\frac{1}{2}\left(\Sigma_{a,J}h_J-\frac{\nu\Sigma_{f,J}h_J}{k_d}\right)\left(f_{0,J+1/2}^{(\ell+1)}+f_{0,J-1/2}^{(\ell+1)}\right)\\
&=\frac{\nu\Sigma_{f,J}h_J}{k^{(\ell+1)}}\phi_J^{(\ell+1/2)}-\frac{\nu\Sigma_{f,J}h_J}{k^{(\ell)}}\phi_J^{(\ell)}\quad. \qquad (7.82)
\end{aligned}
$$

Equations 7.80, 7.81, and 7.82 constitute a tridiagonal system for the cell-edge scalar flux corrections. Finally, substituting Equation 7.66 into Equation 7.75, we have the correction as

$$
\phi_j^{(\ell+1)}=\phi_j^{(\ell+1/2)}+\frac{1}{2}\left(f_{0,j+1/2}^{(\ell+1)}+f_{0,j-1/2}^{(\ell+1)}\right)\quad. \qquad (7.83)
$$

7.2.2 Inconsistently Discretized FDSA

We obtain "inconsistently discretized FDSA" when the transport and acceleration equations are discretized independently. The discretized transport equation and

boundary conditions are given in Equations 7.43 through 7.47. We discretize the acceleration equation, Equation 7.19, in a usual way by integrating it from cell-center to cell-center, with half-width cells at the left and right boundaries. For uniform cell width h, we obtain in the interior of the slab,

$$\begin{aligned} & -\frac{1}{3\Sigma_{t,j-1}h} f_{0,j-1/2}^{(\ell+1)} \\ & \quad + \left[\frac{1}{3\Sigma_{t,j-1}h} + \frac{1}{3\Sigma_{t,j}h} + \frac{h}{2}\left(\Sigma_{a,j-1} + \Sigma_{a,j} - \frac{\nu}{k_d}\left(\Sigma_{f,j-1} + \Sigma_{f,j}\right)\right)\right] f_{0,j+1/2}^{(\ell+1)} \\ & \quad - \frac{1}{3\Sigma_{t,j}h} f_{0,j+3/2}^{(\ell+1)} \\ & = \frac{h}{2}\left[\nu\Sigma_{f,j}\left(\frac{1}{k^{(\ell+1)}}\phi_{0,j}^{(\ell+1/2)} - \frac{1}{k^{(\ell)}}\phi_{0,j}^{(\ell)}\right)\right. \\ & \quad \left. + \nu\Sigma_{f,j+1}\left(\frac{1}{k^{(\ell+1)}}\phi_{0,j+1}^{(\ell+1/2)} - \frac{1}{k^{(\ell)}}\phi_{0,j+1}^{(\ell)}\right)\right] \quad , \quad 1 \le j \le J-1 \quad , \end{aligned} \tag{7.84}$$

and for the left and right boundary conditions,

$$\begin{aligned} \left[\frac{1}{3\Sigma_{t,1}h} + \frac{h}{2}\left(\Sigma_{a,1} - \frac{\nu\Sigma_{f,1}}{k_d}\right) + \frac{1}{2}\right] f_{0,1/2}^{(\ell+1)} - \frac{1}{3\Sigma_{t,1}h} f_{0,j+3/2}^{(\ell+1)} \\ = \frac{\nu\Sigma_{f,1}h}{2}\left(\frac{1}{k^{(\ell+1)}}\phi_{0,1}^{(\ell+1/2)} - \frac{1}{k^{(\ell)}}\phi_{0,1}^{(\ell)}\right) \quad , \end{aligned} \tag{7.85}$$

$$\begin{aligned} -\frac{1}{3\Sigma_{t,J}h} f_{0,J-1/2}^{(\ell+1)} + \left[\frac{1}{3\Sigma_{t,J}h} + \frac{h}{2}\left(\Sigma_{a,J} - \frac{\nu\Sigma_{f,J}}{k_d}\right) + \frac{1}{2}\right] f_{0,J+1/2}^{(\ell+1)} \\ = \frac{\nu\Sigma_{f,J}h}{2}\left(\frac{1}{k^{(\ell+1)}}\phi_{0,J}^{(\ell+1/2)} - \frac{1}{k^{(\ell)}}\phi_{0,J}^{(\ell)}\right) \quad . \end{aligned} \tag{7.86}$$

Solving Equations 7.84, 7.85, and 7.86 yields the correction on the cell edges. The correction is applied to the scalar flux by Equation 7.83.

7.3 Fission Diffusion Synthetic Acceleration Results

We consider all three test problems for deterministic FDSA, and the homogeneous problem and "k_{eff} of the world" problem for FDSA applied to Monte Carlo. We defer our attack on the inherent difficulties Monte Carlo has with the uniform lattice to the

Hybrid Method in the next chapter. We make no differentiation between consistently and inconsistently discretized FDSA because, unexpectedly, they perform virtually the same.

7.3.1 Deterministic FDSA Results

First, we consider the homogeneous slab as shown in Figure 6.1. Using 60 cells and starting 2/3 of the source in the left half and 1/3 in the right half, the deterministic FDSA method (FDSA applied to discrete ordinates) converges in 6 iterations, while the unaccelerated discrete ordinates method requires 722 iterations. The computational speedup was 77. For comparison, the Diffusion Fission Matrix took 10 iterations and 5.7 times longer than FDSA. The convergence of the first and second Fourier mode coefficients are shown in Figures 7.1 and 7.2, respectively.

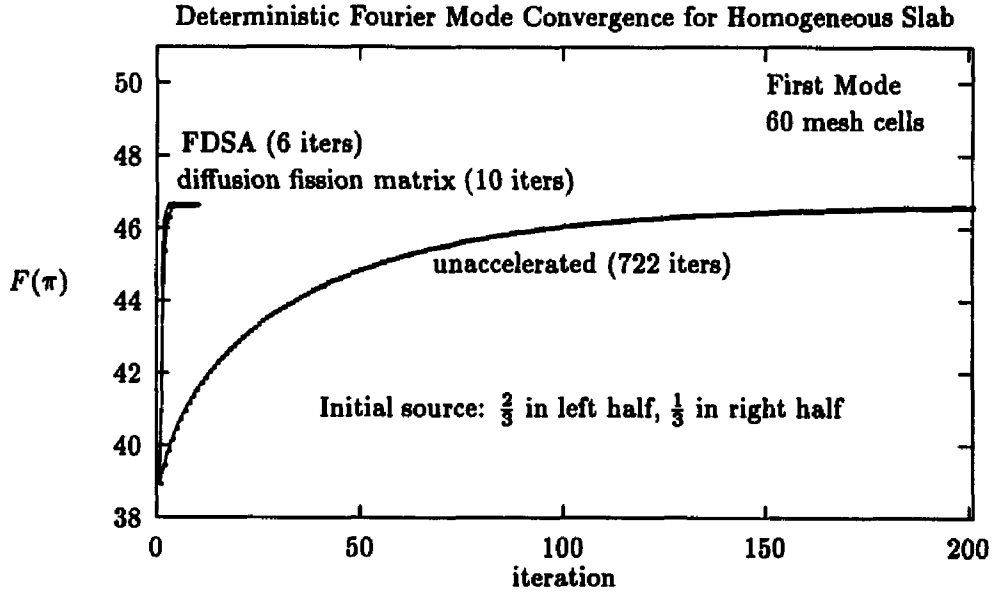

Figure 7.1: The convergence of the first Fourier mode coefficient in the homogeneous slab problem for unaccelerated discrete ordinates, Fission Diffusion Synthetic Acceleration, and, for comparison, Diffusion Fission Matrix acceleration.

Second, we investigate FDSA on the uniform lattice problem, which is shown in

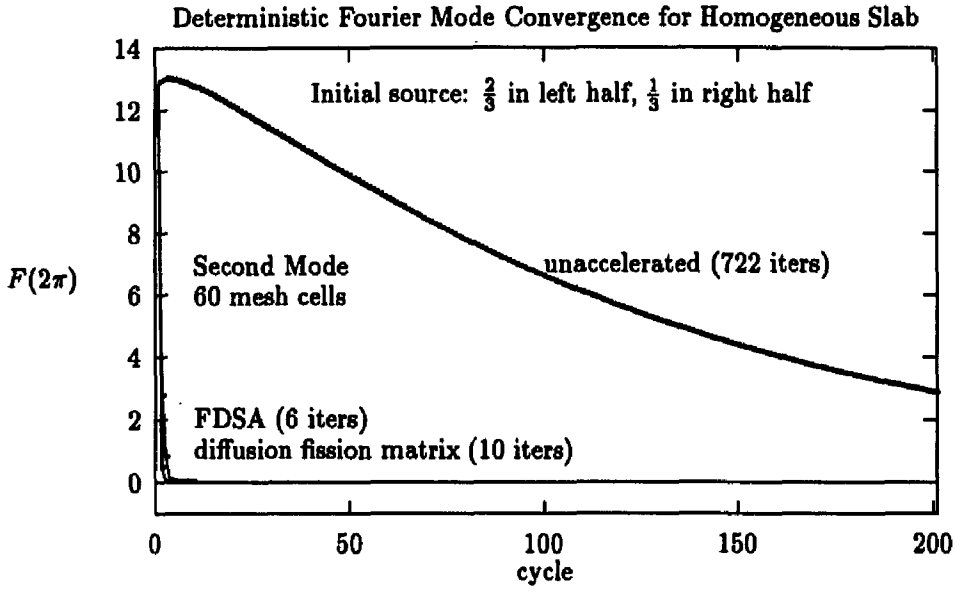

Figure 7.2: The convergence of the second Fourier mode coefficient in the homogeneous slab problem for unaccelerated discrete ordinates, Fission Diffusion Synthetic Acceleration, and, for comparison, Diffusion Fission Matrix acceleration.

Figure 6.2. The discrete ordinates calculation was performed on 464 cells and the acceleration was performed on 116 cells in the 58 mfp system. Again, the initial source was 2/3 in the left half and 1/3 in the right half. The unaccelerated discrete ordinates required 853 iterations to converge and FDSA required only 9, for a computational time speedup of 87.5. The Diffusion Fission Matrix acceleration, for comparison, took 12 iterations and took about 4 times longer than FDSA. The first and second Fourier mode coefficient convergence is shown in Figure 7.3.

Third, we look at the one-dimensional "k_{eff} of the world" problem, which is shown in Figure 6.3. Both the transport and acceleration are on 464 uniform cells in the 58 cm system. This problem was unique for deterministic FDSA because it was the only deterministic problem that required damping. A possible reason that damping was necessary is that the initial source is far from the converged source, the latter of which tends to have no diffusion characteristics. In lieu of showing another

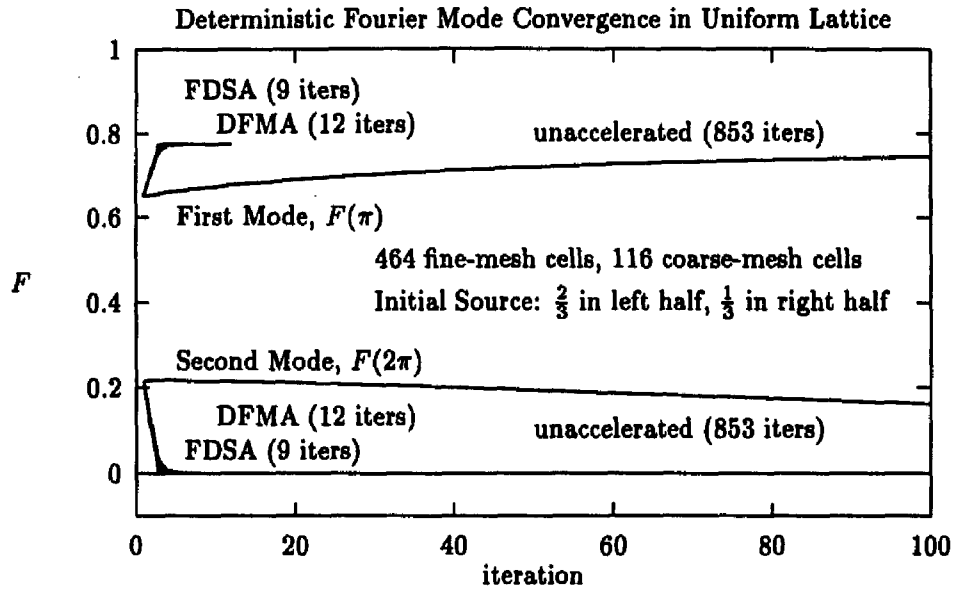

Figure 7.3: The convergence of the second Fourier mode coefficient in the uniform lattice problem for unaccelerated discrete ordinates, Fission Diffusion Synthetic Acceleration, and, for comparison, Diffusion Fission Matrix acceleration.

Fourier plot, we show in Figure 7.4 the iterations and computer time necessary for convergence as a function of damping. The optimal β was 0.6, for a paltry speedup of 2.

7.3.2 Monte Carlo FDSA Results

We apply Monte Carlo FDSA to the homogeneous slab problem. We begin with 2/3 of the source in the left half of the slab and 1/3 in the right half and run 5000 histories per cycle. The diffusion filter parameter is

$$\alpha^2 = \frac{5n}{n+10} \quad . \tag{7.87}$$

α^2 starts out small so the filtering does not accentuate the artificial (high frequency) step in the initial source.

Figures 7.5 and 7.6 show the first and second Fourier mode coefficient convergence for unaccelerated Monte Carlo and for FDSA with β held constant at 0.06. These

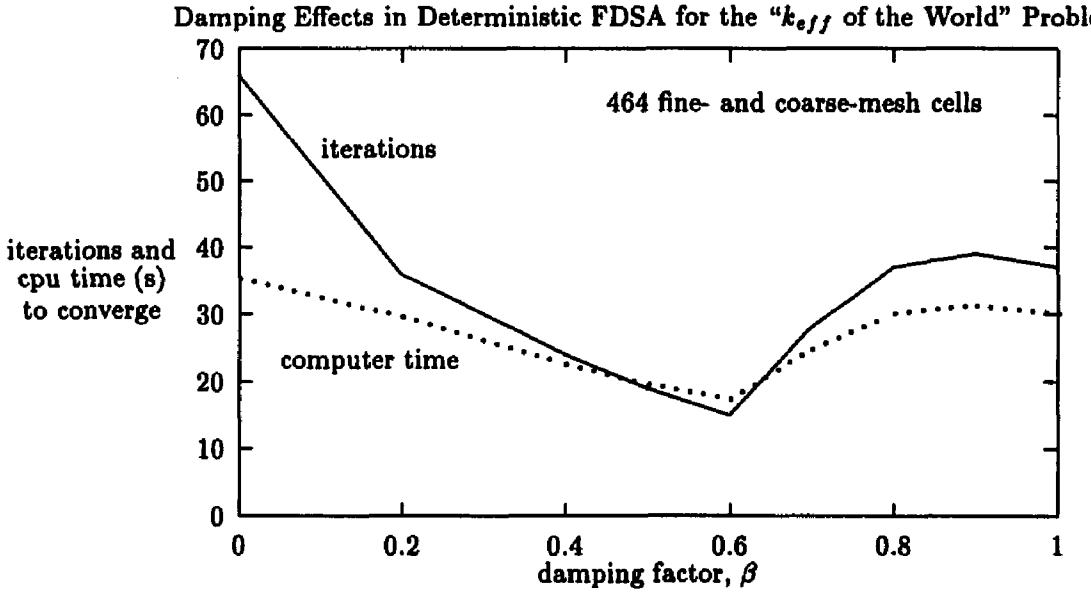

Figure 7.4: The damping effects on the iterations and computer time to converge for deterministic FDSA applied to the "k_{eff} of the world" problem.

problems required severe damping, as one would have expected from inconsistently discretized FDSA. Holding β constant shows how the acceleration converges the source in about 10 or 15 cycles. After that, one can see how the high order statistical noise is translated into lower order fluctuations by the acceleration. Ideally the acceleration should have been shut off after about 13 or 14 cycles.

Setting the damping factor so that the acceleration is tailored to shut off after the source is converged eliminates the adverse effects of trying to accelerate an already-converged source. Therefore, for the next case, we set β as

$$\beta = 0.1 \exp(-5.0 \max(0, n - 11)) \quad , \tag{7.88}$$

so that $\beta = 0.1$ for 11 cycles then goes to zero almost immediately. Convergence of both the first and second Fourier mode coefficients for this case are shown in Figure 7.7. The speedup obtained from the times at the unaccelerated 100th cycle and the FDSA 10th cycle was about 9.3.

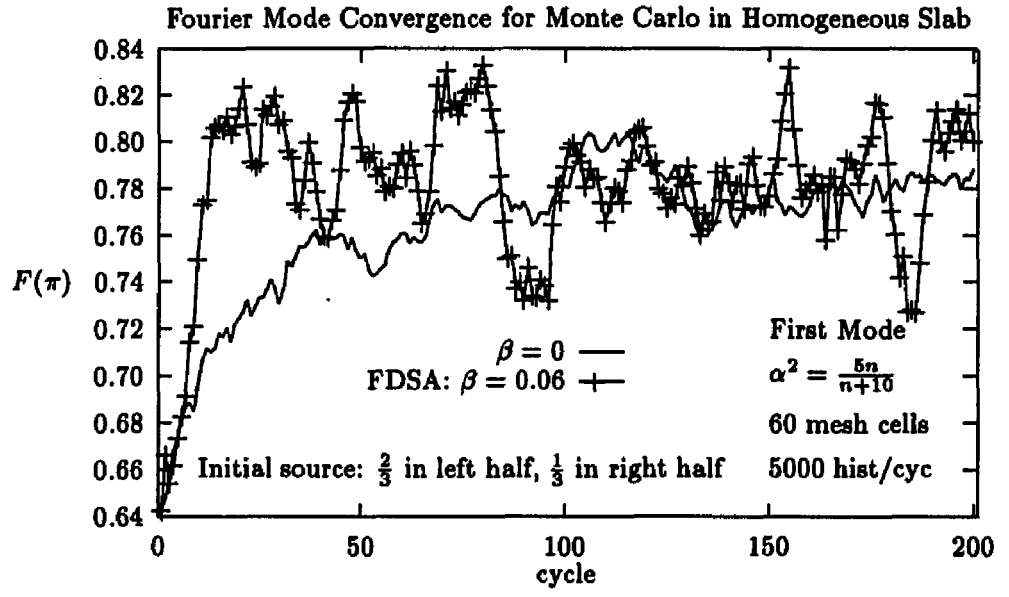

Figure 7.5: The first Fourier mode coefficient convergence for the homogeneous slab with unaccelerated Monte Carlo and FDSA with β=0.06.

Lastly, we apply Monte Carlo FDSA to the one-dimensional "k_{eff} of the world" problem. Damping appeared unnecessary as there was little difference between $\beta = 1.0$ and $\beta = 0.6$. The Fourier mode coefficient convergence is shown in Figure 7.8. Just as with the Fission Matrix Acceleration, the Fourier coefficients seemed almost deterministic because of the high ratio of particles to important fissionable material volume. Comparing the computer times at the unaccelerated 36th cycle and the FDSA 6th cycle, the speedup was about 6.1.

7.4 Summary and Discussion

The Fission Diffusion Synthetic Acceleration (FDSA) method accelerates source convergence by utilizing the diffusion approximation of the exact correction to the angular flux. It is similar to the Fission Matrix Acceleration method in that an exact acceleration equation is approximated. Whereas the Fission Matrix Acceleration method uses the fission matrix as an approximation, FDSA uses the diffusion

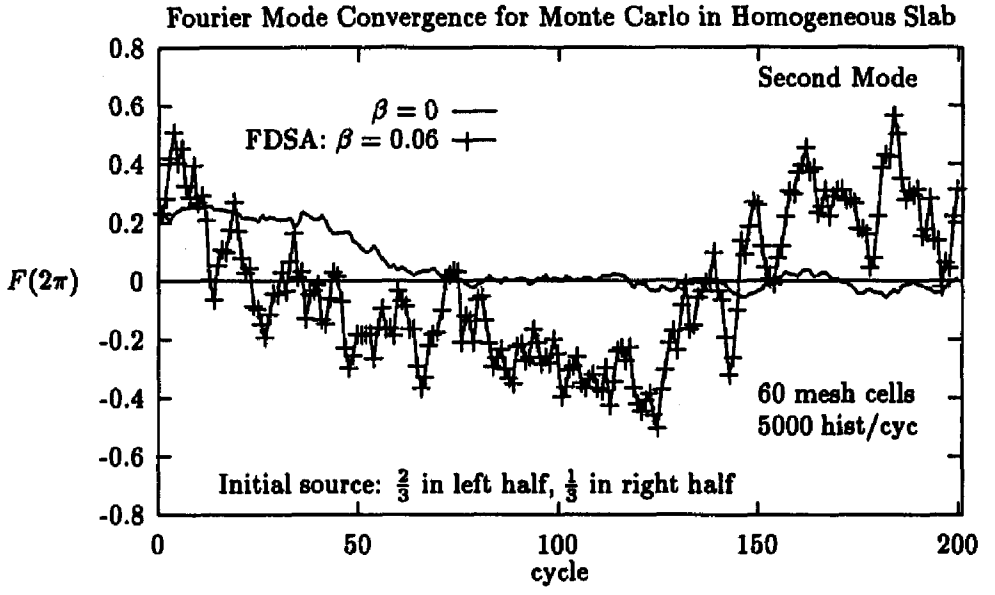

Figure 7.6: The second Fourier mode coefficient convergence for the homogeneous slab with unaccelerated Monte Carlo and FDSA with β=0.06.

approximation–an assumption that scattering is linear in angle. The differences were mostly subtle for the types of problems we considered. However, in the deterministic realm, FDSA required damping for the "k_{eff} of the world" problem. For all other deterministic problems, the optimal acceleration occurred for $\beta = 1$. When applied to the "k_{eff} of the world" problem, FDSA required damping regardless of whether the initial source was flat or had 2/3 in the left half of the slab and 1/3 in the right half. The reason FDSA required damping for that problem is probably because the converged source is very "undiffusion-like," and the initial source contained unphysical high-order components at the center of the slab.

We surprisingly found that inconsistently and consistently discretized deterministic FDSA performed essentially the same. This finding is inconsistent (no pun intended) with the discretization behavior observed in fixed-source DSA. One reason may be that the linear fixed-source Fourier analysis results do not apply to the nonlinear eigenvalue calculation. On the other hand, FDSA applied to Monte Carlo met

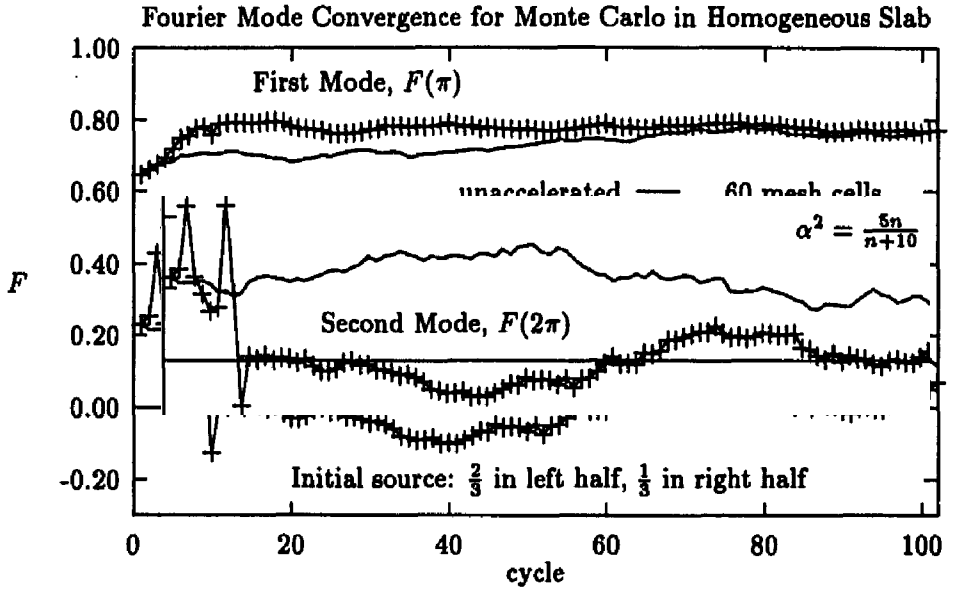

Figure 7.7: The first and second Fourier mode coefficient convergence for the homogeneous slab with unaccelerated Monte Carlo and FDSA with β=0.1 for 11 cycles and essentially zero thereafter.

expectations and behaved like inconsistently discretized FDSA, in that it required (often severe) damping.

For the deterministic FDSA calculations, speedups were about 2 for the "k_{eff} of the world" problem, 77 for the homogeneous problem, and 88 for the uniform lattice. For FDSA applied to Monte Carlo, speedups were 6 for the "k_{eff} of the world" problem, and 9 for the homogeneous problem. We did not attempt the uniform lattice problem. The Monte Carlo calculation speedups may be somewhat misrepresented because all Monte Carlo calculations, as a default, estimate the fission matrix eigenstate at each cycle.

Compared to the Monte Carlo Fission Matrix method, FDSA has the disadvantage of requiring a grid and more precalculation. However, it has the advantage of requiring less calculation at each iteration or cycle.

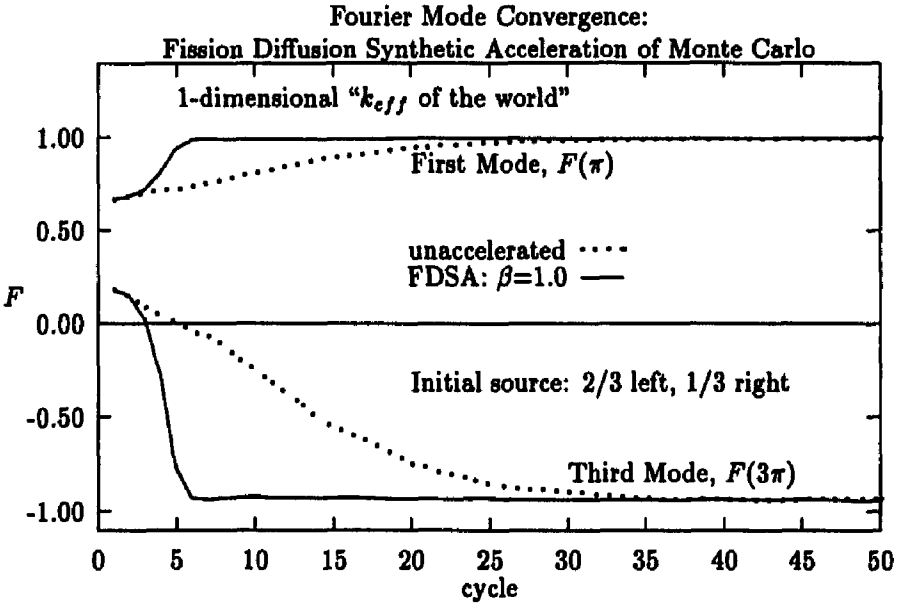

Figure 7.8: The first and second Fourier mode coefficient convergence for the "k_{eff} of the world" problem with unaccelerated Monte Carlo and FDSA with β=1.0.

CHAPTER VIII

A Hybrid Monte Carlo Method for Improved Source Convergence

Unlike the hybrid method in this chapter, the Fission Matrix and Fission Diffusion Synthetic Acceleration Methods are essentially unbiased. That is, they converge to the unaccelerated solution. Converging to the unaccelerated solution is a desirable feature of an acceleration method, unless the unaccelerated method itself has difficulties converging to the correct solution. Such is the case with Monte Carlo criticality calculations for arrays of identical, isolated, and weakly-coupled fissionable components. This type of system has a high dominance ratio. Because of statistics, components in the high dominance ratio system having more particles than expected, will tend to continue having more particles. In fact, for a lattice with no communication between its components, as the number of cycles approaches infinity, all the particles could end up in one component.

We propose a hybrid Monte Carlo method that overcomes this inherent deficiency in Monte Carlo criticality calculations. The hybrid method follows the same format as unaccelerated Monte Carlo by simulating particles on a cycle-by-cycle basis. However, the source for each cycle comes not from the fission sites sampled in the previous cycle, but from the solution of a modified diffusion equation whose parameters are

estimated by Monte Carlo. The modified diffusion equation tends to have smaller statistical errors than regular Monte Carlo. The hybrid method produces two sets of solutions: the modified Monte Carlo solution and the modified diffusion equation solution. Since the hybrid method's Monte Carlo solution is not exactly the same as the regular Monte Carlo solution, the hybrid method is not really an acceleration method. In other words, it is not unbiased. The cause of the bias from the regular Monte Carlo method is that the hybrid method has a spatial truncation error. We will find, however, that the biased nature of the hybrid method is quite beneficial for a lattice of weakly coupled components.

This hybrid method is based upon the Quasi-Diffusion method, which was first proposed in the deterministic arena by Gol'din [Gol64] and successfully applied with newly derived boundary conditions by Miften and Larsen [Mif93].

8.1 Derivation of the Hybrid Monte Carlo Method

Once again, we begin with the monoenergetic, one-dimensional integro-differential transport equation with isotropic scattering. We consider a slab of width L with vacuum boundaries,

$$\mu\frac{\partial\psi(x,\mu)}{\partial x}+\Sigma_t(x)\psi(x,\mu)=\frac{1}{2}\left(\Sigma_s(x)+\frac{\nu\Sigma_f(x)}{k}\right)\int\psi(x,\mu)d\mu \quad , \tag{8.1}$$

$$\psi(0,\mu)=0 \ , \quad \mu>0 \quad , \tag{8.2}$$

$$\psi(L,\mu)=0 \ , \quad \mu<0 \quad . \tag{8.3}$$

Defining ϕ_n, the angular moments of the angular flux ψ, as

$$\phi_n(x)=\int_{-1}^{1}\mu^n\psi(x,\mu)d\mu \quad , \tag{8.4}$$

where ϕ_0 is the scalar flux, we integrate the transport equation, Equation 8.1, over angle and obtain

$$\frac{d\phi_1(x)}{dx} + \Sigma_t(x)\phi_0(x) = \left(\Sigma_s(x) + \frac{\nu\Sigma_f(x)}{k}\right)\phi_0(x) \quad . \tag{8.5}$$

Multiplying Equation 8.1 by μ and integrating over angle, we obtain

$$\frac{d\phi_2(x)}{dx} + \Sigma_t(x)\phi_1(x) = 0 \quad , \tag{8.6}$$

from which we set

$$\phi_1(x) = -\frac{1}{\Sigma_t(x)}\frac{d\phi_2(x)}{dx} \quad . \tag{8.7}$$

Substituting Equation 8.7 into Equation 8.5, we obtain, *without approximation to the transport equation*,

$$-\frac{d}{dx}\frac{1}{\Sigma_t(x)}\frac{d}{dx}\phi_2(x) + \Sigma_a(x)\phi_0(x) = \frac{\nu\Sigma_f(x)}{k}\phi_0(x) \quad . \tag{8.8}$$

Next, we define an "Eddington factor," λ_2,

$$\lambda_2(x) \equiv \frac{\phi_2(x)}{\phi_0(x)} = \frac{\int_{-1}^{1}\mu^2\psi(x,\mu)d\mu}{\int_{-1}^{1}\psi(x,\mu)d\mu} \quad . \tag{8.9}$$

Multiplying and dividing the first term in Equation 8.8 by $\phi_0(x)$, and multiplying and dividing the other two terms in Equation 8.8 by λ_2, we obtain an elliptic equation for $\lambda_2(x)\phi_0(x)$:

$$-\frac{d}{dx}\frac{1}{\Sigma_t(x)}\frac{d}{dx}\lambda_2(x)\phi_0(x) + \frac{\Sigma_a(x)}{\lambda_2(x)}\lambda_2(x)\phi_0(x) = \frac{\nu\Sigma_f(x)}{k\lambda_2(x)}\lambda_2(x)\phi_0(x) \quad . \tag{8.10}$$

The boundary condition at $x = 0$, as derived by Miften and Larsen [Mif93], is found by integrating Equation 8.2 over $\mu > 0$ and manipulating as follows:

$$
\begin{aligned}
0 &= \int_0^1 \mu\psi(0,\mu)d\mu - \int_{-1}^0 \mu\psi(0,\mu)d\mu \\
&\quad + \int_0^1 \mu\psi(0,\mu)d\mu + \int_{-1}^0 \mu\psi(0,\mu)d\mu \qquad (8.11) \\
&= \int_0^1 |\mu|\psi(0,\mu)d\mu + \int_{-1}^0 |\mu|\psi(0,\mu)d\mu \\
&\quad + \int_0^1 \mu\psi(0,\mu)d\mu + \int_{-1}^0 \mu\psi(0,\mu)d\mu \qquad (8.12) \\
&= \int_{-1}^1 |\mu|\psi(0,\mu)d\mu + \int_{-1}^1 \mu\psi(0,\mu)d\mu \quad . \qquad (8.13)
\end{aligned}
$$

Now, we define an Eddington factor for the boundary,

$$\lambda_1(0) = \left(\frac{\int_{-1}^1 |\mu|\psi(0,\mu)d\mu}{\int_{-1}^1 \psi(0,\mu)d\mu}\right) \quad . \qquad (8.14)$$

We also rewrite Equation 8.7 at $x = 0$ by multiplying and dividing the right hand side by $\phi_0(0)$, and substituting Equation 8.9 to obtain

$$\phi_1(0) = -\frac{1}{\Sigma_t(x)}\frac{d}{dx}\lambda_2(0)\phi_0(0) \quad . \qquad (8.15)$$

Noting that the last term in Equation 8.13 is $\phi_1(0)$, we substitute Equations 8.14 and 8.15 into Equation 8.13, obtaining the left boundary condition,

$$0 = \lambda_1(0)\phi_0(0) - \frac{1}{\Sigma_t(0)}\frac{d}{dx}\lambda_2(0)\phi_0(0) \quad , \qquad (8.16)$$

or, multiplying both sides by $\lambda_2(0)/\lambda_1(0)$,

$$0 = \lambda_2(0)\phi_0(0) - \frac{\lambda_2(0)}{\lambda_1(0)\Sigma_t(0)}\frac{d}{dx}\left(\lambda_2(0)\phi_0(0)\right) \quad . \qquad (8.17)$$

The right boundary condition, found in a similar fashion, is

$$0 = \lambda_2(L)\phi_0(L) + \frac{\lambda_2(L)}{\lambda_1(L)\Sigma_t(L)}\frac{d}{dx}\left(\lambda_2(L)\phi_0(L)\right) \quad . \qquad (8.18)$$

Equations 8.10, 8.17, and 8.18 constitute a modified diffusion problem, derived, without approximation, from the transport problem, Equations 8.1, 8.2, and 8.3. The

hybrid method involves estimating the Eddington factors λ_2 and λ_1 with accumulated data from the Monte Carlo simulation. The solution of Equation 8.10 provides the distribution from which the subsequent cycle's fission source is sampled.

8.2 Implementing the Hybrid Method

During the Monte Carlo simulation, data are accumulated for estimating the Eddington factors. For example, on the left boundary, λ_2 is the ratio of an angle-weighted surface current estimate and a surface flux estimate [Lew84],

$$\lambda_2(0) = \frac{\sum_{i=1}^{N} |\mu_i(0)| w_i(0)}{\sum_{i=1}^{N} (w_i(0)/|\mu_i(0)|)}, \tag{8.19}$$

and λ_1 is the ratio of a particle current estimate and a flux estimate at the surface,

$$\lambda_1(0) = \frac{\sum_{i=1}^{N} w_i(0)}{\sum_{i=1}^{N} (w_i(0)/|\mu_i(0)|)}, \tag{8.20}$$

where N is the total number of particles and w_i is the weight of particle i. Required for every cell m in the system, λ_2 is obtained as an average of the angle squared, weighted by the track length flux estimate,

$$\lambda_{2m} = \frac{\sum_{i=1}^{N} \sum_{k(i)=1}^{K(i)} (\mu_i^2 \ell_i w_i)_{k(i)m}}{\sum_{i=1}^{N} \sum_{k(i)=1}^{K(i)} (\ell_i w_i)_{k(i)m}}, \tag{8.21}$$

where ℓ_i is the track length in cell m for track $k(i)$ of particle i.

For two reasons, the variance in the estimates of λ_1 and λ_2 is expected to be less than the variances associated with the regular Monte Carlo estimates of flux. First, the λ's are constrained between zero and one, while flux values throughout the system may differ by many orders of magnitude. Second, the statistical errors would tend, in some sense, to cancel out, since the λ's are ratios of similar quantities.

The method entails running enough cycles of regular, unaccelerated Monte Carlo to get good cumulative estimates of λ_1 and λ_2. Then these estimates are used in

the modified diffusion equation, Equation 8.10, whose solution requires a simple diffusion solver with modified cross sections. The solution is obtained on the cell-edges, allowing the Monte Carlo fission source for the next cycle to be sampled according to a linear fit in each cell.

This hybrid method gives two sets of solutions (flux, fission source, eigenvalue, etc.) of the system, one from the Monte Carlo simulation as usual, and one from the modified diffusion equation. In addition to truncation error [Mif93], the latter has a statistical error associated with it, but this error is less than the error of the Monte Carlo solution.

8.3 Results of the Hybrid Monte Carlo Method

We apply the hybrid method to the uniform lattice test problem, whose dominance ratio is approximately 0.996. The initial source contains 2/3 of the particles in the left half, and 1/3 in the right. The Eddington factors are accumulated over 30 inactive cycles, with 5,000 histories per cycle before the hybrid method is engaged. The Monte Carlo is performed using 58 meshs cells, with survival biasing (weight cut-off of 10^{-4}), and the hybrid diffusion calculation is made on 464 cells. In Figure 8.1, the experimental Fourier analysis shows the first and second Fourier modes, including the converged values from an S_{32} discrete-ordinates calculation. Once engaged, the hybrid method converges faster, and, upon convergence, has smaller statistical fluctuations.

Figure 8.2 shows the Monte Carlo collision fluxes from the unaccelerated and hybrid cases. It is evident that the Monte Carlo flux of the hybrid method is converged with its global cosine shape, while the unaccelerated Monte Carlo flux still retains initial source effects. The one-standard deviation error bars on the unaccelerated

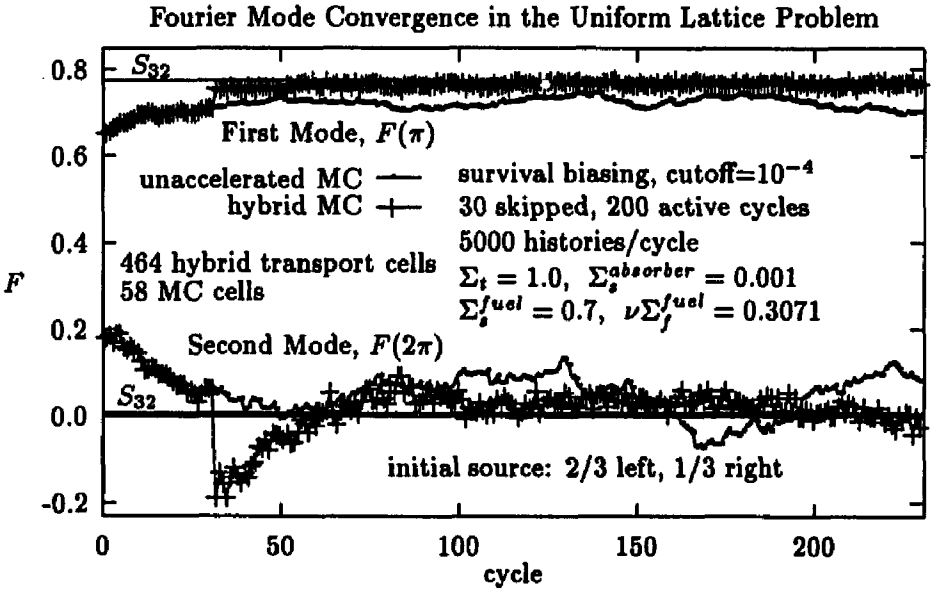

Figure 8.1: Convergence of the first and second Fourier modes for unaccelerated Monte Carlo and hybrid Monte Carlo in the uniform lattice test problem.

Monte Carlo flux show how the variance is grossly underestimated due to the lack of convergence and the high dominance ratio. Even so, the standard deviations of the hybrid Monte Carlo flux were nearly a factor of two smaller. Given that the unaccelerated flux error is underestimated, the actual factor of reduction is much larger than the apparent factor of two. We cannot easily quantify this actual factor because the unaccelerated fission source is not even converged.

For this problem, where the fuel cells are identical and the system is large, the eigenvalue, an integral quantity, is not overly sensitive to the fission source shape. Thus, the method shows no apparent improvement in estimating the eigenvalue.

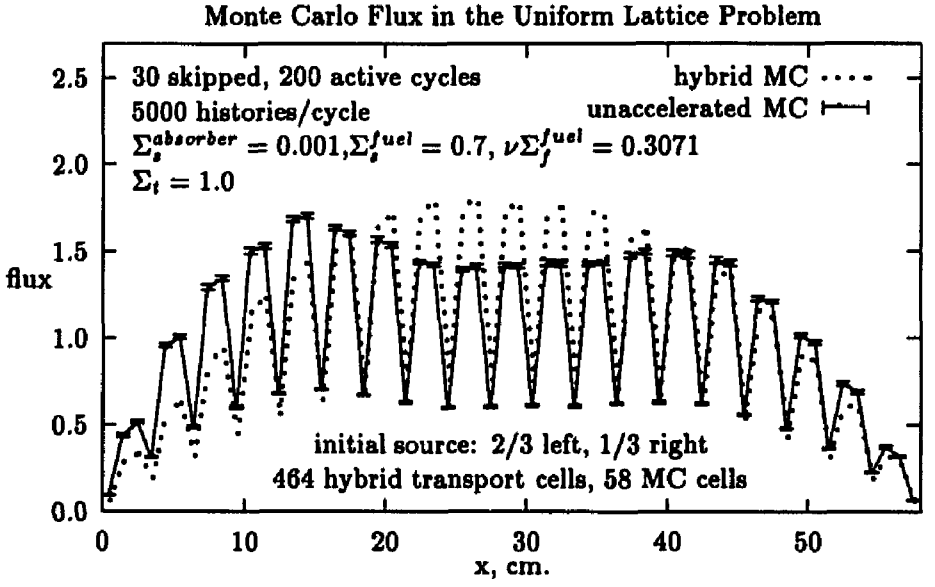

Figure 8.2: Collision flux estimate after 230 total cycles for unaccelerated Monte Carlo and hybrid Monte Carlo in the uniform lattice test problem.

CHAPTER IX

Summary, Conclusions, and Future Work

9.1 Summary and Conclusions

We have presented three new methods possessing improved source convergence properties in criticality calculations for systems with high dominance ratios. The three methods are the Fission Matrix Acceleration method, the Fission Diffusion Synthetic Acceleration (FDSA) method, and a Hybrid Monte Carlo method. Currently, practical Monte Carlo and deterministic criticality calculations are based on the source iteration method, which converges very slowly for systems with high dominance ratios. In fact, for some difficult problems, the Monte Carlo method will not converge to the correct solution. Systems that have high dominance ratios are those that have weak neutron communication between their distant regions. Typical high dominance ratio systems are large thermal nuclear reactors and arrays of barrels of nuclear waste.

The Fission Matrix Acceleration and FDSA methods are unbiased acceleration methods. They converge to the same solution as the unaccelerated calculation. Both methods approximate an exact acceleration equation for the fission source. Solving the approximate equation yields an additive correction for the fission source. The acceleration requires extra work at each iteration or cycle, but the source convergence

is accelerated by requiring fewer iterations or cycles.

The Fission Matrix Acceleration equation uses the fission matrix as a low-order operator in approximating an exact acceleration equation. The fission matrix may be estimated deterministically or by Monte Carlo. Fission Matrix Acceleration may be implemented in different ways. For instance, a diffusion fission matrix may be used to accelerate diffusion, discrete-ordinates, or Monte Carlo calculations. A Monte Carlo fission matrix can be used to accelerate a Monte Carlo calculation. The latter implementation is important because the absence of a deterministic acceleration equation deems a regular spatial grid unnecessary. Unfortunately, the statistical noise is amplified by the acceleration method and, therefore, needs to be filtered out. To do this we use a diffusion-like filter that requires a regular spatial grid, but filters exist that do not require a regular grid.

We test the feasibility of all three methods in a testbed consisting of idealized problems. Although these problems are far from reality, they contain enough realistic properties to serve as a valid testbed.

We have applied the Fission Matrix acceleration to three one-dimensional test problems. These were a homogeneous slab, a uniform lattice array, and a one-dimensional model of the "k_{eff} of the world" problem. Their dominance ratios are 0.991, 0.996, and 0.823, respectively. For deterministic calculations, we observed computational time speedups of about 20-34 for the homogeneous slab and uniform lattice problems. The deterministic speedup for the 1-D "k_{eff} of the world" problem was only 3.8 because the dominance ratio is not very high and, hence, there is little gain to be had. The speedups for Monte Carlo fission matrix acceleration were about 5 for the homogeneous slab and the 1-D "k_{eff} of the world" problem. The uniform lattice problem proved too difficult for unaccelerated–and therefore, accelerated–

Monte Carlo to converge to the correct fission source.

We have implemented the new Fission Matrix Acceleration method in the production Monte Carlo code MCNP. Applied to the three-dimensional "k_{eff} of the world" problem, results for the "real" problem were impressive. Fission matrix data were accumulated for 20 cycles after which the acceleration was turned on. The accelerated Monte Carlo solution converged in about 3 to 4 cycles, while the unaccelerated Monte Carlo required another 70 cycles. The dominance ratio of the three-dimensional "k_{eff} of the world" problem is about 0.92, which is higher than its one-dimensional representative test problem. The similarity of the method's behavior in this real problem to that in the simplified problems verified the validity of the testbed of idealized problems.

The Fission Diffusion Synthetic Acceleration (FDSA) method is similar to the Fission Matrix Acceleration method except that the acceleration equation is approximated by using the diffusion approximation. This acceleration method can be applied to discrete-ordinates or Monte Carlo transport and it requires a grid for solving the diffusion-like acceleration equation. FDSA requires less storage than the Fission Matrix Acceleration method. Applied to Monte Carlo, we saw speedups of 6 to 9. For deterministic calculations, we saw speedups of 77 and 88 for the homogeneous slab and uniform lattice, and a speedup of only 2 for the 1-D "k_{eff} of the world" problem.

The strength of the diffusion-like filter is controlled by a parameter α. The filter is intended to remove the high-frequency statistical noise from accelerated Monte Carlo calculations. We often found it necessary to damp the additive correction with a parameter β that varied between 0 and 1. Damping scales back all frequencies of the correction. The parameters α and β are not independent. If the filtering

does not remove enough noise, then the entire correction may have to be damped. Using β to do the work of filtering and keep the acceleration stable results in a loss of acceleration, because the low frequencies of the acceleration are scaled back also. Unfortunately, the selection of α and β is not automated.

Unaccelerated Monte Carlo was unable to converge for the uniform lattice test problem. In this case, attempts to accelerate convergence with an unbiased acceleration method also failed. We presented a Hybrid Monte Carlo method that is not an unbiased acceleration method because it does not converge to the unaccelerated Monte Carlo fission source due to its second order truncation error. Therefore, quantifying speedup is difficult, except to say that the Hybrid Method converges while, practically, the unaccelerated Monte Carlo does not. The Hybrid Monte Carlo method has a truncation error, but in the uniform lattice problem, it proved superior in converging the source and greatly reducing the statistical error. The method, for this problem, realized nearly a factor of two reduction in the *apparent* standard deviation of the collision flux estimate, but a much larger reduction in the *actual* standard deviation.

In conclusion, we have successfully accelerated fission source convergence in both deterministic and Monte Carlo criticality calculations. By filtering statistical noise, we have incorporated deterministic attributes into the Monte Carlo calculations in order to speed their source convergence. We have used both the fission matrix and a diffusion approximation to perform unbiased accelerations. The Fission Matrix Acceleration method has been implemented in the production code MCNP and successfully applied to a real problem. When the unaccelerated calculations are unable to converge to the correct solution, they cannot be accelerated in an unbiased fashion. A Hybrid Monte Carlo method weds Monte Carlo and a modified diffusion calcu-

lation to overcome these deficiencies. The Hybrid method additionally possesses reduced statistical errors.

9.2 Future Work

We now discuss a few items from the potentially endless list of "things to do."

1. Automate the selection of α and β. We know that as the number of Monte Carlo histories per cycle increases, the calculation appears more deterministic and filtering requirements diminish. So, α should be inversely proportional to the number of histories per cycle. The damping factor β may be dependent on the dominance ratio, ρ. If the dominance is near unity, very little information is gained each iteration or cycle. So, it may be that $\beta \sim (1 - \rho)$.

2. Implement a Kalman filter. The diffusion-like filter we use spatially smooths the fission source. For a severely heterogeneous system, spatial smoothing may introduce unphysical and unwanted errors. A Kalman filter would determine the optimal fission source in a region based on all previous cycles.

3. Use powers of the fission matrix. For high dominance ratio problems where little information is gained each cycle, it may be that one cycle or iteration is too small of a "snapshot" to get a view of the big picture. If instead of collecting the fission matrix over one cycle, suppose its n-th power was collected over n cycles. Then the acceleration could be applied every n cycles and be more effective. See Appendix A for a brief discussion.

4. Implement FDSA in a marriage between a deterministic production code and a Monte Carlo production code.

5. Combine FDSA and the Hybrid method.

6. Accelerate the fission matrix. Currently, the fission matrix is estimated after the unaccelerated cycle or iteration. Thus, the acceleration effects do not show up in the fission matrix until the next cycle or iteration, and, then, only implicitly. Accelerating the rows of the fission matrix may prove beneficial.

7. Further investigate using the adjoint fission source as an importance function, as suggested by Goad and Johnston [Goa59]. We considered using an importance function inversely proportional to the adjoint fission source during the inactive cycles to speed convergence, and proportional to the fission source during the active cycles to reduce the system-wide variance. However, initial results were not encouraging.

8. Study the adaptation of Halton's sequential Monte Carlo methods [Hal94] to criticality calculations.

APPENDICES

APPENDIX A

Using Powers of the Fission Matrix

If the fission matrix is accumulated from Monte Carlo results, the possibility exists to use multiple powers of the fission matrix in source convergence acceleration. The advantage of using the fission matrix to the, say, n-th power to accelerate source convergence is that it has a smaller dominance ratio. If, for instance, the dominance ratio of the fission matrix is ρ, the dominance ratio of the fission matrix to the n-th power is ρ^n. For systems with high dominance ratios, this modification in the fission matrix acceleration may prove useful and maybe even benefit the cases where unaccelerated Monte Carlo has difficulty converging to the correct solution.

After three cycles of source iteration (accelerated or otherwise) we would have

$$f_{1/2} = \frac{1}{k_0} L f_0 \quad , \tag{A.1}$$

$$f_{3/2} = \frac{1}{k_{1/2}} L f_{1/2} \quad , \tag{A.2}$$

$$f_{5/2} = \frac{1}{k_{3/2}} L f_{3/2} \tag{A.3}$$

$$= \frac{1}{k_{3/2} k_{1/2} k_0} L^3 f_0 \quad . \tag{A.4}$$

The last equation may be written

$$f_{5/2} = \frac{1}{\ell} K f_0 \quad , \tag{A.5}$$

where

$$\frac{1}{\ell}K = \frac{1}{k_{3/2}k_{1/2}k_0}L^3 \quad . \tag{A.6}$$

The elements of the matrix K would be constructed from the cumulative production in cell i at cycle m due to a source in cell j at cycle $(m-n)$ and the source at cycle $(m-n)$. This method would require extra storage because the normally-used single power fission matrix would still be required. The construction of K would require at least a uniform source in its initiating cycle.

The derivation of a fission matrix acceleration equation follows:

$$f - f_{5/2} = \frac{1}{k}Lf - f_{5/2} \tag{A.7}$$

$$= \frac{1}{k}L(f - f_{5/2}) + \frac{1}{k}Lf_{5/2} - f_{5/2} \quad . \tag{A.8}$$

So,

$$(I - \frac{1}{k}L)(f - f_{5/2}) = \frac{1}{k}Lf_{5/2} - f_{5/2} \tag{A.9}$$

$$= \frac{1}{k}Lf_{5/2} - \frac{1}{\ell}Kf_0 \tag{A.10}$$

$$= \frac{1}{k}L(\frac{1}{\ell}Kf_0) - \frac{1}{\ell}Kf_0 \tag{A.11}$$

$$= (\frac{1}{k}L - I)(\frac{1}{\ell}Kf_0) \tag{A.12}$$

$$= \frac{1}{\ell}K(\frac{1}{k}L - I)f_0 \tag{A.13}$$

$$= \frac{1}{\ell}K(\frac{1}{k}Lf_0 - f_0) \tag{A.14}$$

$$= \frac{1}{\ell}K(\frac{k_0}{k}f_{1/2} - f_0) \quad . \tag{A.15}$$

Then, as before, the appropriate spatial projections are made and the particular solution for the correction is obtained by setting k equal to

$$k = k_0\frac{(f^*, \frac{1}{\ell}Kf_{1/2})}{(f^*, \frac{1}{\ell}Kf_0)} = k_0\frac{(f^*, \frac{1}{\ell}Kf_{1/2})}{(f^*, f_{5/2})} \quad . \tag{A.16}$$

Here, f^* is the eigenvector of the adjoint L. The determination of k would require an extra matrix multiply, since $Kf_{1/2}$ is not explicitly known.

The idea is that the fission source for the i-th cycle can be accelerated by using a fission matrix to the n-th power and the fission sources from the $(i-n)$-th and $(i-n+1)$-th cycles. Extra storage would be required, as well as bookkeeping over n cycles, not just one.

This approach could enhance stability and possibly reduce some of the cycle-to-cycle correlation effects. It would only be applicable to the case where the Monte Carlo fission matrix is used.

APPENDIX B

Poetic Summary

I needed to know k
had computer time to burn
needed Monte Carlo
nowhere else to turn

sampling and pdf's
those are its wares
I like Monte Carlo
even though it has errors

I made up the input
so nice and clear
"I'll get me that number,"
I said without fear

material and densities
cross sections to discern
I guessed at a source
and hit carriage return

I waited and waited
for that thing to converge
killing the job
was my greatest urge

Along came Ed Larsen
luckily sooner than later
he said all I need
is a low-order operator

"I've been talking to Art
we've got the fix
just get yourself
a good fission matrix!"

so, hold the Mt. Dew
no shootin' the breeze
that run is completed
it converged with ease

what once took hours
now takes minutes
who can believe it?
it's gotta be nuts!

but proof of spare time
before you sits
I tried to write poetry
yep. it's the pits

BIBLIOGRAPHY

BIBLIOGRAPHY

[Ait57] A.C. Aitken, "Statistical Mathematics," Eighth Edition, Oliver and Boyd, Edinburgh and London (1957).

[Alc77] R.E. Alcouffe, "Diffusion Synthetic Acceleration Methods for the Diamond-Differenced Discrete-Ordinates Equations," *Nuclear Science and Engineering*, **64**, 344-355 (1977).

[Asa74] T. Asaoka, et al., "Coarse-Mesh Rebalancing Acceleration for Eigenvalue Problems," ANL-75-2, NEA-CRP-L-118, Argonne National Laboratory, July 1-3, (1974).

[Bel70] George I. Bell and Samuel Glasstone, *Nuclear Reactor Theory*, reprinted by Robert E. Krieger Publishing Company, Malabar, Florida, 1985, original edition printed by Van Nostrand Reinhold Co., New York (1970).

[Blo95] R.N. Blomquist, "VIM Continuous Energy Monte Carlo Transport Code," *Proceedings of the International Conference on Mathematics and Computations, Reactor Physics, and Environmental Analyses*, April 30–May 4, 1995, Portland, Oregon (1995).

[Bow83] H. Bowsher, E.M. Gelbard, P. Gemmel and G. Pack, "Magnitude of Bias in Monte Carlo Eigenvalue Calculations," *Trans. Am. Nucl. Soc.*, **45**, 324 (1983).

[Bow95] S.M. Bowman, "New Enhancements to SCALE for Criticality Safety Analysis," *Proceedings of the International Conference on Nuclear Criticality Safety (ICNC)*, September 17-22, 1995, Albuquerque, New Mexico (1995).

[Bri86] R.J. Brissenden and A.R. Garlick, "Biases in the Estimation of K_{eff} and Its Error by Monte Carlo Methods," *Ann. Nucl. Energy*, **13**, No. 2, 63-83 (1986).

[Bri93] J.F. Briesmeister, Editor; "MCNP^{TM}-A General Monte Carlo N-Particle Transport Code, Version 4A," LA-12625-M, Los Alamos National Laboratory (1993).

[Car69] L.L. Carter and N.J. McCormick, "Source Convergence in Monte Carlo Calculations," *Nuclear Science and Engineering*, **36**, 438-441 (1969).

[Car75] L.L. Carter and E.D. Cashwell, *Particle Transport Simulation with the Monte Carlo Method*, TID-26607, ERDA Critical Review Series, Technical Information Center, U.S. Energy Research and Development Administration, Oak Ridge, TN (1975).

[Cas67] Kenneth M. Case and Paul F. Zweifel, *Linear Transport Theory*, Addison-Wesley Publishing Company, Reading, Massachusetts (1967).

[Dic76] Deanne Dickinison and G.E. Whitesides, "The Monte Carlo Method for Array Criticality Calculations," *Nuclear Technology*, Volume 30, page 166, August 1976.

[Dud76] James J. Duderstadt and Louis J. Hamilton, *Nuclear Reactor Analysis*, John Wiley & Sons, Inc., New York (1976).

[Elp85] T. Elperin and A. Dubi, "On the Markov Chain Analysis of Source Iteration Monte Carlo Procedures for Criticality Problems: I," *Nuclear Science and Engineering*, **91**, 59-76 (1985).

[Eno90] M. Enosh, D. Shalaitin and Y. Yeiven, "The Bias in Monte Carlo Eigenvalue Calculations," *Prog. Nucl. Energy*, **24**, 1-3, 259 (1990).

[For94] R.A. Forster, S.P. Pederson, and T.E. Booth, "Ten New Checks to Assess the Statistical Quality of Monte Carlo Solutions in MCNP," *Proceedings of 8th International Conference on Radiation Shielding*, American Nuclear Society, Arlington, Texas, p. 414 (1994).

[Gas75] R.C. Gast and N.R. Candelore, "Monte Carlo Eigenfunction Strategies and Uncertainties," *Proceedings of the NEACRP Meeting of a Monte Carlo Study Group*, ANL-75-2, NEA-CRP-L-118, Argonne National Laboratory, July 1-3, (1974).

[Gel74] E.M. Gelbard and R.E. Prael, "Monte Carlo Work at Argonne National Laboratory," ANL-75-2(NEACRP-L-118), Argonne National Laboratory, 202 (1974).

[Gel81] E.M. Gelbard, "Unfinished Monte Carlo Business," *Proc. ANS/ENS Int. Meeting on Adv. in Mathematical Methods of Nuclear Engineering Problems*, Munich, Germany, April 27-29, 1981, European Nuclear Society (1981).

[Gel90] E.M. Gelbard and R. Prael, "Computation of Standard Deviations in Eigenvalue Calculations," *Progress in Nuclear Energy*, **24**, 237-241 (1990).

[Gel91] E.M. Gelbard, "Monte Carlo Eigenvalue Biases: Generalization Beyond the Absorption Estimate," *Trans. Am. Nucl. Soc.*, **64**, 302 (1991).

[Gel94] E.M. Gelbard and A.G. Gu, "Biases in Monte Carlo Eigenvalue Calculations," *Nuclear Science and Engineering*, **117**, 1 (1994).

[Goa59] W. Goad and R. Johnston, "A Monte Carlo Method for Criticality Problems," *Nucl. Sci. Eng.*, **5**, 371 (1959).

[Gol64] V.Ya. Gol'din, "A Quasi-Diffusion Method for Solving the Kinetic Equation," *Zh. Vych. Mat. I Mat. Fiz.* **4**, 1078 (1964). English translation in *USSR Comp. Math. and Math. Phys.* **4**, 6, 136 (1967).

[Gre68] H. Greenspan, C.N. Kelber, and D. Okrent, Editors, *Computing Methods in Reactor Physics*, Chapter 5, "Monte Carlo Methods in Reactor Computations," M.H. Kalos, F.R. Nakache, and J. Celnik, Gordon and Breach Science Publishers, New York (1968).

[Hal94] John H. Halton, "Sequential Monte Carlo Techniques for the Solution of Linear Systems," *Journal of Scientific Computing*, **9**, 2, June 1994, pages 213-257 (1994).

[Ham64] J.M. Hammersley and D.C. Handscomb, *Monte Carlo Methods*, John Wiley & Sons, New York (1964); reprinted with minor corrections by Barnes & Noble, Inc., New York (1965).

[Hir88] Charles Hirsch, "Numerical Computation of Internal and External Flows, Volume 1: Fundamentals of Numerical Discretization," John Wiley & Sons, Chichester, 1988.

[Kad91] Hiroyuki Kadotani, Yoshiharu Hariyama, Masayuki Shiota, and Tomoyuki Takada, "Acceleration of Fission Distribution Convergence Using Eigenvectors from Matrix K Calculations in the KENO Code," *Proceedings of the International Conference on Nuclear Criticality Safety*, September 9-13, 1991, Oxford, UK (1991).

[Kal86] Malvin H. Kalos and Paula A. Whitlock, *Monte Carlo Methods, Volume I: Basics*, John Wiley & Sons, New York (1986).

[Kap58] E.L. Kaplan, "Monte Carlo Methods for Equilibrium Solutions in Neutron Multiplication," UCRL-5275-T, Lawrence Livermore National Laboratory, (1958).

[Kap74] Hans G. Kaper, Arthur J. Lindeman, and Gary K. Leaf, "Benchmark Values for the Slab and Sphere Criticality Problem in One-Group Neutron Transport Theory," *Nuclear Science and Engineering*, **54**, 94-99 (1974).

[Kap84] Wilfred Kaplan, *Advanced Calculus*, Third Edition, Addison-Wesley Publishing Company, Reading, Massachusetts (1984).

[Kre78] Erwin Kreyszig, *Introductory Functional Analysis with Applications*, John Wiley & Sons, New York (1978).

[Lar82] Edward W. Larsen, "Unconditionally Stable Diffusion-Synthetic Acceleration Methods for the Slab Geometry Discrete Ordinates Equations. Part I: Theory," *Nuclear Science and Engineering*, **82**, 47-63 (1982).

[Lar84] Edward W. Larsen, "Diffusion-Synthetic Acceleration Methods for Discrete-Ordinates Problems," *Transport Theory and Statistical Physics*, 13 (1&2), pages 107-126 (1984).

[Lee94] S.R. Lee, et al.,"Unified GUI for the Los Alamos Radiation Transport Code System," *Trans. Am. Nucl. Soc.*, **71**, 402 (1994).

[Lew84] Lewis, E.E. and Miller, W.F. Jr., *Computational Method of Neutron Transport*, John Wiley & Sons, New York (1984).

[Lux91] I. Lux and L. Koblinger, *Monte Carlo Particle Transport Methods: Neutron and Photon Calculations*, CRC Press, Florida (1991).

[Mac73] D.B. MacMillan, "Monte Carlo Confidence Limits for Iterated-Source Calculations," *Nucl. Sci. Eng.*, **50**, 73 (1973).

[Men68] M.R. Mendelson, "Monte Carlo Criticality Calculations for Thermal Reactors," *Nucl. Sci. Eng.*, **32**, 319 (1968).

[Mif93] M.M. Miften and Edward W. Larsen, "The Quasi-Diffusion Method for Solving Transport Problems in Planar and Spherical Geometries," *Transport Theory and Statistical Physics*, 22(2&3), 165-186 (1993).

[Mih67] J.T. Mihalczo, "Multiplication Factor of Uranium Metal by One-Velocity Monte Carlo Calculations," *Nuclear Science and Engineering*, **27**, 557 (1967).

[Mor56] K.W. Morton, "Criticality Calculation by Monte Carlo Methods," AERE T/R 1903, Harwell (1956).

[Mor66] G.W. Morrison, J.T. Mihalczo, and D.C. Irving, "REACT and CONVERG Fortran Subroutines for Determining Source Convergence for the O5R Monte Carlo Neutron Transport Code," ORNL-TM-1325, Oak Ridge National Laboratory (1966).

[Pet92] L.M. Petrie, Oak Ridge National Laboratory, private communication (1992).

[Ree71] W.H. Reed, "The Effectiveness of Acceleration Techniques for Iterative Methods in Transport Theory," *Nuclear Science and Engineering*, **45**, 245-254 (1971).

[Smi95] N.R. Smith, "An Introduction to MONK 7," *Proceedings of the International Conference on Nuclear Criticality Safety (ICNC)*, September 17-22, 1995, Albuquerque, New Mexico (1995).

[Spa69] Jerome Spanier and Ely M. Gelbard, *Monte Carlo Principles and Neutron Transport Problems*, Addison-Wesley Publishing Company, Reading, Massachusetts (1969).

[Spi68] Murray R. Spiegel, *Mathematical Handbook of Formulas and Tables*, Schaum's Outline Series, McGraw-Hill Book Company, New York (1968).

[Stu08] Student, "The Probable Error of a Mean," *Biometrika*, Volume VI, No. 1, March (1908).

[Swa72] Richard Edward Swaja, *Application of Stochastic Optimal Estimation Principles to Monte Carlo Eigenfunction Convergence*, Ph.D. dissertation, Carnegie-Mellon University, Pittsburgh, Pennsylvania, October, 1972, recorded as 1973 in the reprint by University Microfilms International, Ann Arbor, MI (1993).

[Tho73] A.F. Thomas and F. Abbey, "Calculational Methods for Interacting Arrays of Fissile Material," Pergamon Press, Oxford (1973).

[Urb95] Todd J. Urbatsch, R. Arthur Forster, Richard E. Prael, and Richard J. Beckman, "Understanding the Three-Combined k_{eff} Confidence Intervals in MCNP," *Proceedings of the International Conference on Nuclear Criticality Safety (ICNC)*, September 17-22, 1995, Albuquerque, New Mexico (1995). See also "Estimation and Interpretation of k_{eff} Confidence Intervals in MCNP," *Nuclear Technology*, **111**, 169-182, August (1995).

[Van93] K.A. Van Riper, *Sabrina User's Guide*, Los Alamos Report LA-UR-93-3696 (1993).

[Wal95] Wallace F. Walters and Todd A. Wareing, "An Accurate, Strictly-Positive, Nonlinear Characteristic Scheme for the Descrete-Ordinate Equations," *Transport Theory and Statistical Physics*, to be published.

[Whi71] G.E. Whitesides, "A Difficulty in Computing the k-effective of the World," *Trans. Am. Nucl. Soc.*, **14**, 680 (1971).